

Investigation of Tx-Rx Mutual Inductance Eddy Current System for High Lift-Off Inspection

A doctoral thesis submitted for the degree of Doctor of Philosophy

Denis Ijike Ona



Intelligent Sensing and Communications Research Group
(ISC)

School of Engineering, Newcastle University

February 2020

CERTIFICATE OF ORIGINALITY

This is to certify that the work submitted in this thesis is my own work except as specified in acknowledgements. Neither the work nor the thesis has been submitted to any other institution for another degree. Where the work formed comes from jointly-authored publications, my contribution and those of the other authors to this work have been explicitly indicated. Also, I confirm that appropriate credit has been given within the thesis where reference has been made to the work of others. The work presented in Chapter 4 was previously published in [175]. The studies were conceived by all the authors. I carried out all the modelling, design, simulation and experimental validation of the work under the guidance of the remaining authors.

..... (Signed)

..... (Candidate)

To my wife, the boys & Chimere-uche

Table of Contents

Table of Contents	v
List of Figure	ix
List of Tables	xi
List of publications	xii
Abbreviations	xiii
Acknowledgements	xv
Abstract.....	xvi
Chapter 1. Introduction.....	1
1.1 Research Background	1
1.2 Research Aim and Objectives	2
1.3 Scope of the Research.....	3
1.4 Main Achievements	4
1.5 Thesis Layout.....	5
1.6 Chapter Summary	7
Chapter 2. Literature Review.....	8
2.1 Review of Electromagnetic NDT&E Techniques for Defect Detection.....	8
2.2. Eddy Current Pulse Thermography (ECPT)	9
2.3 Ground Penetrating Radar (GPR)	10
2. 4 Magnetic Field Leakage.....	12
2.5 Alternating current field measurement (ACFM)	13
2.6 Electromagnetic Acoustic Transducers (EMAT).....	14
2.7 Synopsis of NDT&E Techniques for Defect Detection and Characterisation.....	15
2.8 Review Eddy current (EC) testing	16
2.8.1 EC Probe configurations	17
2.8.2 EC Signal conditioning	18
2.8.3 EC excitation modes.....	19

2.9 Background of EC Testing System.....	22
2.9.1 Principle of eddy current testing	22
2.9.2 Principle of Pulse eddy current testing.....	24
2.9.4 PEC signal interpretation	27
2.9.5 PEC technique features	28
2.9.6 PEC Feature extraction	28
2.10 Inspection of Conductive Material at High Lift-off with Tx-Rx EC Probe.....	29
2.11 Challenges and Problems Identification	31
Chapter 3. Prototype Tx-Rx PEC system and Research methodology	33
3.1 Defect Detection and quantification	33
3.2 Tx-Rx probe configuration	34
3.3 Signal Conditioning of Tx-Rx PEC System.....	35
3.4 Excitation Modes of EC Testing System	36
3.5 Prototype Tx-Rx PEC System Configuration and Setup	36
3.6 Research Methodology	37
3.6.1 Study 1: Optimization of Mutual Inductance Based on Tx-Rx Probe	38
3.6.2 Study 2: Investigation of Signal Conditioning of Tx-Rx Probe.....	38
3.6.3 Study 3: Comparative Study of Excitation Modes of Tx-Rx Probe.....	38
3.7 Chapter summary.....	39
Chapter 4. Optimization of Tx-Rx probe for high lift-off inspection.....	40
4.1 High Lift-off Inspection with Tx-Rx Eddy current Probe	40
4.2 Design and Optimisation of Mutual Inductance based Tx-Rx Probe	42
4.3 Mutual Inductance Based Tx-Rx probe Testing Method.....	43
4.4 Numerical Simulation Study.....	46
4.4.1 Lift-off Influence.....	47
4.4.2 Coil Gap Influence	49
4.5 Experimental Study and Validation	50
4.5.1 Lift-off Influence Analysis.....	50

4.5.2 Coil Gap Influence Analysis	51
4.5.3 Comparison of Simulations and Experimental Results.....	53
4.5.4 Performance Evaluation of the Proposed Technique for Crack Detection	54
4.4 Chapter summary	56
Chapter 5. Investigation of signal conditioning of Tx-Rx probe for high lift-off inspection.	57
5.1 Introduction.....	57
5.3 Proposed Signal Conditioning Circuit	62
5.4 Experimental Setup.....	65
5.5 Experimental Results and Discussions	67
5.5.1 Lift-off Influence and linearity range.....	67
5.5.2 Sensitivity to Crack Detection and SNR.....	72
5.5 Performance Comparison	74
5.6 Chapter summary	75
Chapter 6. Selection of Excitation Mode for High Lift-off Inspection	76
6.1 Introduction.....	76
6.2 Experimental Studies	77
6.3 Experimental Setup and Samples	78
6.4 Results and Discussion	80
6.4.1 Influence of lift-off on Rx time domain response of PEC and SFEC.....	80
6.4.2 PEC time domain and SFEC crack detection at different Lift-offs.....	81
6.4.3 QNDE of crack depths with PEC and SFEC at different lift-offs.....	82
6.4.4 PEC Frequency Domain Vs SFEC Crack Detection.....	84
6.5 Performance evaluation and Comparison	86
6.6 Chapter Summary	87
Chapter 7. Conclusion and Further Work.....	88
7.1 Research Conclusions	88
7.2 Future work Suggestions	89
References	92

List of Figure

Figure 1.1 A general schematic of electromagnetic NDT&E	1
Figure 1.2 Structures that require high lift-off inspection	2
Figure 2.1 Summary of the different electromagnetic NDT&E techniques	9
Figure 2.2 Basic configurations of pulse eddy current thermography system	10
Figure 2.3 Block diagram of generic GPR system	12
Figure 2.4 A typical MFL inspection technique for pipeline inspection	13
Figure 2.5 Current and magnetic field distribution in ACFM	14
Figure 2.6 EMAT Testing	15
Figure 2.7 coplanar rectangular coil Tx-Rx probe above a conductor	18
Figure 2.8 Different excitation modes of EC testing	21
Figure 2.9 Principle of eddy current	22
Figure 2.10 Different types of EC probes	24
Figure 2.11 PEC time-domain parameters	28
Figure 2.12 Typical PEC signals obtained by using a Hall-device-based probe	29
Figure 2.13 Lift-off influence and principle of Tx-Rx probe eddy current testing	30
Figure 3.1 The basic architecture of EC defect detection and quantification	34
Figure 3.2 Direct and indirect coupling of Tx-Rx probe	35
Figure 3.3 Impedance change and self-impedance of the Rx coil	36
Figure 3.4 PEC-based system setup	37
Figure 3.5 Research diagram for PEC inspection system	37
Figure 4.1 Influence of lift-off and coil gap on Rx output of Tx-Rx probe	42
Figure 4.2 Driver-Pickup PEC probes	44
Figure 4.3 Equivalent circuits of PEC probes	44
Figure 4.4 Simulation model showing driver, pick-up coils and test sample	47
Figure 4.5 Lift-off influence on reference-subtracted signal from simulation	48
Figure 4.6 Coil gap influence on reference-subtracted signal from simulation	49
Figure 4.7 Experimental setup for PEC probe	50
Figure 4.8 Reference-subtracted pick-up voltage vs lift-off at different coil gaps	51
Figure 4.9 Reference-subtracted signal pick-up voltage vs coil gap at different lift-offs	52
Figure 4.10 Comparison of crack detection at different lift-offs with fixed coil gap	55
Figure 5.1 Tx-Rx equivalent circuit	60
Figure 5.2 Different Signal Conditioning Circuit	64
Figure 5.3 Tx-Rx probe above test sample with conditioning circuit	65
Figure 5.4 Experimental setup	67

Figure 5.5 Response signal of Rx with repeated pulse excitation of Tx coil	68
Figure 5.6 Static characteristic curve of Tx-Rx probe.....	70
Figure 5.7 Percentage deviation from the ideal linearity.....	71
Figure 5.8 Measurement errors of the Circuits.....	72
Figure 5.9 Crack detection of the aluminium sample.....	73
Figure 6.1 System block diagram for the study.....	78
Figure 6.2 Experimental setup.....	79
Figure 6.3 Aluminium test sample with artificial cracks.....	80
Figure 6.4 Sample and scan dimensions.....	80
Figure 6.5 Lift-off influence of PEC and SFEC at fixed Coil gap	81
Figure 6.6 Crack detection of PEC and SFEC at different Lift-offs	81
Figure 6.7 Crack depth mapping of PEC and SFEC responses at different Lift-offs.....	83
Figure 6.8 Frequency domain response of PEC and SFEC.....	85
Figure 6.9 Crack depth detection of PEC based on frequency domain.	86

List of Tables

Table 2. 1 Commonly used NDT techniques.	16
Table 4. 1 Mesh convergence study	47
Table 4. 2 Influence of lift-off and coil gap on the sensitivity of driver pickup probe	48
Table 4. 3 Experimental and simulations results at selected lift-off and coil gaps	53
Table 5. 1 SNR and peaks of Maxwell's bridge and modified Maxwell's bridge	74
Table 6. 1 Performance of PEC and SFEC in crack depth detection	82
Table 6. 2 Repeatability of PEC measurements	84
Table 6. 3 Repeatability of SFEC measurements	84
Table 6. 4 Comparison of PEC and SFEC performances for high lift-off testing.....	87

List of publications

- [1] D. I. Ona, G. Y. Tian, R. Sutthaweekul, and S. M. Naqvi, "Design and optimisation of mutual inductance based pulsed eddy current probe," *Measurement*, vol. 144, pp. 402-409, 2019/10/01/, 2019.

- [2] D. I. Ona, G. Y. Tian, and S. M. Naqvi, "Investigation of Signal Conditioning for Tx-Rx PEC Probe at High Lift-off Using a Modified Maxwell's Bridge" Submitted to *IEEE Sensors*, 2019.

- [3] H. Song, L. Yang, G. Liu, G. Tian, D. Ona, Y. Song, and S. Li, "Comparative Analysis of In-line Inspection Equipment and Technologies." *IOP Conf. Series: Materials Science and Engineering*. **382** 032021, 2018

Abbreviations

AC	Alternating Current
ACFM	Alternating Current Field Measurement
ACPD	Alternating Current Potential Drop
ADC	Analog-to-Digital Converter
AMR	Anisotropic Magneto-Resistance
CNC	Computer Numerical Control
DAS	Data Acquisition System
DC	Direct Current
EC	Eddy Current
ECPT	Eddy Current Pulsed Thermography
ECT	Eddy Current Testing
EM	Electromagnetic
EMAT	Electromagnetic Acoustic Transducer
EMF	Electromagnetic Field
GMR	Giant Magnetoresistance
GPIB	General Purpose Interface Bus
GPR	Ground Penetrating Radar
IR	Infra-Red
LPT	Line Printer Terminal
MFEC	Multi-Frequency Eddy Current
MFL	Magnetic flux leakage
NDT&E	Non-destructive Testing and Evaluation
PC	Personal Computer
PCA	Principal Component Analysis
PEC	Pulse Eddy Current
PIG	Pipe Line Integrity Gauge
PII	Pipe Line Integrity
PMFL	Pulsed Magnetic Field Leakage
PRF	Pulse Repetition Frequency
PZT	Piezo Electric Transducer
QNDE	Quantitative Non-destructive Evaluation

RL	Resistor-Inductor
Rx	Receiver
SFEC	Sweep Frequency Eddy Current
SNR	Signal-to-Noise Ratio
SQUID	Superconducting Quantum Interference Device
SUT	Sample Under Test
TP	Time-to-Peak
Tx	Transmitter
TZC	Time-to-Zero Crossing
UWB	Ultra-Wide Band

Acknowledgements

This thesis would not have been possible without the support and encouragement of many people who contributed and extended their valuable co-operation in the completion of the research work. I feel short of words in expressing my appreciation for their help at various stages of this work. First and foremost, I would like to express my sincere gratitude to my supervisor Prof. G.Y. Tian for his guidance, his patience and his continuous support from the beginning to the completion of this work. I thank Dr Mohsen Naqvi whose red pen made most of this work presentable. I specifically give many thanks to Dr Emmanuel Ogundimu for his encouragement, insightful advice and help during the course of this work. Special thanks to all the technicians for assistance with sample fabrication. My sincere appreciation goes to all my colleagues past and present. Some of them are Adejo Achonu, Ruslee Sutthaweekul, Adi Marinda, Mohammed Buhari, Chaoqing Tang, Monica Roopak, Yachao Ran and Lawal Umar and everyone in the research group for their valuable and worthwhile discussions throughout the research period. My warm appreciation also goes to committee of friends in Newcastle upon Tyne especially in the church who through their friendship and love made my stay worthwhile. Thanks to the Tertiary Education Trust Fund (TETfund) for sponsoring this research work through the overseas scholarship scheme. Finally, my sincere gratitude goes to God Almighty, the source of wisdom and all inspirations, in whom I live, move and have my being.

Abstract

Eddy current (EC) testing is a popular inspection technique due to its harsh environment tolerance and cost-effectiveness. Despite the immense research in EC inspection, defect detection at high lift-off still poses a challenge. The weakening mutual coupling of EC probe and sample due to the increase in lift-off degrades signal strength and thus reduces the detection sensitivity. Although signal processing can be used to mitigate lift-off influence, it is laborious and time consuming. Therefore, in this study, a Tx-Rx probe system is proposed to deal with high lift-off inspection.

The parts of the study of the Tx-Rx EC system includes optimisation of probe configuration, improvement of signal conditioning circuit and comparative study of excitation modes. In optimisation of probe configuration, lift-off and coil gap are optimized to mitigate the offset caused by the direct coupling of Tx-Rx coils. The optimum coil gaps of Tx-Rx probe for different lift-offs are found by observing the highest signal strength. The optimisation of coil gap against lift-off extends the detection sensitivity of the EC system to a lift-off of about 30 mm which is by far higher than 5 mm lift-off limit of a single-coil EC probe. In signal conditioning aspect, a modified Maxwell bridge circuit is designed to remove the offset due to self-impedance of the Rx coil. The proposed circuit mitigates the influence of the self-impedance of Rx coil and improves signal-to-noise ratio SNR. In the excitation mode, pulse and sweep frequency signals are compared to study detection sensitivity, SNR and crack quantification capability. The result of the comparative study reveals that pulse excitation is good for crack sizing while sweep frequency excitation is better for crack detection. Simulations and experimental studies are carried out to show the efficacy of the Tx-Rx EC system in high lift-off crack detection.

Chapter 1. Introduction

This chapter provides a brief background of non-destructive testing and evaluation (NDT&E) of electrically conductive materials. Project motivation, research aim and objectives, scope of the research, main achievements and the structure of the thesis are presented.

1.1 Research Background

Non-destructive testing and evaluation (NDT&E) refers to methods of testing materials for defects without damage to its serviceability. Performing such tests without damaging a component or shutting down of a plant improve profitability due to higher plant availability factors [1]. Defects in components arise from the presence of flaws in the raw material itself, and defects arising from fabrication processes such as welding, casting, machining and assembling. Environment and loading conditions which the components are subjected to during transportation, storage and usage are also sources of damage to components. These defects include cracks, corrosion, fatigue, creep and wall thinning. In a case of rail tracks and storage structures, this may lead to leakages threatening the development of the national economy, lives and properties are also lost. To forestall the occurrence of these leakages and accidents, regular inspections of structures are required for health and safety [2]. A general overview of NDT&E system is shown in figure 1.1. An NDT&E system is made up of three modules; excitation, reception and feature extraction modules. In the excitation part, a particular form of energy is injected into the object under test. The energy is transformed depending on the material properties and presence of flaws in the object. The transformed signal is detected by the reception unit. Finally, the received signals are processed to extract information about the object under test.

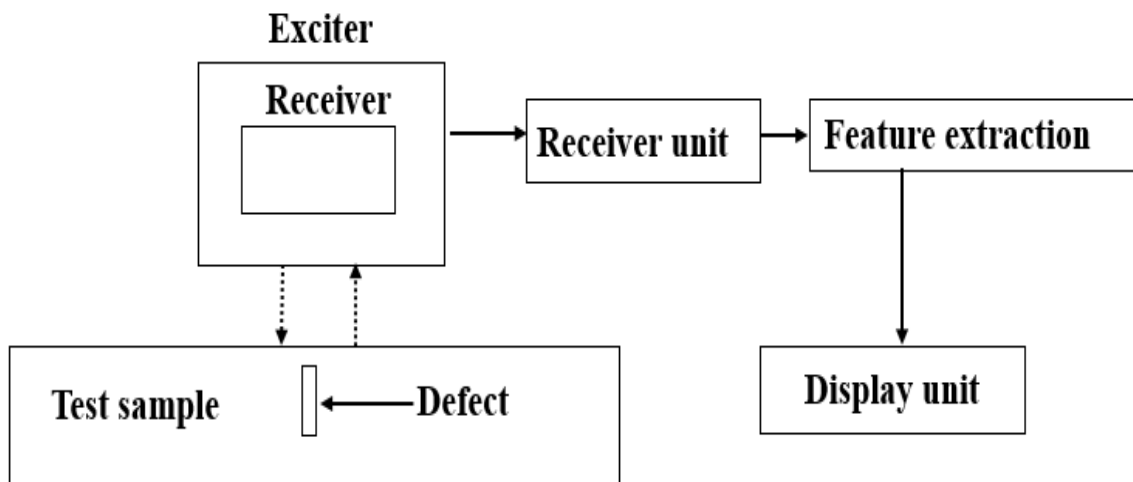


Figure 1.1 A general schematic of electromagnetic NDT&E

Some structures are buried underground, thick insulated or have weld areas as shown in figure 1.2 [3]. Also some storage tanks especially industrial tanks store high-temperature fluids making them very hot for inspection at low lift-off. Hence inspection of such structures is required to be done at high lift-off.

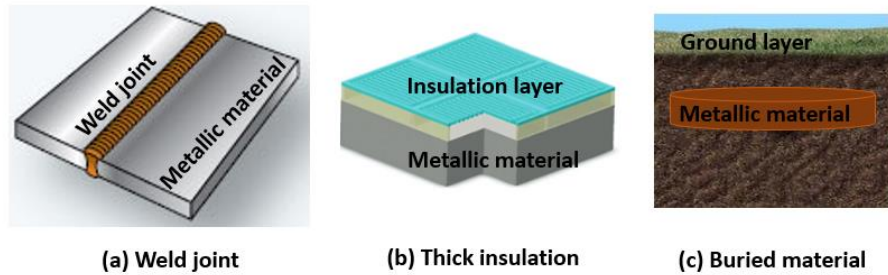


Figure 1.2 Structures that require high lift-off inspection

Various (NDT&E) techniques are used for testing including ultrasonic technique [4, 5], magnetic flux leakage (MFL) [6, 7], electromagnetic acoustic transducers (EMAT) [8], alternating current field measurement (ACFM) [9], alternating current potential drop (ACPD) [10] and EC (eddy current) [11]. None of these methods can claim superiority to another; they all have their own attractive features and limitations. However, most of the (NDT&E) techniques require the removal of the insulation layer for effective inspection. EC technique is a widely used electromagnetic NDT&E technique for detection and sizing of the surface as well as near subsurface flaws in insulated or weld surfaces. In this technique, flaws are detected by measuring changes in impedance of a coil excited with an alternating current or by measuring induced voltage in an adjacent receiver coil. Different probe configurations can be optimised for specific applications of EC inspection system. EC testing is a simple and portable NDT&E technique used for testing of components such as heat exchanger tubes, aircraft structures and industrial pipes. Different EC signals including multi-frequency, sweep-frequency and pulse are used as excitation signals of EC probe [12]. The excitation signals can be represented in time domain as PEC and frequency domain as multi-frequency or sweep-frequency. A time-domain signal like PEC possesses a wide range of a continuum of frequency components. Hence, it contains more information compared to a single-frequency excitation [13].

1.2 Research Aim and Objectives

The main aim of the project is to design and investigate a mutual inductance based Tx-Rx (driver-pickup) PEC system for high lift-off NDT&E application such as thick insulated or buried structures and weld areas.

To develop this system, the objectives of the study are as follows:

- To investigate the influence of Tx-Rx coil gap and Lift-off on detection sensitivity.
- To design and optimise mutual inductance based Tx-Rx PEC probe for inspection at lift-off range of 0 to 30mm.
- To design and investigate a modified AC bridge based on operational amplifier (opamp) configuration for front-end signal conditioning for high lift-off testing.
- To compare different excitation signals for quantitative non-destructive testing and evaluation.
- To demonstrate experimentally the use of mutual inductance based Tx-Rx PEC probe for crack detection and characterization at high lift-off.

1.3 Scope of the Research

In this research, a mutual inductance based Tx-Rx PEC probe is proposed to assess its usage in high lift-off inspection. Three parts of the inspection system are studied to address the challenges of sensitivity degradation, Low SNR and small linearity range of the probe at high lift-off. The study selected samples with known defect geometry and electromagnetic properties. Further, signal processing techniques with feature extraction techniques are then exploited to determine the efficacy of the method in the detection of crack on an aluminium plate.

The initial feasibility study is carried out to investigate the optimal coil gap and lift-off configuration of TX-Rx probe using numerical simulations and experiments for high lift-off inspection. The main target is to detect crack with optimal sensitivity at a given lift-off on the conductive sample, a situation normally encountered in thick insulation or weld area inspection. The optimal coil gap and lift-off are used to detect crack and based on the results compared to detection at other lift-off values. It was found that detection at the optimal coil gap and lift-off can be used to get better sensitivity.

From the feasibility study, a mutual inductance based Tx-Rx PEC probe is investigated. The study uses optimisation of coil gap and lift-off to mitigate the effect of the degrading sensitivity and direct coupling of Tx and Rx coils which characterize high lift-off inspection. And opamp based modified Maxwell's bridge circuit was designed to remove the influence of self-impedance of Rx coil which degrades SNR of the output signal. An experimental study is then conducted to show the efficacy of the approach in artificial crack on an aluminium sample. More importantly, the improvement in linearity range and measurement errors based on

modified Maxwell's inductance bridge over conventional bridges through qualitative analysis is demonstrated.

To conclude the study, a comparative study of different excitation modes including pulse, multi-frequency and sweep frequency excitations for defect detection and characterization is carried out. Experimental studies are used to validate the approach in crack detection of the aluminium sample.

1.4 Main Achievements

The first contribution of this study proposed an optimisation design of mutual inductance based PEC Probe to improve sensitivity at high lift-off. Simulation and experimental study on the influence of lift-off and coil gap on mutual inductance of Tx-Rx PEC probe and aluminium sample are carried out. Results validate that both coil gap and lift-off have significant effects on resultant mutual inductance of Tx-Rx PEC probes above test samples and hence its sensitivity. In addition, the probe sensitivity is enhanced at a given (optimal) lift-off for a fixed coil gap. The increase in detection lift-off with coil gap could be optimised for specific lift-off requirements. The second contribution proposed a modification of Maxwell's bridge signal conditioning circuit for Tx-Rx PEC testing at high lift-off. In Tx-Rx probe, self-impedance of the Rx coil dominates the output signal, reducing SNR especially at high lift-off. This limits the subsequent amplification of the output signal by the signal conditioning circuit. In practice, Maxwell's inductance bridge based measurement circuit is used to mitigate this challenge but results in small linear range input-output characteristic. Electromagnetic interference and stray capacitance effects also cause measurement errors. A modified Maxwell's bridge is investigated in comparison with conventional Maxwell's bridge for high lift-off inspection. The simple modified operational amplifier based bridge circuit removes the Rx coil self-impedance to improve SNR and to make output signal proportional to impedance change only. Results show improved SNR, linearity range and higher lift-off crack detection sensitivity in comparison to conventional Maxwell's bridge circuit. The third contribution is on comparative study of different excitation modes including single frequency, multi-frequency, sweep-frequency and pulse excitations modes of Tx-Rx PEC probe for defect detection and characterization at high lift-off. The combined effects of high lift-off and crack depth makes the interpretation of the response signal difficult. Also, at high lift-off, the impedance change of Tx-Rx probe as may be brought about by cracks becomes minimal, making crack depth measurement a challenge. Hence excitation mode with high SNR and signal strength are required for high lift-off testing. Unfortunately, each type of the excitation modes presents merits and demerits that prevent the selection of an absolute best excitation mode. Hence a

comparative study of different EC excitation modes is carried out to select the excitation mode that can provide as much information as possible about the presence and geometry of defects at high lift-off. Two excitation modes namely Sweep- frequency eddy current (SFEC) and pulse eddy current (PEC) are experimentally compared based on SNR, lift-off influence and accuracy of crack depth estimation. Following this, experiments for estimation of crack depth at high lift-off were carried out for both excitation modes. PEC response shows more linear relationship with depth cracks whereas, SFEC shows more signal strength therefore are better for cracks detection at high lift-off.

The techniques presented in this thesis demonstrates that synergistic integration of the optimised Tx-Rx probe configuration, modified Maxwell's bridge signal conditioning circuit with appropriate excitation mode ensures reliable detection and quantification of crack at high lift-off. The major findings made in this study are that the coil gap and lift-off have significant effects on resultant mutual inductance of Tx-Rx probe above test samples. In addition the probe sensitivity is enhanced at a higher lift-off as coil gap increases. Also the SNR of Tx-Rx probe can be improved by removing the offset due to direct coupling of Tx-Rx coils and self-impedance of the Rx coil. Furthermore, the sensitivity of Tx-Rx probe depends significantly on excitation mode in relation to lift-off value. The study developed a possible way to extend the inspection lift-off of a single-coil probe which loses sensitivity at a lift-off beyond 5mm to about 30 mm lift-off by Tx-Rx probe optimisation. Structures that requires a target high lift-off within 30mm can be inspected. The optimised Tx-Rx probe developed in this thesis can also be used to design a printed circuit Tx-Rx EC probe for a predetermined inspection lift-off by fixing the coil gap. Also for a varied lift-off inspection, the coil gap can be controlled to achieve the optimal lift-off as the inspection lift-off varies like in structures with varied insulation thickness or pipelines with varied diameters.

1.5 Thesis Layout

This thesis consists of seven chapters and a summary of the content of each is given below

In Chapter 1, a detailed research background of the study is presented. The motivation of the work, aims and objectives of the research work, the scope of the work and main achievements related to the study are presented.

Chapter 2 presents an in-depth literature review of different NDT&E techniques. Different areas related to eddy current signal waveforms, probe configurations, signal conditioning, Lift-off Problem and techniques that deal with high lift-off are reviewed. Both their advantages and disadvantages are discussed. The study also looks at the theoretical background of the EC

testing system explained in terms of electromagnetic field interactions of probe and sample. The EC testing system, EC signal interpretation, instrumentation and signal conditioning, and EC features system are then discussed. Research challenges and problems of high lift-off EC inspection system are identified and solutions to some of the problems are proposed.

In Chapter 3, a prototype Tx-Rx EC inspection system is explained. The research methodology is then presented with a target to investigate mutual inductance based Tx-Rx EC system for high lift-off inspection. This is carried out in the three aspects namely, optimisation of coil gap and lift-off for sensitivity improvement, removal of Rx coil self-impedance for SNR and linearity improvement. And a comparative study of Tx-Rx probe excitation modes for application in high lift-off inspection is carried out.

Chapter 4 deals with the study of coil gap and lift-off influence on defect detection sensitivity. The influence of the weakening interaction between probe and test sample as lift-off increases on sensitivity is analysed by numerical simulations and experiments for design and optimisation of Tx-Rx PEC probes. Results validate that both coil gap and lift-off have significant effects on resultant mutual inductance of driver-pickup PEC probes above test samples. In addition, the probe sensitivity is enhanced at a given (optimal) lift-off at any fixed coil gap. The increase in detection lift-off with coil gap can be optimised for specific lift-off requirement.

In Chapter 5, the second study of the PEC system for high lift-off inspection is the investigation of a modified Maxwell's inductance bridge for high lift-off testing. The conventional Maxwell's bridge is modified and implemented based on opamp circuit configuration. This is to remove the offset signal caused by self-impedance of Rx coil to improve linearity range and SNR. The performance evaluation of the modified circuit is carried out in comparison to the conventional Maxwell's inductance bridge circuit through experimental study. Results showed improved SNR, linearity range and higher lift-off crack detection sensitivity in comparison to Maxwell's inductance bridge circuit.

Chapter 6 presents a comparative study of different excitation modes for defect detection and characterization at high lift-off. This is because, each type of the excitation modes presents strengths and weaknesses that prevent the selection of an absolute best excitation signal. Hence, different excitation modes including single frequency, multi-frequency, sweep-frequency and pulse excitations are reviewed to ascertain their strength and weaknesses for high lift-off inspection. An experimental study was conducted with PEC and SFEC excitation modes results obtained shows that PEC is a good candidate for QNDE, while SFEC is better for defect detection

Chapter 7 summarises the thesis work and contribution, presents the research conclusions and outlines further work based on the current findings

1.6 Chapter Summary

This chapter introduces a brief background of the EC testing system. The problems and challenges the research sets out to solve are presented and explained. The aims and objectives of this research including the scope of the work are discussed. The main achievements of the research are also presented. Lastly, the layout of the thesis along with the contents of each chapter is summarised.

Chapter 2. Literature Review

This chapter presents a literature review of different NDT&E techniques used in defect detection and characterization of structures. A general review of electromagnetic NDT&E techniques most commonly used in the detection and characterization of defects are presented. Next is the review of EC system, focusing specifically on probe configurations, signal conditioning and, excitation modes for defect characterization. Challenges in this area are identified and the chapter concludes with proposed steps to mitigate some of the identified challenges.

2.1 Review of Electromagnetic NDT&E Techniques for Defect Detection

NDT&E has been widely used in inspecting materials for defect detection and evaluation. Advancements in sensing technology and signal processing have expanded the application of NDT&E. Many areas including material science and other areas where sophisticated systems are designed make NDT&E applications unlimited. For non-contact inspection, eddy current techniques have been topics of research for the past decade and have found widespread applications in conductive materials inspection [11]. In general, all Electromagnetic (EM) methods used in NDT&E are based on the principle of Maxwell's equations which cover a broad range of the EM spectrum whether static or direct current (DC). EM NDT&E involves sending some form of EM energy through the test material and analysing the response to understand its interaction with the test material. From the interaction, anomalies such as defects, residual stress and microstructural variations can be detected and characterized. It also relates anomalies to location, quantity, size, shape and orientation. These defects need to be removed or repaired, to avoid loss of structural integrity of material or components.

This chapter provides an in-depth literature review of research on sensing systems used for NDT&E applications. The review is grouped under eddy current pulse thermography (ECPT), ground-penetrating radar (GPR) magnetic Field Leakage (MFL) electromagnetic acoustic transducer (EMAT), Alternating current field measurement (ACFM) and Eddy Current. As the centre of this research is in EC system, different types of EC probe configurations, signal conditioning and Excitation modes are reviewed. The review of each technique, presents its advantages and disadvantages and their area of applications. The challenges in application of EC in high lift-off inspection including degradation in sensitivity and SNR, probe linearity characteristics and excitation modes are identified. As no one inspection method is suitable for detecting and evaluating all kinds of defects, in some cases, two or more techniques are fused

or integrated together to form a robust sensing system. Therefore, a detailed comparison between each of the NDT techniques is provided to evaluate their appropriateness to crack detection and characterization. A summary of the different techniques is shown in figure 2.1.

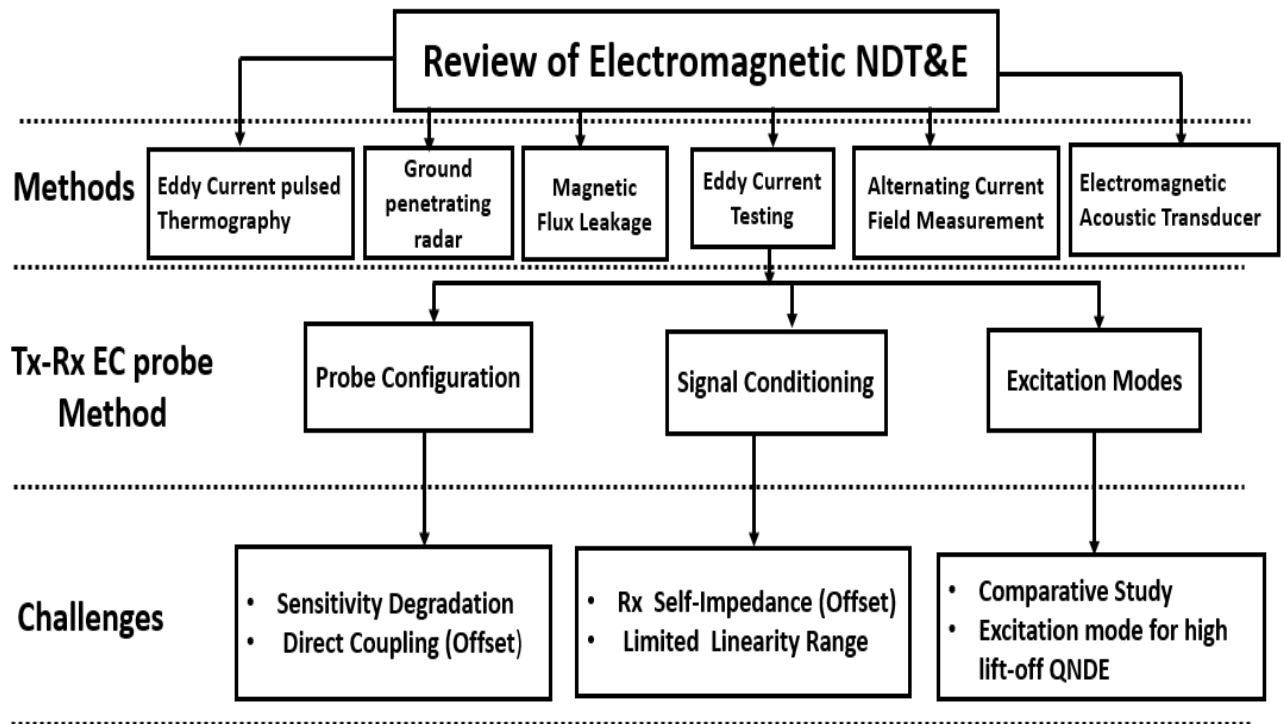


Figure 2.1 Summary of the different electromagnetic NDT&E techniques

2.2. Eddy Current Pulse Thermography (ECPT)

Eddy current thermography involves the usage of a high-frequency electromagnetic wave at a higher current on the structure which is to be inspected for a time typically about 20ms to 1 s [14]. Induced eddy current is focused on the discontinuity of the material under inspection which leads to increase or decrease in the eddy current density within the area. The areas with higher eddy current density will encounter higher level of heating and thus identify any presence of damages from the infrared (IR) image sequences during the phase of the heating and cooling [15].

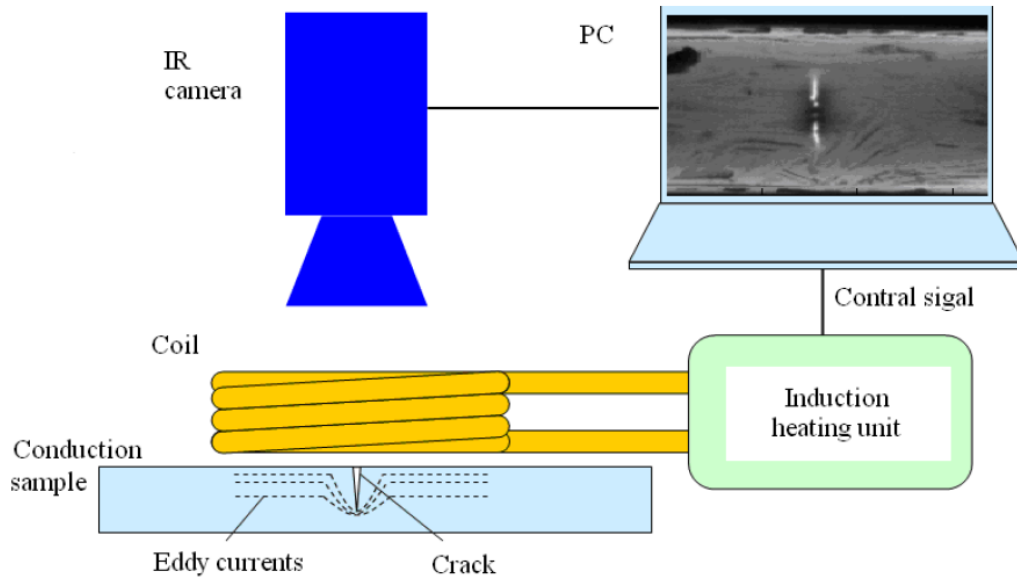


Figure 2.2 Basic configurations of pulse eddy current thermography system

The system shown in figure 2.2 [16] includes an induction heating system that is used to induce eddy currents on the sample under inspection where the heat produced on the surface of the sample is captured by the IR camera which is then displayed on the PC. In [17], corrosion blisters in mild steel under insulation were investigated using ECPT and hidden cracks on corroded metal surfaces were detected. Different damages were used to study the eddy current density distribution and heat conduction. In [18], ECPT was used to detect surface cracks on the tungsten carbide matrix of polycrystalline diamond compact bit. To improve the sensitivity of the detection, principal components analysis (PCA) was used for processing of the IR image sequences. Also recently, surface condition on free form surfaces have been measured and evaluated using thermal pattern reconstruction of ECPT [19]. Also early-stage fatigue crack has been detected by Peng et al [20]. They used different feature extraction techniques to quantify the fatigue crack using ECPT. The proposed method showed an enhancement in the crack detection capability for railway.

However, one major drawback of the ECPT system is that it can only detect defect in conductive materials. And also the equipment required for carrying out the experimental work is quite bulky in addition to the high current requirement.

2.3 Ground Penetrating Radar (GPR)

GPR operates by emitting electromagnetic waves that penetrate the ground then returns to the surface. The velocities of the waves depend on the dielectric property of the subsurface [21]. The time of flight of the electromagnetic waves as they leave the transmitting antenna into media and reflect back to the receiving antenna at the surface is a function of the depth of the

reflection point and the electric properties of the media. Thus, interpretation of this reflected energy may yield information on subsurface structural variation and condition of the media. Significant work needs to be done to process GPR data and signals [3]. Conventional GPR systems use two or three antennas with different frequencies to interrogate the structure of the surrounding soil, the interface between the soil and pipes, and the structure of the pipe [21]. GPR can potentially identify leaks in buried oil pipeline either by detecting underground voids created by the leaking oil or by detecting anomalies in the depth of the pipe as the radar propagation velocity changes due to soil saturation with leaking water [3]. The GPR technique has been used to detect and quantify the degree of internal leaking of hydroxides in asbestos-cement pipes [22]. Also a GPR system has been designed for under water oil pipeline detection device for China Petroleum [23]. Another type of GPR called Ultra-Wide Band (UWB) GPR is a short-range radar that remotely senses and images objects that are buried in-ground. It radiates a sequence of short electromagnetic pulses in the Nano and Pico-seconds ranges into the ground and measures the reflected signals that arise due to the difference in the electrical properties between the ground and the buried object [24]. For the inspection of buried pipes, it is desirable to operate in the picoseconds range because pulse widths in this region are equal to or less than the wall thickness of most non-ferrous buried pipes. The pulse repetition frequency (PRF) ranges from thousands to several billion pulses per second [21]. Numerical experiments demonstrated the potential of this technique for pipe condition assessment. The use of ultra-short duration pulses makes it possible to obtain relatively high-resolution results. Numerical simulation for P-Scan has been carried out and a pre-commercial prototype is still under development and not available yet. An improvement of UWB GPR was reported in [25] using Continuous Wave Stepped Frequency. To improve measurement sensitivity of continuous wave GPR [26] proposed a canceller based on microwave interferometer. Results showed improved sensitivity compared to the standard continuous wave radar measurements.

The challenge of signal dispersion which limits the penetration of GPR signals was mitigated by [27] using a compact slot antennas. And its high resolution and good penetrating capability was validated with experiments. In [28] GPR imaging was improved by removing internal antenna effects and antenna medium interactions based on full-wave inversion technique. An easier interpretation in terms of medium structures was achieved.

The merit of GPR inspection is that it offers a location technique which is independent of the pipeline material and therefore has a direct application to the problem of locating non-metallic pipes. Despite its merits a number of drawbacks limit the use of GPR. Although the maximum depth of utility detection is typically about 3 m in favourable conditions, the pulses lose strength

very quickly in conductive materials, such as clay and saturated soils, thereby affecting the depth of penetration and unless employed intelligently. A typical GPR system is shown in figure 2.3. It consists of a transmitter, a receiver, a processor and a display.

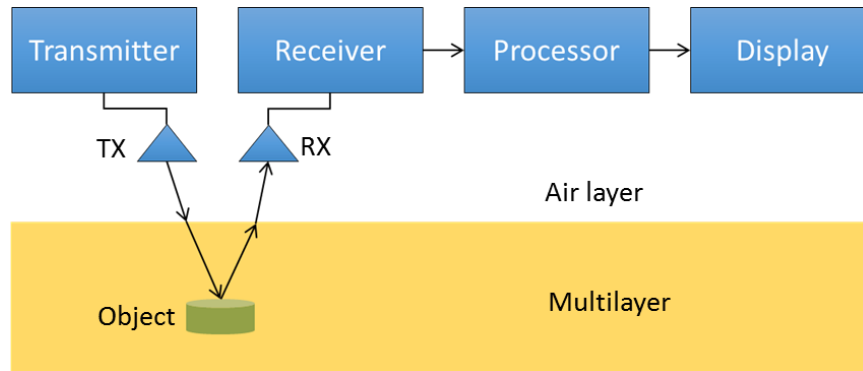


Figure 2.3 Block diagram of generic GPR system

2. 4 Magnetic Field Leakage

MFL operates by sending a strong magnetic field to a ferromagnetic material, any geometrical discontinuity in the test object will cause the field to leak out of the object into the air. The flux leakage can be monitored by a magnetic field sensor and used to estimate the dimensions of the defect. A typical schematic of an MFL imaging system is shown in figure 2.4. It can be clearly seen that because of the effects of induction on magnetic lines at the discontinuity, the surface leakage flux occurs at high magnetization level. When a defect is present, the MFL sensors picks up the defect information before passing the information for processing [29]. This technique is commonly used because of its simplicity [30]. The MFL has advantage of volumetric corrosion detection but its sensitivity is limited and cannot detect small axial defects. However, an improved MFL measurements called Tri-axial MFL was able to detect and size defects located at the internal pipe wall but with no significant improvement for those at external surface [31]. The specific challenge is that eddy current distribution in conductors induced by relative movement between the MFL probe and a test object alters the profile and intensity of magnetic field leakage and distort the profile of MFL signals. This brings about difficulty in the signal interpretation and description of defects [32]. Performance of MFL also depends on the magnetization of the specimen. Magnetization should be adequate to saturate the material to force the magnetic field to leave the material in presence of a metal loss. Different techniques have been deployed towards improvement of MFL. Some of the approaches include pulse magnetic field leakage (PMFL), rotation and dual axial MFL [33].

MFL which is popular in the inspection of ferrous material like steel pipes is suitable for uniform wall loss and pitting corrosion[34]. However, cracks at the same line as the magnetic fields are not easily detected due to non-orthogonality of the crack to the excitation flux [35]. MFL is not suitable for insulated pipes because of their limitation to small lift-off [36]. But more work is required to improve the sensitivity by optimisation of MFL sensors. Despite the advancement and attempt to improve the MFL through excitation signals and sensor optimization there are other challenges. Such challenges are the volume and weight of the sensor, the requirement of the magnetic circuitry and the sample type such as the thick insulated pipes and weld zones which require high lift-off inspection.

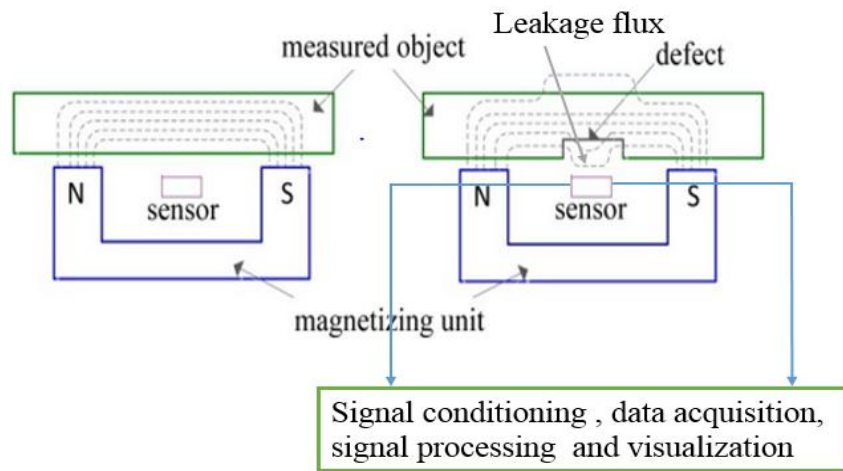


Figure 2.4 A typical MFL inspection technique for pipeline inspection

2.5 Alternating current field measurement (ACFM)

ACFM inspection techniques work by measuring the alternating magnetic field disturbances. The disturbances increase when the induced electric current is disturbed by the presence of a surface-breaking crack [37]. Through an electric current induction system, the ACFM probe introduces an electric current locally in the test sample and measures the associated electromagnetic fields close to the surface [38]. The presence of a defect disturbs the associated fields and the information is graphically presented to the system operator. This technique can detect surface or near surface-breaking cracks both in ferromagnetic and non-ferromagnetic structures [39]. As can be seen in Figure 2.5, two fields components are measured i.e. B_z and B_x which gives the information about the length and depth respectively. Although, ACFM was developed for underwater weld inspection, it has been used in other applications like inspection of pipes, vessels, rail tracks and stress measurement [40]. ACFM also finds applications in detection and sizing of surface-breaking cracks in metallic components and welds[41]. The main advantage of ACFM is that it requires no electrical contact with the workpiece and

maintains steady field at a given lift-off [42] . This gives it uniform and robust lift-off characteristics. However the performance is limited by speed of operation [9] and the difficulty in correct rankings for all the detected defects [43].

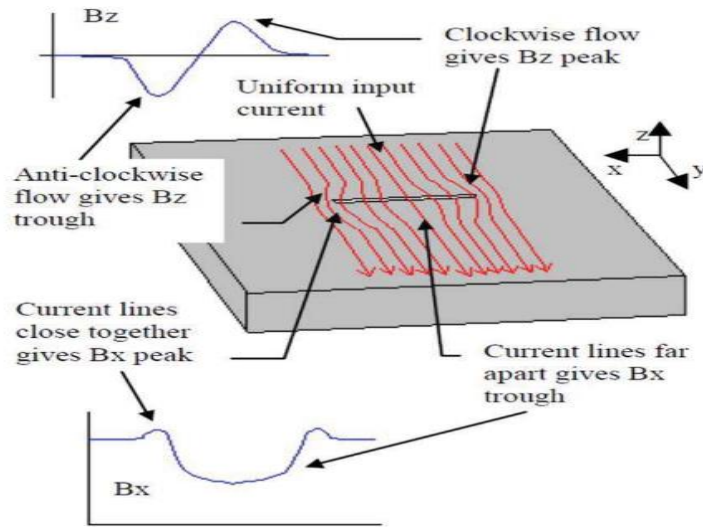


Figure 2.5 Current and magnetic field distribution in ACFM

2.6 Electromagnetic Acoustic Transducers (EMAT)

EMAT is beneficial because it does not require any coupling liquid and are able to generate a wide range of waves-modes. Other merits of EMAT include non-contact operation, ability to generate shear waves, Rayleigh waves lamb waves and its capability to operate at high temperature environment [44] EMAT normally consists of a magnet (either a permanent or an electromagnet) and a wire located above the metal surface and in the magnetic field. A wire carrying an alternating current and held close to a conductor will induce eddy-currents in the conductor. Eddy-currents under the magnetic field is subject to stress. Under the alternating stress, the stress wave is prone to be generated in the metals. When the frequency is over 20 kHz, it will be considered as the ultrasonic wave. On the other hand, the reflected ultrasonic wave will affect the wave vibration, acoustic vibrations inside the conductor move to the surface under the receive wire. In the presence of a magnetic field, this motion produces eddy current in the conductor surface that produces a magnetic field that extends across the air gap to induce a current in the near-by wire connected to a preamplifier. TransCanada, a Canadian company in collaboration with PII company started an attempt to apply the EMAT technology in pipeline inspection equipment [45]. The problem of ultrasonic coupling of EMAT is a challenge which techniques such as laser induced ultrasonic and air coupling have been introduced to mitigate[46] . However, the principle of EMAT which generates ultrasonic in a conducting material using eddy currents as shown in figure 2.6 makes it a potential technique for detecting flaws in metallic materials. A piezoelectric transducer (PZT) is an alternative to EMAT but

requires fluids like air or oil for ultrasonic coupling [47]. Hence, the main advantages of EMAT shown in figure 2.6 over PZT include the fact that couplant and surface preparation is not required during measurement. Thus, the cost of surface preparation during measurement and irregularities that arise from the use of couplant are eliminated.

However, the high voltage of hundreds of volts at which EMATs are commonly operated is a challenge. In addition to the bulky electronics, EMAT is not used in an explosive environment. Also the transduction efficiency is lower than that of PZT. The signal an EMAT generates is not as strong as the ones obtained by other means and hence, extra care is required in the signal processing and power conditioning circuits when using this approach [48]. In some applications, a combination of EMAT and PZT is used to improve these limitations as reported in [49]. However, the major drawbacks of EMAT's is their relatively poor signal-to-noise ratio (SNR), and the inherently low efficiency of the transduction effect. The low efficiency makes any small lift-off variation to cause a notable drop in the power transferred to the metallic sample.

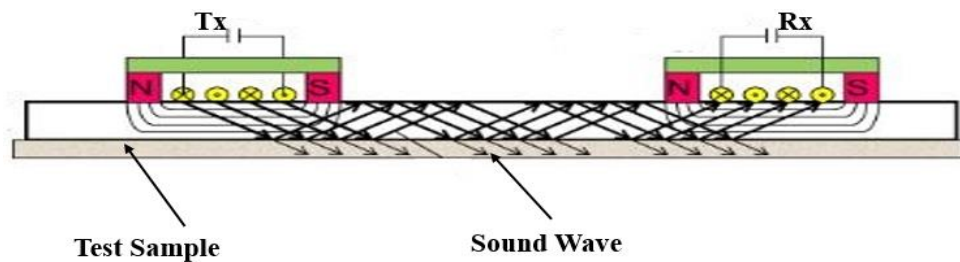


Figure 2.6 EMAT Testing

2.7 Synopsis of NDT&E Techniques for Defect Detection and Characterisation

So far, the review focused on NDT&E methods for defects detection and characterization. A comparison of the techniques in terms of its overview along with the merits and demerits of the techniques are provided in table 2.1. These methods can be performed on metals, plastics, ceramics, composites, cement, and coatings in order to identify cracks, internal voids, surface cavities, delamination, incomplete defective welds and any type of flaw which would lead to premature failure. There are a lot of requirements that need to be considered before selecting any NDT&E techniques discussed thus far. These requirements include application scenario, accessibility, portability, the material under inspection, inspection size and its area, type of defects and costs. Some of the techniques perform well under certain conditions and are better used for certain applications than the others giving qualitative and quantitative information. However, they may only be effective for limited materials, while other techniques may perform better when other factors are taken into consideration. Eventually, the overall target of

inspection is to provide an accurate and time-efficient technique that can advance the repair/replacement in a cost-effective manner.

Table 2.1 Commonly used NDT techniques.

Technique	Capabilities	Limitation	Working range (lift-off)
ECPT	Surface flaws	Material must be good conductor of heat and electricity, bulky equipment and high current requirement	5-10 mm [50]
GPR	Location of non-metallic material	Lose strength very quickly in conductive materials (low depth of penetration)	2-10 cm [51]
EMAT	Beneficial for its non couplant requirement	Presence of low coupling efficiency, sensitive to small lift-off changes	0 – 6 mm [52]
MFL	Magnetic field and low cost	High false alarm rate, not feasible for non-metallic detection	0 – 10 mm [53]
ACFM	Insensitivity to lift-off variations and detection of surface and welds cracks	Low speed of operation	0-30 mm [9]

2.8 Review Eddy current (EC) testing

EC testing technique has been used for detection of coating thickness and plate thickness of conducting plates [54] . Later, its variant, pulse eddy current technique was used for inspection of pipes, vessels, aircraft structures and numerous other applications. Some of the established applications of the EC technique are listed below

- a. Detection of surface and subsurface flaws [55, 56]
- b. Estimation of wall thickness loss due to corrosion [57, 58]
- c. Sorting of materials based on electrical conductivity [59, 60]
- d. Detection of flaws due to corrosion in multilayer structures [61-63]

e. Measurement of coating thickness [64-66]

f. Measurement of stress in materials [67, 68]

Most of the EC applications involve detection of wall thickness loss, coating thickness, surface as well near-surface cracks. As can be seen from the literature, several researchers attempted development of several techniques based on Probe configurations, signal conditioning and excitation methods for the targeted applications. Therefore, next sections concentrate on review of EC under probe configuration, signal conditioning and excitation modes.

2.8.1 EC Probe configurations

Probe is an essential part of EC system and probe configuration affects EC system performance including penetration depth, spatial resolution and sensitivity [69]. In this context, there is a definite need to design and optimize the EC probe for high lift-off inspection. This can be accomplished either by experimentation or by numerical modelling. Various researchers have reported different types of probe configurations and for detection of localized flaws and cracks in metallic structures. In the literature, the most widely used probe configurations are double-d, rectangular, cup-core, ferrite core and air core. In [70] an EC probe based on a rectangular Tx coil and an axial parallel Rx coil were proposed and investigated for the purpose of metal loss evaluation and imaging. Experimental results illustrated that metal loss depth can be estimated effectively by the peak amplitude of the EC A-scan response. In [71] a transmit-receive (Tx-Rx) type probe configuration was proposed. The sensor was configured in such a way that the offset due to the direct field coupling from the Tx coil to the Rx coil is removed and provides additional advantage of reduced common-mode noise. The configured probe has been able to detect the presence of metallic samples and the variations of glucose in human blood. In [72] a design optimization of eddy current probe was carried out for detection of deep sub-surface defects in thick stainless steel plates. Results indicated that the cup-core probe shows better sensitivity for detection of deep sub-surface defects. A linear relationship between phase angle and defect depth below the surface has been observed, apart from discrimination of sub-surface and surface defects. To reduce the effects of surface characteristics of materials and background noise of a magnetic excitation field, a new sensor with magnetic shielding was developed for eddy-current (EC) testing in [73]. Results show that the magnetic shielding core can increase the EC density in the test material. External magnetic field shielding can effectively improve the defect detection sensitivity. In [74] a rectangular excitation probe was proposed for identification of edge of the flaws in a thick aluminium sample and for imaging of flaws. When the probe is scanned along the length of the flaws, EC signal parameter showed a positive and negative maximum corresponding to the movement of the coil entering and

leaving edge of the flaw, which is used to generate imaging of the flaws and therefore, evaluation of flaw length. In [75] the electromagnetic field and mutual inductance between two rectangular eddy current coils in transmit-receive mode has been calculated analytically for different sizes and for arbitrary misalignment above a planar conductor. A relation between coil gap and lift-off for Tx-Rx rectangular probe was developed based on mutual inductance. It was shown that the mutual inductance of a Tx-Rx probe above a planar test sample can be optimised based on coil gap and lift-off. A validated analytical flat plate model of eddy current response to gap was used to examine the effect of Tx-Rx coil gap on lift-off in [76]. Results obtained showed that both coil gap and lift-off have a significant effect on the response which was used for in-reactor measurements. A typical rectangular coil Tx-Rx probe above a conductor is shown in figure 2.7.

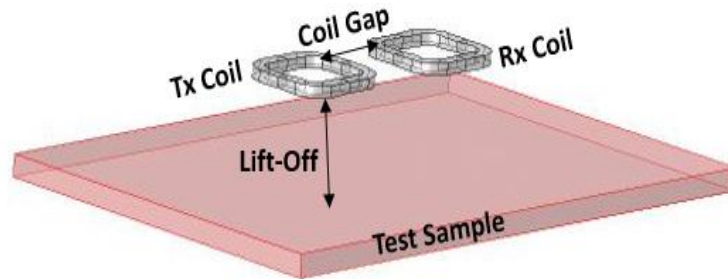


Figure 2.7 coplanar rectangular coil Tx-Rx probe above a conductor

It is observed that by using a rectangular Tx-Rx EC probe configuration, coil gap and lift-off can be optimised and effective lift-off can be increased for thick insulated, buried materials or weld area inspection [75]. Inspired by the mutual inductance dependence on coil gap and lift-off of coplanar rectangular Tx-Rx types of probes, systematic studies can be focused to develop and optimize Tx-Rx type EC probes for high lift-off inspection.

2.8.2 EC Signal conditioning

Signal conditioning plays an important role in pulse eddy current testing. The signal conditioning circuit should be able to convert the impedance change of the PEC probe coils as may be brought about by defects into electrical signals. It should also be able to detect and amplify the feeble response signals influenced by noise. Several researchers have reported the development of signal conditioning circuit for detection of flaws, metal loss and thickness measurement of plates. In [77] a commercially available transient eddy-current system (TRECSCAN) were used for estimation of metal loss due to corrosion in multilayer structures.

They used an air-core coil excited with current-controlled bipolar square-wave pulses and measured the normal component of the magnetic field on the axis of the coil using a Hall sensor. After suitable amplification and filtering, the signals were digitized using a 16-bit ADC card. The instrument was able to measure the wall thickness variation up to 3.6 mm with a lift-off 2.5 mm. In [78] a signal conditioning method was proposed which yielded a signal feature that behaves as a function of thickness. The signal feature has a desirable characteristic of low lift-off influence. It was used for measuring ferromagnetic material thickness at 12mm lift-off. For a Tx-Rx probe with variable mutual couplings, sensitivity decreases significantly as lift-off increases. And the percentage of the Rx self-impedance in the output signal of the circuit becomes very much higher than the coil impedance change that bears the required information [79, 80]. Typically, the variation in coil impedance falls in the range of 5% to 10% of the self-impedance [81]. The inherent self-impedance of the Rx coil is also one of the sources of nonlinearity of the Rx output signal [82]. Due to the self-impedance of the Rx coil, in addition to multi-parameter influence, the required information is sometimes masked in noise. This limits the subsequent amplification of the output signal, which is the key in applications with a low SNR [71]. The impedance change can be converted into electrical signals such as current, voltage, frequency, and phase using different circuits. Such circuits include an amplitude modulation circuit [83], a frequency modulation circuit, and bridge circuits [84, 85]. Frequency output sensors can also be used as signal conditioning through oscillation for instance as in [82, 86, 87]. However, to balance the influence of coil self-impedance and improve sensitivity, bridge circuits are normally used as part of signal conditioning to convert the impedance change into electrical signal [88]. Ac bridge circuit is operated in a balanced mode to null the offset due to self-impedance of Rx coil and to detect the impedance change as the balance is disturbed. Conventional ac bridges including Maxwell's inductance bridge, are used for this purpose but limited by nonlinearity and measurement errors [89]. Hence, there is a strong need to develop a sensitive signal conditioning circuit to mitigate the challenge of the conventional ac bridges.

2.8.3 EC excitation modes

Detection and quantification of defects using eddy current techniques depend on excitation signals especially at high lift-off. EC excitations that can provide as much information as possible about the presence and geometry of defects for specific application are needed. Signals with a wide spectral content capable of penetrating different layers of test sample are taking over single frequency sinusoidal excitation. In literature, different excitations were reported for detection and quantification of flaws based on applications. It was reported in [90] that a single frequency EC performance depends much on the frequency and lift-off chosen for the

investigation. They suggested that this factor should be appropriately selected depending on the sample and application. Lower frequencies are selected for subsurface defect in many cases with reduced SNR and higher frequencies for surface defect [91]. [92] and [93] suggested the range of 100 Hz–10 MHz as standard inspection frequencies of EC. However [94] characterized metallic coatings and detected surface defects at high frequency of 25 MHz. The high frequency applied for the inspection of small discontinuities occurred in the near-surface. The major weakness of single frequency EC is the limitation to a single penetration depth [95].

To mitigate the challenge of single depth penetration, multi-frequency testing has been applied to ensure multi-layer penetration and to cancel out undesired signals in order to improve the SNR. Multi-frequency testing has been used to improve SNR up to 1100% over traditional single-frequency excitation [96]. [97] presented an integrated multi-frequency injection with dimensional spatial domain called pyramid fusion method. The SNR improved due to reduction in noise sources which demonstrated the potential of signal enhancement via fusion method or raster scanning. Variations in temperature, material geometrical and probe lift-off [97] have been eliminated using a differential sensor with multi-frequency excitation. By acquiring data at a given frequency and by subtracting a second data collected at another frequency the influence of a bracket was reduced in estimation of a tube thickness. Multi-frequency testing has been also accomplished by combining the results obtained at different frequencies in the spatial domain [11]. [98] improved the characterization of the crack depth based on the use of a suitable multi-frequency excitation signals and of digital signal processing algorithms. Although Multi-frequency testing acquires data with more information, the response contains only depth information corresponding to the skin depth of the selected excitation frequencies. This low spectral resolution may provide low resolution on the depth of cracks [99].

Another excitation mode of EC is sweep-frequency eddy current system which can operate up to 50MHz. Sweep-frequency EC has been developed for electromagnetic non-destructive characterization of residual stresses [100]. Sweep-frequency eddy current has also been used to estimate the thicknesses of the top and lower layers of multi-layered structures [101]. The main advantage of this method is that the signal contains sinusoidal tones of the same amplitude, penetrating different depths with constant signal strength [102]. In addition, a better frequency resolution can be achieved. However, the sweep-frequency technique can be difficult and time-consuming as it relates to data acquisition and analysis. To reduce energy and time of inspection, comparable quantitative information can be obtained in a single excitation cycle using a single broadband pulse eddy current (PEC) excitation to probe the test specimen instead of excitation with different single-frequency signals.

The earliest study of PEC for crack detection in layered structures with installed fasteners was conducted by Harrison[103]. Giguere et al [104] also studied the detection of cracks beneath rivet heads using the transient EC techniques. It has been used in the inspection of aircraft, oil/gas pipelines, nuclear steam pipes, and high-speed rails. [105] demonstrated the advantage of PEC to detect holes and notches beneath rivet heads in subsurface layers of stratified samples without the need for reference samples through the varied pulse width feature. [106] employed the finite element modelling with the PEC in detecting deep-lying cracks originating near boltholes in the inner layers of aircraft lap joints with ferrous fasteners present. Differential signals from both the top layer and the bottom layer cracks in different orientations and with different probe displacements were analysed using a modified principal components analysis (PCA) to differentiate cracks from empty spaces. The advantage of PEC as it relates to crack depth estimation is that its response contains depth information in the entire spectrum of frequency-domain. Quantitative information can hence be obtained in a single excitation cycle and with high-frequency resolution. However, the signal energy is not evenly distributed among the frequency components. Low-frequency components possess higher strength while high-frequency components possess lower strength. Hence different frequency components penetrate different depth with unequal signal strengths. Furthermore, time-domain features like PEC features are prone to noise [107]. Different EC excitation modes including single frequency, sweep frequency, multi-frequency and pulse are shown in figure 2.8

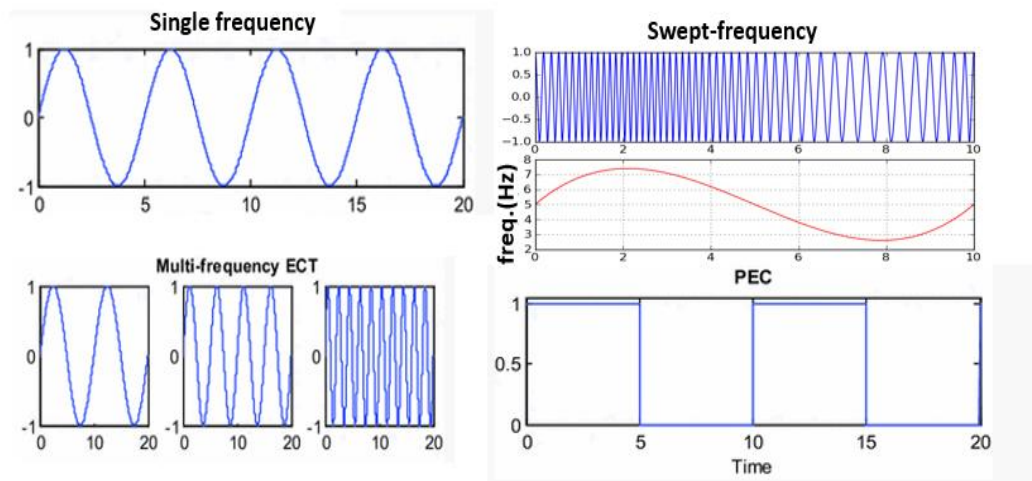


Figure 2.8 Different excitation modes of EC testing

As can be seen from the review each type of the excitation signals presents merits and demerits that prevent the selection of an absolute best excitation signal. The excitation signals can be represented in the time domain as PEC and frequency domain as multi-frequency or sweep-frequency. A time-domain signal like PEC possesses a wide range of a continuum of frequency

components. Hence, it contains more information compared to a single-frequency excitation. However, time-domain features are prone to noise [107] and demand calibration data to achieve defect quantification [108]. Frequency-domain signals on the other hand give room for the selection of the exciting tones that form the composite signal and are simpler in terms of signal processing. But are more demanding in physical realization. Another factor to consider is the frequency range of a magnetic coil which also poses a challenge in choice of excitation signals. Hence it is required to carry out a comparative study of the performance of the excitation modes at high lift-off.

2.9 Background of EC Testing System

2.9.1 Principle of eddy current testing

ECT system is one of the electromagnetic techniques used to inspect and evaluate conductive materials. ECT system uses signals within the range group of 100Hz–10MHz [109]. EC technique shown in figure 2.9 lies on the principle of Faraday’s law where current is induced in a conductive material in changing magnetic field. A primary magnetic coil is excited with a time changing voltage or current signal to generate magnetic field. The flow of eddy current in a conductive material within this field develops a secondary field which opposes the main field inducing the eddy current [110]. This opposition changes the impedance in the primary magnetic coil. As defects in the material distorts the eddy current distribution, there is a corresponding effect in the main field which is analysed to determine and characterize the defect [111].

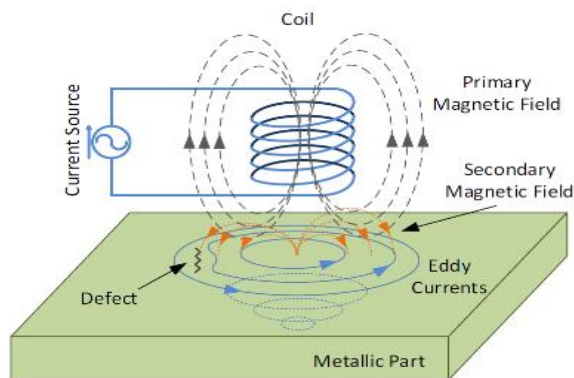
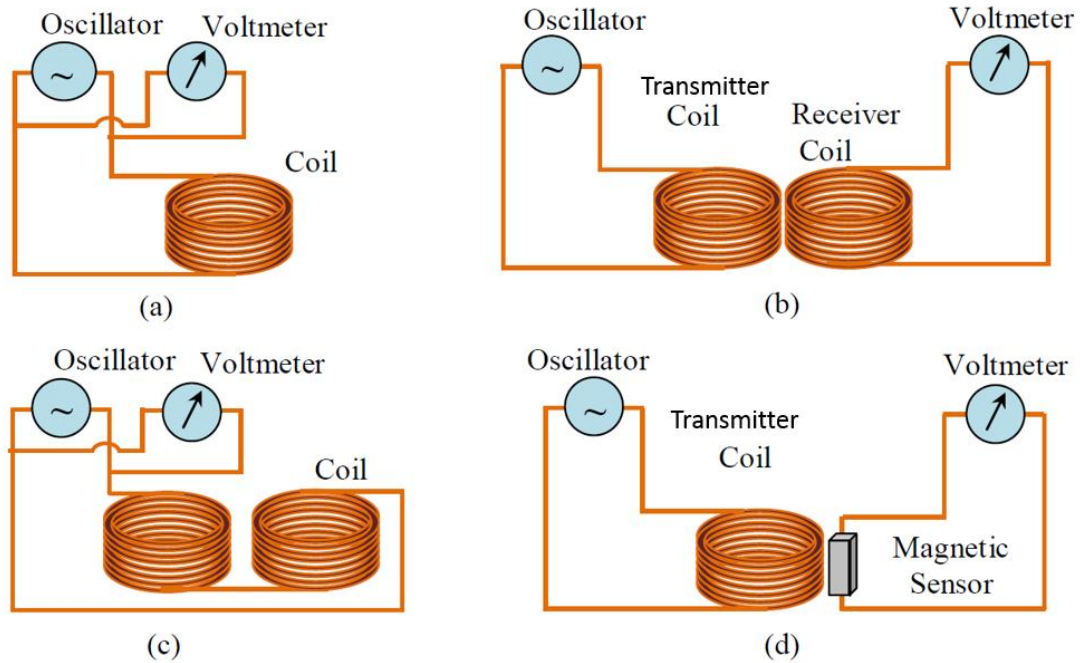


Figure 2.9 Principle of eddy current

The primary and secondary magnetic fields are detected by measuring the electromotive force (emf) across a receiver coil or by using a magnetic sensor such as Hall element. The demand for various applications results in the existence of different types of EC probe configurations in the literature for the excitation source and detection sensor which are chosen based on the application [112, 113]. In many applications, inductive coils are used for both excitation and

sensing. Hence, the eddy current probes are categorized according to their configuration and mode of operation. The probe configuration is closely related to the way the probe covers the testing area. The probe operation mode is grouped into reflection, differential, absolute and hybrid modes, whereas some of the standard configurations include the outside diameter probes, inside diameter (bobbin) probes, bolt hole probes and surface probes [114]. Figure 2.10 shows the commonly used EC probe configurations for testing materials. Figure 2.10 (a) shows a probe having only excitation coil, also called as absolute probe, in which the change in the impedance of the excitation coil itself is used for detection of flaws [115]. The absolute impedance variation measured by this type of PEC probe configuration reveals much information about the tested sample, but the resistor-inductor (RL) circuit used to measure the response signal is too sensitive to temperature variations [11]. Figure 2.10 (b) Tx-Rx type of probe having separate Tx and Rx coils. In this case, the induced voltage in the Rx coil is used for detection of flaws. Figure 2.10 (c) shows a probe connected in a differential mode. The differential-Mode probe consists of two connected coils that are placed on adjacent parts of the test sample. One of the sensing coils is wound to oppose the magnetic field of other coil to reduce the offset voltage caused by the primary magnetic field. The output of the probe is zero when there is no defect on the sample. The non-zero output results when the defect alters the voltage offset of the Rx coil [116]. The transmitter coil of this type of probe is commonly connected to an RL circuit while the Rx coil output signal may be applied directly to the input of differential amplifier. Figure 2.10 (d) shows probe with the solid-state magnetic sensor to measure the direct magnetic field [117]. In this configuration, the coil is used for excitation while the magnetic sensor is used to receive the response signal.



(a) Absolute (b) Tx-Rx with pickup coil (c) differential (d) Tx-Rx with magnetic sensor.

Figure 2.10 Different types of EC probes

2.9.2 Principle of Pulse eddy current testing

Pulse eddy current testing is a new emerging technology in electromagnetic non-destructive testing (NDT). The main advantage is that, compared to single frequency EC, PEC inherently has a broadband of frequencies. This is advantageous for any eddy-current-based NDT&E techniques due to the frequency-dependant skin effect. PEC can potentially be applied in shorter time for inspection of different depths as PEC applies a wideband of frequencies in a single pulse. This reduces the measurement time depending on the sample characteristics [118]. PEC works on the principle of Faraday's law of electromagnetic induction. As discussed in Section 2.9.1, the resultant magnetic fields can be measured as the induced emf across an Rx coil or by using a magnetic sensor. Eddy currents are induced in the test structure during the excitation pulse rise time and fall time. The induction process does not happen at other times of the excitation pulse [119]. Therefore, the PEC technique is also called a transient eddy current technique. The rate of change of rising time of the current pulse is crucial as it determines the frequency components contained in it. The higher the rate of change, the more the high-frequency components, as a result the lower the depth of penetration of eddy currents and surface diagnostic information extraction and vice versa[120]. As the pulse diffuses into the specimen, it is broadened by dispersion and also influenced by flaws in the object. The flaws closer to the surface affect the eddy current response pulse earlier than those at deeper locations.

Hence, there is a sweep of frequencies in a single pulse excitation in PEC technique [121] . A long-duration pulse consists of a continuum of frequencies, and is especially rich in low-frequency components, which are essential for subsurface flaw detection [122]. PEC technology has the potential to identify a large number of parameters, such as detection of flaws in thick materials, non-contact measurements at higher probe lift-off [123] . In most of the PEC applications, coils are used for both magnetic field excitation and pickup. The amount of induced voltage in the pickup coil depends on the rate of change of magnetic flux (ϕ) and number of turns in the coil (N) shown in (2.1).

$$V = -N \frac{d\phi}{dt} \quad (2.1)$$

The decrease in excitation signal frequency decreases the rate of change of the magnetic flux and consequently, decreases the induced voltage in the Rx coil. Thus, at very low frequencies the response signal magnitude decreases to a level where signal-to-noise ratio (SNR) is too low for reliable detection. To improve the excitation coil sensitivity, increasing the flux through the excitation coil is a possibility. The magnetic flux (Φ) passing through a circular coil is given by (2.2)

$$\phi = B\pi r^2 \quad (2.2)$$

Where B is the magnetic flux density, r is the radius of the excitation coil. Higher detection sensitivity can be achieved theoretically by building a larger excitation coil as it would allow a higher depth of penetration of the magnetic fields. On the other hand, if the same large size Rx coil is used for detection purpose, resolution and sensitivity would be compromised [124] . Use of a smaller diameter excitation coil would provide better sensitivity and resolution but it would limit the eddy current penetration in the test object. Therefore, better solution would be to use a large diameter excitation coil and a small diameter Rx coil to achieve good resolution and better detection sensitivity. These types of probes are less sensitive to low-frequency electromagnetic fields and magnetic field sensors such as Hall, GMR, AMR and SQUID [125, 126] are currently used in place of the Rx coil to mitigate this weakness. The magnetic sensors have advantages over the induction coils. Firstly, they measure the direct magnetic field itself instead of the rate of change of the magnetic field measured by the pickup coils and possess constant sensitivity down to zero frequency. Secondly, the size of the magnetic sensor is generally much smaller than excitation and receiver coils, and this contributes to higher spatial resolution. However, the magnetic sensor frequency response is limited by bandwidth. This allows the measurement of magnetic field intensity directly from DC to an upper frequency limit which depends on the chosen sensor, but it is in general in excess of 100 kHz [127]. They can be used as detectors in pulse eddy current probes. Although magnetic sensors are used

because of their advantages, some strength of coil-based Tx-Rx makes it outstanding for PEC applications. Advantages of Tx-Rx PEC probe including improved signal to noise ratio in the presence of changing lift-off, directional properties, capability of optimization of individual coils of the probe made it a good choice of PEC probe [128].

2.9.3. PEC governing equations

The governing partial differential equation of the pulse eddy current technique can be derived from the following Maxwell's equations of electromagnetics:

$$\nabla \times E = -\frac{\partial B}{\partial t} \quad (2.3)$$

$$\nabla \times B = \mu J \quad (2.4)$$

Where E is electric field intensity, B is magnetic flux density, μ is the magnetic permeability of the material and J is current density. The magnetic flux density is expressed in terms of the vector potential A as given below.

$$B = \nabla \times A \quad (2.5)$$

Differentiating both sides of (2.5) with respect to time

$$\frac{\partial B}{\partial t} = \frac{\partial(\nabla \times A)}{\partial t} \quad (2.6)$$

From (3.3)

$$\nabla \times E = -\frac{\partial(\nabla \times A)}{\partial t} \quad (2.7)$$

or

$$\nabla \times \left(E + \frac{\partial A}{\partial t} \right) = 0 \quad (2.8)$$

As the sum of the two vector quantities in parenthesis of (2.8) is curl free, it can be written as the gradient of a scalar. Hence (2.8) is written as

$$E + \frac{\partial A}{\partial t} = -\nabla V \quad (2.9)$$

$$E = -\nabla V - \frac{\partial A}{\partial t} \quad (2.10)$$

Where V is the electric scalar potential. The current density in equation (2.4) is a combination of applied excitation current density (\mathbf{J}_s) and the induced eddy current density (\mathbf{J}_e) in the material i.e. $\mathbf{J}=\mathbf{J}_s+\mathbf{J}_e$ where $\mathbf{J}_e=\sigma\mathbf{E}$, and σ is electrical conductivity of the material. Substituting this equation in (3.5) results in

$$\nabla x(\nabla x A) = -\sigma \mu \frac{\partial B}{\partial t} - \sigma \mu \nabla V + \mu J_s \quad (2.11)$$

Applying Coulomb gauge condition (A) equation (3.11) reduces

$$\nabla^2 A = \sigma \mu \frac{\partial B}{\partial t} - \sigma \mu \nabla V - \mu J_s \quad (2.12)$$

Equation (3.12) is the governing partial differential equation to be solved for understanding the PEC technique. An analytical solution to equation (2.12) is difficult due to multiple interfaces and boundaries, especially in the presence of flaws. Finite element method based numerical techniques are extensively used due to their versatility as well as computational efficiency and they are attractive for solving equation (2.12)

2.9.4 PEC signal interpretation

In PEC testing a reference PEC signal is first obtained by scanning the PEC probe over a flaw-free region on test object or by keeping the probe in air. A PEC difference signal is obtained by subtracting the reference signal from that of a flaw signal. Thus, the PEC response appears zero until the probe is moved to a position where the geometry of the structure is changed or due to the presence of a flaw in the test object. Time-domain parameters viz. Peak amplitude (V_p), Time-to-peak (T_p) and Time-to-zero crossing (T_{zc}) are obtained from the PEC difference signal and used for detection of a flaw and for determining its location [129, 130]. Typical PEC signal and time domain parameters are shown in figure 2.11. These parameters are also useful to classify flaws:

- a. The peak amplitude depends on the location and size of a flaw, in other words it is proportional to the amount of metal loss in the test object [70, 131].
- b. Eddy currents are attenuated and dispersed as they travel deeper into the test material. Hence, the time-to-peak is related to the position of a flaw in the test object[132, 133].

c. In theory, there are several numbers of time-to-zero crossing points that are possible. However, only a few are visible in the measurements. Change in the thickness of cladding alters the zero crossing point. T_{zc} is also related to the location of a flaw [134-136].

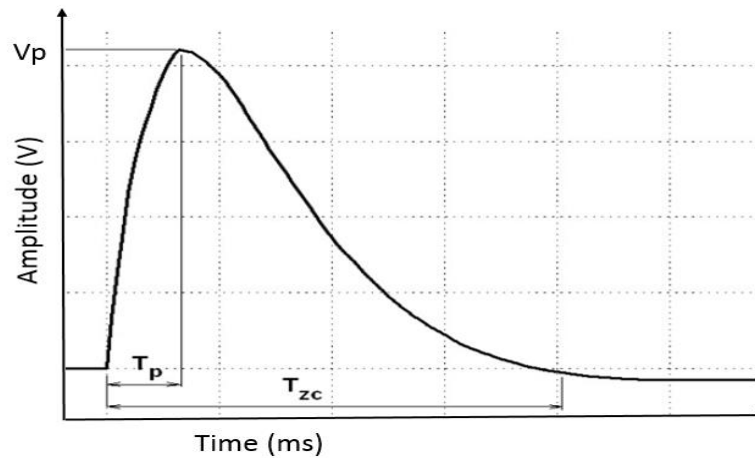


Figure 2.11 PEC time-domain parameters

2.9.5 PEC technique features

Some of the attractive features of PEC technique[137] are:

- a. Pulse has a continuum of frequency components hence, multiple depth of investigation at once,
- b. Detection of flaws at deeper depth with improved sensitivity,
- c. Non-contact scanning large areas of a complex structure without the need for couplant,
- d. Less heating effects because of its low average power and pulsing

2.9.6 PEC Feature extraction

Different factors influence PEC signals, such as electrical conductivity, lift-off, and magnetic permeability, the thickness of the sample and inhomogeneity of the material. The other challenges faced by researchers in obtaining useful information from the signals are the noise and the low-level signals in some cases. Consequently, the right signal processing, signal analysis, feature extraction and classification model must be implemented in order to attain the desired parameters, such as coating thickness, size and position of defects, and to isolate them from the undesired parameters, such as lift-off variation. Several techniques have been investigated for defect and crack detection and characterization of conductive materials

[3, 138-141]. Normally, a reference signal which is measured from a defect-free reference sample is used in most of PEC techniques. A difference signal is obtained by subtracting the reference signal from the test one as shown in figure 2.12 [125].

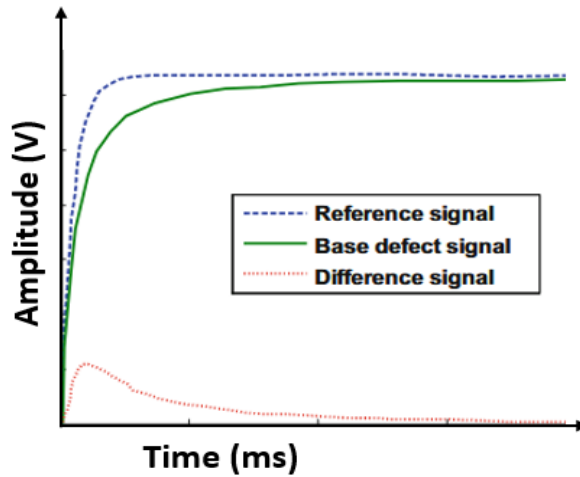


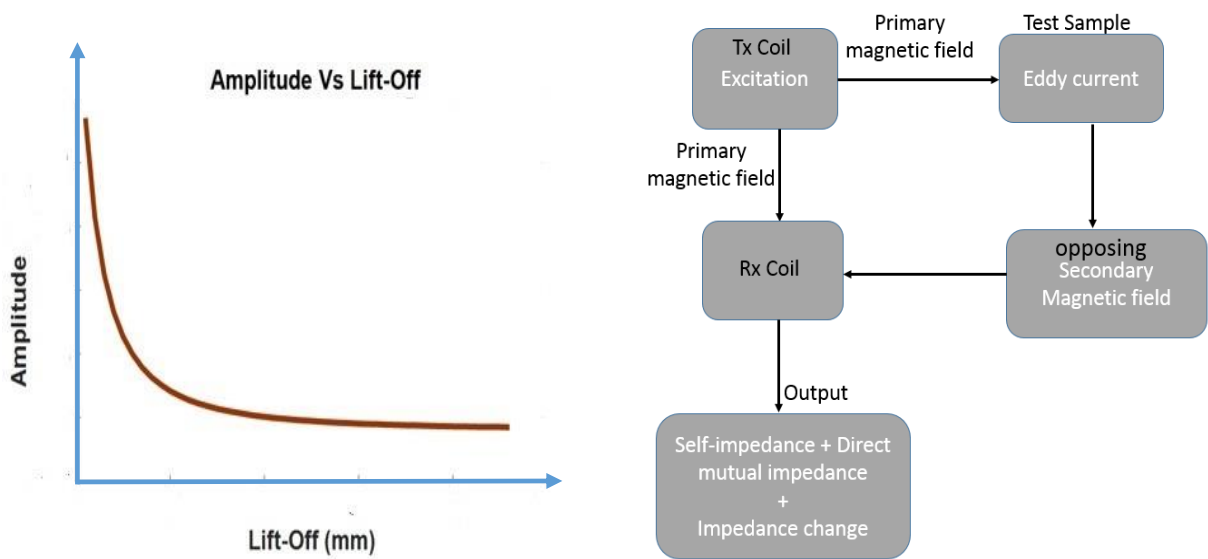
Figure 2.12 Typical PEC signals obtained by using a Hall-device-based probe

Different types of signal are collected depending on whether a coil or a magnetic sensor is used. A coil will capture the time-derivative of the magnetic field while a magnetic sensor will sense the field itself. PEC time responses can be normalized in order to reduce the effects of lift-off variation and varying magnetic permeability prior to the calculation time-domain features[142]. In some cases, like the principal component analysis technique, researchers try to optimize the discrimination within the range of the parameters, which require them to employ data dimensionality reduction techniques. The obtained features can be subsequently fed into a classifier in order to either classify or quantify the defects.

2.10 Inspection of Conductive Material at High Lift-off with Tx-Rx EC Probe

Inspecting structures at high lift-off brings the challenges of signal attenuation and signal degradation. As a result, the information regarding the defective structure might be lost making inspecting materials under high lift-off a difficult task. ECT is strongly affected by the amount of lift-off which can be defined as the separation distance between the probe surface and the conducting material surface. This distance changes the mutual inductance of the circuits as the lift-off increases[143]. The amplitude of the eddy current induced electromagnetic force (emf) at the Rx coil decreases significantly, which can result in the misinterpretation of the signals. At a significant lift-off, no detectable emf will be induced in the Rx coil due to the test sample [144, 145]. To understand the scenario of high lift-off inspection, consider figure 2.13a in which a single-coil probe distance from the tangent surface of the test sample is defined by the lift-off. The effect of high lift-off is particularly prominent when using sinusoidal excitations, which lose sensitivity beyond 5mm lift-off. Figure 2.13b shows the principle of Tx-Rx based PEC probe. As can be seen, the interaction of the Tx coil, Rx coil and the sample generates a response detected by the Rx coil as superposition of direct mutual impedance of Tx coil and Rx coil, self-

impedance of Rx coil and Rx coil impedance change. In Tx-Rx probe configuration the Rx coil detects the response (output) signal which is expected to bear the information about the test sample. However the major challenge of Tx-Rx probe is that the response signal detected by the Rx coil is the impedance change of the Rx coil superimposed on direct mutual impedance of Tx and Rx coils, and self-impedance of the Rx coil. Among these components of the response signal, it is only the signal due to impedance change that bears the required information about the test sample. Whereas, the other components form the offset which in this case is equivalent to noise. The impedance change becomes very minimal compared to other components at high lift-off.



(a) Decay of EC signal with lift-off for one coil probe (b) Principle of Tx-Rx probe EC testing

Figure 2.13 Lift-off influence and principle of Tx-Rx probe eddy current testing

Although it is not required to have a zero lift-off, it is imperative to try and maintain a consistent lift-off, since the variation in the coupling between probe and test piece will significantly affect the received signal. There are methods to mitigate the problem of lift-off effects in the eddy currents testing. For instance, [146] researched dual excitation frequencies and coil design to minimize the lift-off effect. Research about processing the data was also conducted to minimize the lift-off effect. [147] proposed the use of wavelets to remove the eddy current probe wobble noise from the steam generator's tubes. Reduction in the lift-off effect was also attempted by optimizing the coil design and sensor array [148]. Tian et al [149] had researched the reduction of lift-off effects via normalization techniques. The technique can be applied to the

measurement of metal thickness beneath the non-conductive coatings and to the measurement of cracks, where the output is highly sensitive to the lift-off effect.

2.11 Challenges and Problems Identification

The literature survey carried out in this chapter, highlights the most common types of NDT&E techniques for defect detection. However, most of the methods are restricted in terms of high lift-off detection and quantification of defects due to the thick insulation layer, buried material, weld zones or high-temperature structures. The Solution to these problems will require using bulky, expensive equipment with much higher power or removal of the insulation layer which will include operation shutdown or using inspection holes to send signals along the structure. EC technique is a good option for the reviewed techniques. However, from the review of the EC testing system, the main challenges posed by defect detection and quantification at high lift-off are numerous. Some of these challenges are high lift-off, complex or curved surface and natural defects such as stress corrosion crack, and rolling contact fatigue. This research is focused on solving the problem of high lift-off using mutual inductance based Tx-Rx EC probe system. Hence, some challenges and problems of Tx-Rx based probe that must be mitigated for its high lift-off application are as follows:

- I. For the mutual inductance based EC probe testing system, defect detection sensitivity depends on mutual inductance of the probe and test sample and are vital for detection and quantification of defects. This can be achieved by using appropriate EC probe configuration. However, the sensitivity of the probe to defect detection degrades as lift-off increases. This is a big challenge in the detection of defects especially when the geometry of cracks as position, length, width and depth is required to be estimated.
- II. For the Tx-Rx EC probe, the direct mutual inductance of Tx coil and Rx coil which is a major source of noise is a challenge. Thus, the direct mutual inductance is required to be eliminated to improve detection sensitivity.
- III. For the Tx-Rx EC probe, the defect detection sensitivity depend on both direct and indirect coupling through a test sample which invariably depends on coil gap and lift-off. Thus, coil gap and lift-off needs to be optimised for improved sensitivity at high lift-off.
- IV. The mutual impedance changes which bear the required information about the test sample are required to be converted to electrical signals like current, voltage by the signal conditioning circuit. In Tx-Rx probe the self-impedance of the Rx coil is enormous compared to impedance change and dominates the output signal. These

decreases the SNR and limits the amplification of output signal especially at high lift-off. Hence signal conditioning circuit should be designed to eliminate the large Rx coil self-impedance and improve SNR.

- V. In high lift-off eddy current testing system performance depends on excitation modes. This is because each type of the excitation signals presents merits and demerits that prevent the selection of an absolute best excitation signal.
- VI. Hence different excitation modes including single-frequency multi-frequency, sweep-frequency and pulse excitation modes should be comparatively studied for high lift-off QNDE (quantitative non-destructive evaluation).

To tackle some of the aforementioned problems identified from the literature, the study focused on the design and investigation of mutual inductance based Tx-Rx EC system for high lift-off inspection. The demand for high lift-off inspection emanates from thick insulation, buried structure, weld zones and high-temperature structures.

Chapter 3. Prototype Tx-Rx PEC system and Research methodology

In this chapter, the theory related to Tx-Rx pulse eddy current testing system and the research methodology is presented. Following the challenges and problems highlighted in chapter 2, a method is developed to solve some of the challenges identified based on these challenges namely, degrading sensitivity at high lift-off, SNR and linearity improvement, and comparative study of excitation modes used in eddy current testing for QNDE. Tx-Rx probe configuration and its defect detection process are presented. The chapter concludes by presenting the research methodology with the method to investigate and mitigate the challenges outlined.

3.1 Defect Detection and quantification

Materials and engineering structures are often subjected to fatigue stress, cyclic loading and environmental influences. This results in defects/cracks initiated usually at the microscopic level on the structure's surface and degenerates to bigger sizes [150]. The defects cause material discontinuities and also reduced the local stiffness of the structure. As a preventive measure, early detection is needed in order to avoid possible failures [151]. The defect detection is the process of detecting the defect on the structures using any of the NDT&E processing techniques. Through visual inspection and surveying tools, the surface condition defects can be analysed and evaluated [152]. However, for a fast and reliable surface defect analysis, automatic crack detections methods are needed instead of the slower subjective traditional human inspection methods. This result in an increased interest in various techniques of NDT&E. For EC technique, the major challenges are the degrading sensitivity as lift-off increases and the low SNR condition as a result of noise. But because of the simplicity in the processing of eddy current signal, several probe configuration, signal conditioning and excitation methods has been proposed. The basic architecture of defect detection and characterization approach is shown in figure 3. 1. It is divided into two categories namely, the data acquisition section and the data processing section. The data acquisition section comprises excitation unit (signal generator) used to generate interrogating signal and the EC probe. The EC probe is connected to a movable platform called the x-y scanner. The scanning can either be A-, B- or C-scan and once the probe position is determined, the control unit then sends a trigger signal to the signal generator and an excitation signal is sent to the sample under test (SUT) EC probe. The captured raw data is then sent to the data processing unit which is first pre-processed and then passed to the processing unit .Once the data acquisition and storage are completed, the data is processed, and the features are extracted through quantitative and qualitative analysis. QNDE methods were used for defect detection and quantification.

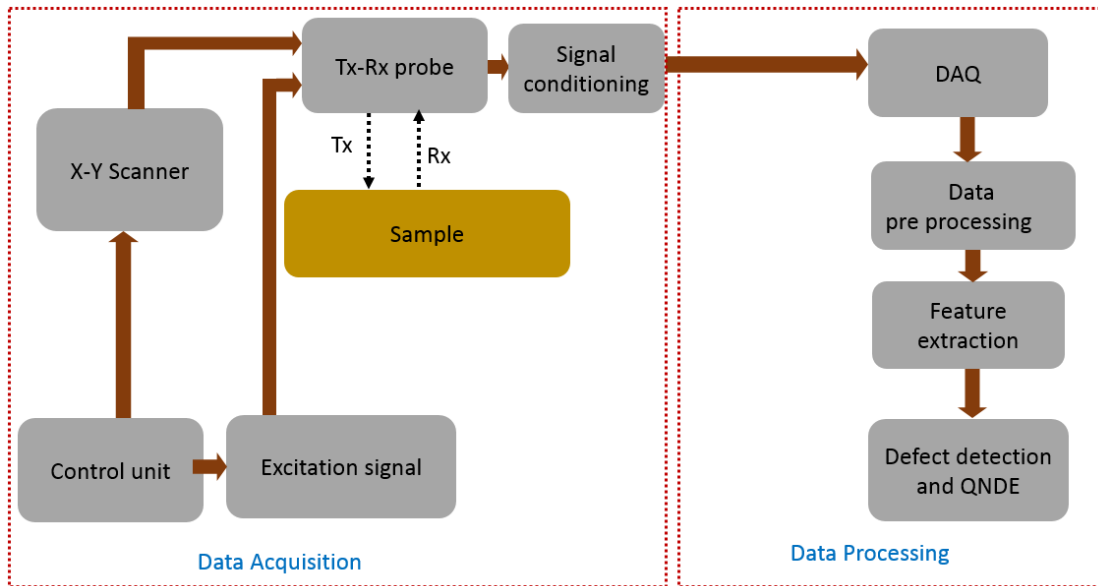


Figure 3.1 The basic architecture of EC defect detection and quantification

3.2 Tx-Rx probe configuration

The Tx-Rx probe consists of two coils that separately function as the transmitter and the receiver. Tx-Rx probes are advantageous over single-coil probes due to their sensitivity, SNR and resistance to thermal drift, as well as the fact that Tx and Rx coils can be separately designed for a specific application. Furthermore, Tx-Rx probe approach allows greater flexibility in PEC probe design. Size, shape, orientation, and separation of Tx-Rx coils (coil gap) are all parameters which can be optimized. In Tx-Rx probe configurations, a time changing current excites the Tx coil, which induces eddy currents in the test sample. The resulting magnetic field induces a voltage in a separate Rx coil [153]. The presence of eddy currents in a metallic sample is indicated by a change in the secondary coil voltage, which causes a change in mutual impedance between the Tx coil and the Rx coil, as well as the self-impedance of an individual coil. Since the coil positions determine the detection area, Tx-Rx coils are very direction sensitive. The direction of the Tx-Rx unit can be a huge advantage when looking for very specific directional flaws. The major challenge of Tx-Rx probe is that the Tx coil will interfere with the Rx coil creating crosstalk (direct mutual coupling)[75, 154]. As shown in figure 3.2, the direct coupling forms an offset in the Rx circuit and degrades the SNR. This is because only the coupling of Tx and Rx coil through the sample bears the information about the test sample.

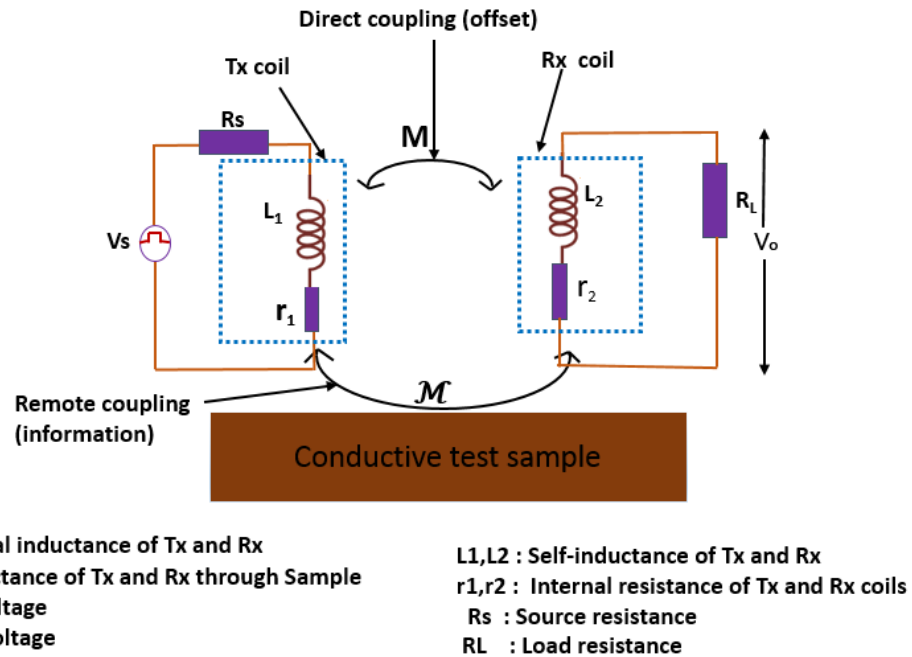
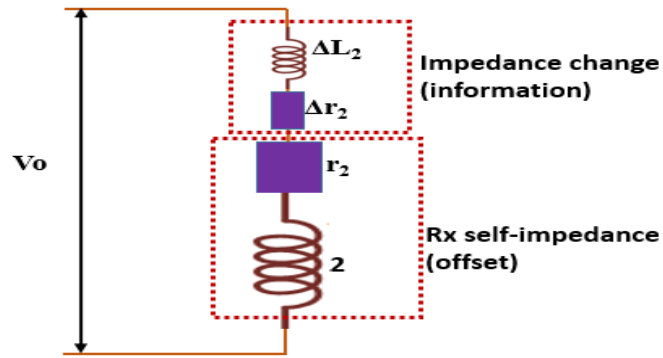


Figure 3.2 Direct and indirect coupling of Tx-Rx probe

3.3 Signal Conditioning of Tx-Rx PEC System

The main function of the signal conditioning circuit of Tx-Rx probe is to extract the required information signal while rejecting noise. In Tx-Rx probe the main sources of noise are the direct coupling offset of Tx and Rx coil as stated in section 3.3. In addition, the self-impedance of the Rx coil also forms an offset (noise) which dominates the output signal as shown in figure 3.3. Ac bridges are generally used as part of the signal conditioning circuit to remove the Rx coil self-impedance. This is to make output signal proportional to impedance change only. After which, the output can be fed to instrumentation amplifier where gain can be suitably adjusted. The output of the instrumentation amplifier is subsequently given to an analog-to-digital converter (ADC). Digitized output is then fed to the computer (PC) via data acquisition system (DAS). And low pass filtering reduces the effect of interference and noise on the output [89]. However, a setback of Ac bridge circuits is limited linear range input-output characteristic [155, 156] and the measurement error due to stray capacitance between bridge nodal point and ground, and stray inductance of the inductive coils [157]



L_2 : Self-inductance of Rx coil
 r_2 : Internal resistance of Rx coil
 V_o : Output voltage
 Δr_2 : change in Rx coil resistance
 ΔL_2 : change in Rx coil inductance

Figure 3.3 Impedance change and self-impedance of the Rx coil

3.4 Excitation Modes of EC Testing System

Different excitation modes are used for EC probes based on applications. EC excitations that can provide as much information as possible about the presence and geometry of defects for a specific application are needed [12]. Signals with a wide spectral content capable of penetrating different layers of test sample are taking over single frequency sinusoidal excitation. However, each type of excitation modes presents merits and demerits that prevent the selection of an absolute best excitation mode [158]. Hence, performance of excitation modes needs to be evaluated for specific applications.

3.5 Prototype Tx-Rx PEC System Configuration and Setup

Following excitations, Tx-Rx probe configuration and signal conditioning, the overall system setup are designed and validated through simulation and experimental validation. The equipment setup for the EC based NDT&E system is shown in figure 3.4. The system comprises a personal computer with a Windows operating system and MATLAB software, CNC scanner. The computer is connected at one end to the x-y scanner through its controller via a parallel port interface (LPT). Whereas the signal conditioning circuit connected to the PC through an interface bus (GPIB). The control software for the x-y scanner movement and the data acquisition from the signal conditioning circuit are written in MATLAB script using the manufacturer's guidelines provided in the library.

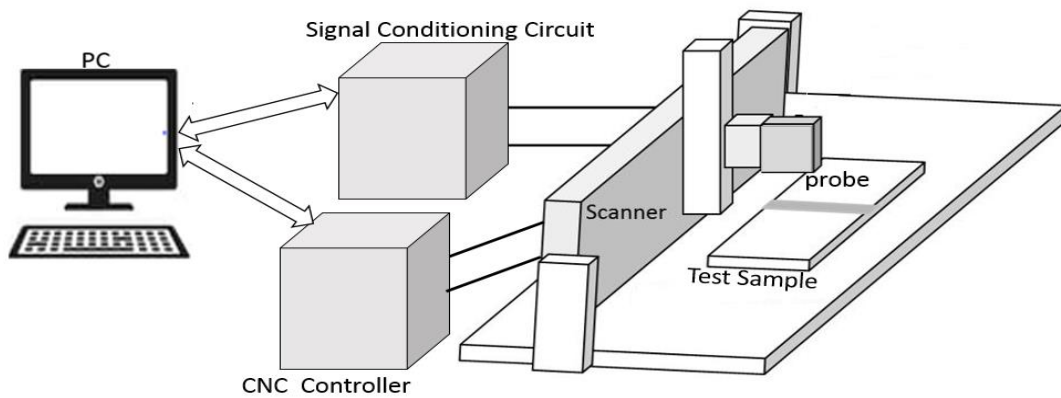


Figure 3.4 PEC-based system setup

3.6 Research Methodology

The research carried out in this thesis involves the design, modelling, simulation and experimental investigation of mutual inductance based pulse eddy current system that can be used for high lift-off inspection. The major challenges the study tries to address are the problem of degrading sensitivity at high lift-off, dealing with the direct mutual inductance of Tx coil and Rx coil, dominance of output signal by the self-impedance of Rx coil, and lastly a comparative study of excitation signals of Tx-Rx PEC probe for defect detection and quantification. Therefore, major attention was given to the improvement of sensitivity of Tx-Rx PEC probe to detect, identify, quantify and evaluate defects resulting from high lift-off inspection. A detail of how the aforementioned challenges were addressed are shown in each of the subsequent Chapters that follow. The proposed research method flow diagram is shown in figure 3.5.

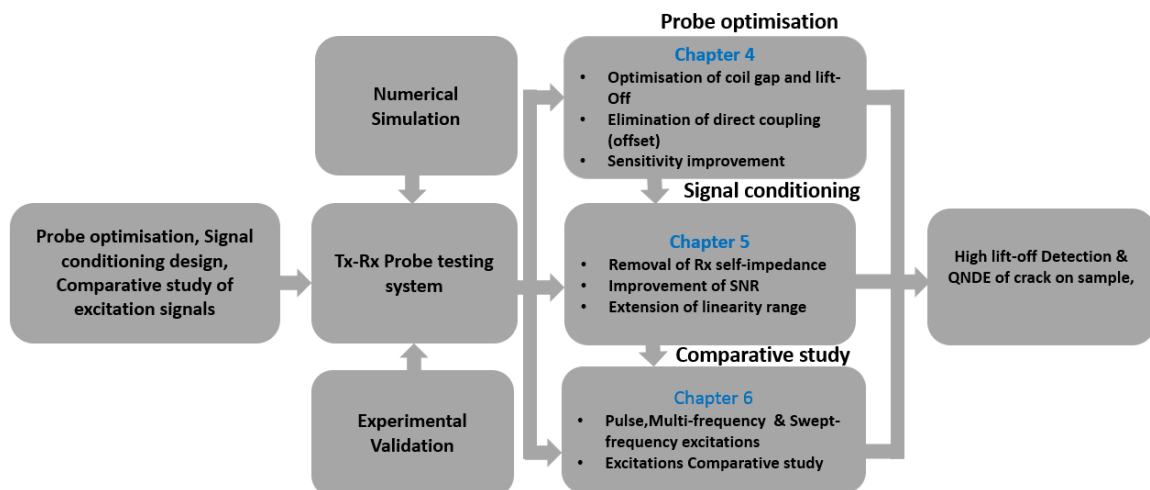


Figure 3.5 Research diagram for PEC inspection system

3.6.1 Study 1: Optimization of Mutual Inductance Based on Tx-Rx Probe

This study proposed an optimisation design of Tx-Rx PEC probe to minimize direct mutual impedance offset of Tx and Rx coil to enhance sensitivity at high lift-off. This is because to obtain high sensitivity, a robust system that can eliminate the offset content of the signal is needed. Through simulation and experimental study using aluminium plate, the capability of the Tx-Rx probe in high lift-off testing was demonstrated. The manmade crack in the aluminium plate was detected at a lift-off higher than the limited 5.0 mm of one coil probe (a big challenge in EC testing system). The performance indicator of amplitude change was used to evaluate the sensitivity of the Tx-Rx probe at the target lift-off of about 30 mm. The results show that the proposed Tx-Rx approach produces better-sensitivity compared to one coil probe and the approach enables the probe to determine the optimal lift-off for any fixed coil gap. The higher the coil gap the higher the optimal lift-off though with reduced sensitivity. Therefore, sensitivity can be traded for higher optimal lift-off depending on the required sensitivity and lift-off.

3.6.2 Study 2: Investigation of Signal Conditioning of Tx-Rx Probe

The second study presents the elimination of offset caused by the self-impedance of Rx coil on the output signal. This is because at high lift-off, the impedance change brought about by defect becomes a small fraction of the output signal while the self-impedance of the Rx coil dominates the output signal. The effect of this dominance is that the SNR of the output signal is highly reduced. To eliminate the offset, Maxwell inductance bridge is modified based on opamp configuration using two Rx coils connected in such a way that their self-impedances cancels out. Results obtained shows improved SNR, linearity range and reduced measurement error. The modified circuit was evaluated by crack detection of aluminium sample at a lift-off 30mm and compared with the conventional Maxwell's inductance bridge in terms of SNR and linearity range. The modified circuit performed better in SNR and linearity range. However, it is easier to map crack geometry with Maxwell's inductance bridge than the modified circuit.

3.6.3 Study 3: Comparative Study of Excitation Modes of Tx-Rx Probe

The third study is on the comparative study of different excitation modes performance for high lift-off inspection. Single frequency, multi-frequency, sweep-frequency and pulse excitations were reviewed for high lift-off detection and quantification of crack depth. After which PEC and SFEC were selected for experimental study. Experiments for estimation of crack depth at high lift-off are carried out for both excitation modes. Pulse features show more linear relationship with depth cracks. Whereas, SFEC is better for cracks detection at high lift-off. Hence feature selection and combination is to be investigated further for high lift-off defect detection and QNDE

3.7 Chapter summary

This chapter looked at the theoretical background of Tx-Rx PEC probe system that can be used for NDT&E inspection. The prototype Tx-Rx system geometry, probe configuration, excitation modes and signal condition circuits are discussed. Thereafter, the Tx-Rx system setup is presented looking at the different approaches that can be used for defect detection and quantification at high lift-off. The research methodology showing different studies that will be carried out are outlined.

The remaining chapters of the thesis will demonstrate the simulation and experimental studies carried out based on the studies outlined in the research methodology. The effective techniques developed to address the challenges identified are presented and analysed. Critical analysis and the discussion of the results are provided.

Chapter 4. Optimization of Tx-Rx probe for high lift-off inspection

In chapter 3, the theory related to the Tx-Rx PEC system and the research methodology was discussed. In this chapter, the study looks at the design and optimisation of mutual inductance based Tx-Rx PEC probe system for high lift-off inspection. A Tx-Rx PEC model is developed for the high lift-off inspection. An optimisation of coil gap and lift-off is proposed to enhance the sensitivity at high lift-off. Numerical simulations are used to investigate the influence of coil gap and lift-off on detection sensitivity using amplitude change as a performance indicator. This indicator is also used to investigate the effect of coil gap and lift-off on crack detection sensitivity for a different number of coil gap/ lift-off combinations. Experimental validation of the approach is carried out for detection of artificial crack on an aluminium sample. The results show that the proposed approach produces a better sensitivity to crack for an optimal lift-off at a given coil gap. The results also show that for every coil gap, there is an optimal lift-off at which highest sensitivity is achieved. The chapter concludes that the techniques can be applied on inspection of buried objects, structures with thick insulation and weld areas where high lift-off inspection is unavoidable.

4.1 High Lift-off Inspection with Tx-Rx Eddy current Probe

Despite the aforementioned developments in EC probe as reviewed in Chapter 3, the sensitivity of the EC probe decreases significantly with increase in lift-off. This is because, in the case of EC probe, as lift-off increases, the eddy current field from the test sample reaching the probe weakens resulting in sensitivity degradation [159]. Research to improve sensitivity based on lift-off has been reported in [160]. However, normalization technique as used in the reports definitely degrades sensitivity. The approach in [161] used the peak value of the difference signal to reduce lift-off but with a complicated measurement. A transformer approach was used through electrical equivalent circuit analysis in [159] to mitigate the effect of lift-off in thickness measurement. However, only one coil probe is considered but exploiting the potentials of Tx-Rx probe will better enhance sensitivity. Many difficult or impossible inspection problems with a single-coil impedance EC type probes could be overcome with Tx-Rx probes containing separate excitation and receive coils [112]. The Tx-Rx probe approach allows greater flexibility in EC probe design. Size, shape, orientation and separation of Tx-Rx coils (coil gap) are some parameters of Tx-Rx probe which could be optimized. The excitation coil(s) induces eddy currents and the receive coil(s) detects the resultant magnetic field distortion caused by defects. However, the direct coupling of Tx and Rx coils (offset) is the major challenges which limits its applications as highlighted in section 3.3.

The mutual inductance of a driver-pick-up EC probe above a conductor is a superposition of mutual inductances emanating from magnetic couplings of driver-pick-up coils and test sample. One is between driver coil and pick-up coil in free space and another is due to the coupling through the conductor. One contributed by the conductor gives the information about the defect in the test sample not the one between driver-pick-up coils in space. In fact, the mutual inductance between coils in free space causes excitation signal to induce an intrinsic offset voltage in the pick-up coil. Because analysis and quantification of defects mainly depend on eddy current signal, the induced intrinsic offset voltage in the pick-up coil is equivalent to noise [75].

Different techniques have been used to reduce the direct coupling between coils in order to improve sensitivity. Coil winding is used to induce phase shift between two excitation coils to cancel out the offsets in the pick-up coil in [71]. However this technique is limited by nonlinearity errors and sensor drift emanating from magnetic hysteresis. In [162], ferrite sheet was used to reduce the direct coupling between driver and pick-up coils with improved sensitivity. The limitation of this technique lies in the fact that some part of eddy current generated field would also be diverted by the ferrite thereby reducing the information signal strength [163]. Another limitation of the driver-pick-up probe is low defect detection especially at low frequency. Although magnetic field sensors [126] are currently used in place of the pickup coils to mitigate this weakness, some strength of driver-pick-up probe makes it outstanding for EC applications. Enhanced capabilities for driver-pick-up EC probe, including improved SNR in the presence of changing lift-off, directional properties, capability of optimization of individual coils of the probe made it a good choice for EC probe [128].

Although much research to mitigate lift-off effect and direct coupling of the driver-pick-up probe has been done, there is still a challenge to inspect at high lift-off. In [75] the electromagnetic field and mutual inductance between two rectangular EC coils in driver-pick-up mode have been calculated analytically for different sizes and for arbitrary misalignment above a planar conductor. A relation between coil gap and lift-off for Tx-Rx rectangular probe was developed based on mutual inductance. It can be observed that the mutual inductance of a driver-pick-up probe above a planar test sample can be optimized based on coil gap and lift-off. Furthermore, a validated analytical flat plate model of EC response to gap was used to examine the effect of driver-pick-up coil gap on lift-off in [164]. Result showed that both coil gap and lift-off have a significant effect on the response.

Inspired by the work of [75] and [164], a coplanar rectangular driver-pick-up probe is systematically optimised based on coil gap and lift-off influence on sensitivity for high lift-off

inspection. Rectangular coils are considered because of its merits when compared to other coil shapes. The merits of rectangular coils include high sensitivity to surface scratches and subsurface defects, directional property, capability of creating uniform eddy current flow. In addition, it can be configured to operate in differential and driver-pick-up mode [165].

4.2 Design and Optimisation of Mutual Inductance based Tx-Rx Probe

The design and optimisation of mutual inductance based probe are based on mutual coupling of driver coil, pickup coil and test sample. The direct and indirect mutual inductances depend on coil gap and lift-off. Eddy currents in the sample generate a secondary magnetic field which is captured by the pickup coil as a voltage signal plus the voltage generated by pickup coil due direct coupling. Hence, the pickup coil detects the vector sum of both exciting and EC fields as voltage. The EC field opposes the Tx coil field and the Rx coil subtracts the EC field from the Tx coil field and produces a voltage corresponding to the resultant field. When the probe is very close to the test sample (low lift-off) high EC density is induced in the sample. The high eddy current increases the secondary field and lowers the resultant field of the pickup coil which results in lower pickup coil voltage. As the lift-off increases, low EC density is induced. The low EC density decreases the secondary field and increases the resultant field of the pickup coil which results in high pickup coil voltage.

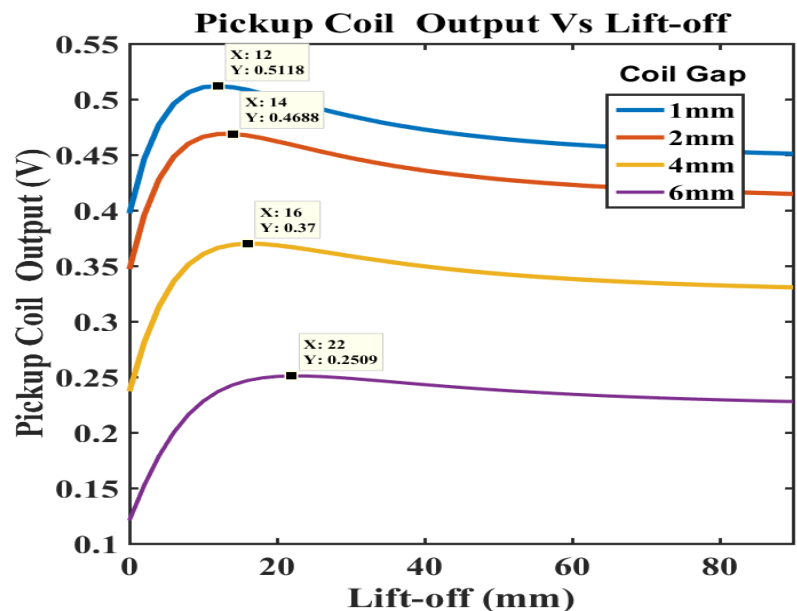


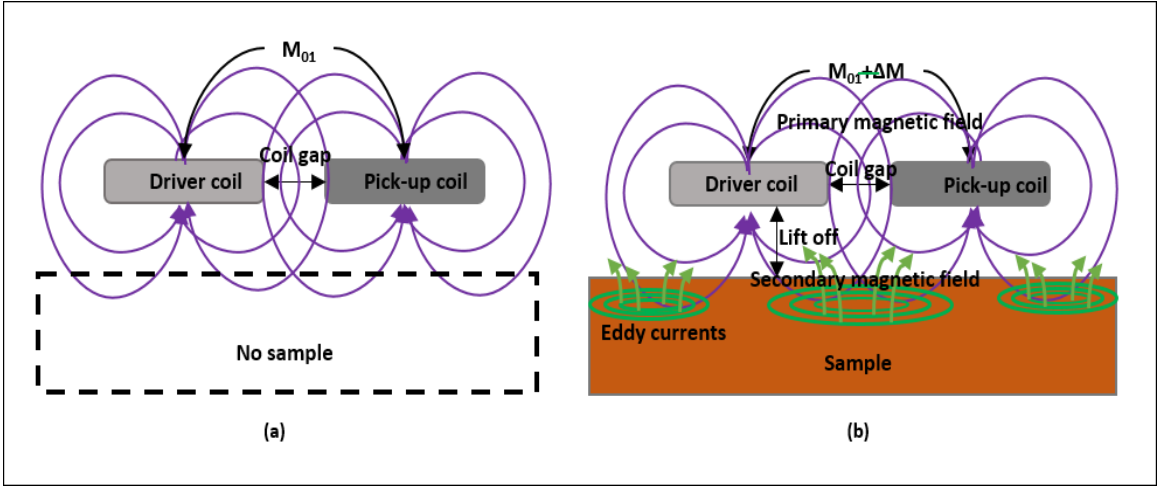
Figure 4.1 Influence of lift-off and coil gap on Rx output of Tx-Rx probe

From figure 4.1, it can be seen that as lift-off increases the Rx output voltage increases up to a lift-off where the Rx coil voltage is maximum. After the maximum point the Rx coil voltage

starts to decay and tends to the value of Rx coil voltage drop due to Rx coil self-impedance. The lift-off at which Rx coil voltage is maximum is the optimum lift-off at which highest sensitivity is achieved for that coil gap. For every coil gap there is an optimal lift-off at which highest sensitivity is achieved and increase in coil gap increases the optimal lift-off. However, increase in optimal lift-off due to increase in coil gap is penalized by decrease in sensitivity. For instance at 1mm coil gap (maximum lift-off = 12mm, sensitivity= 0.5118), 2 mm coil gap (maximum lift-off = 14 mm, sensitivity = 0.4688), 4mm coil gap (maximum lift-off = 16 mm, sensitivity = 0.37), 6 mm coil gap (maximum lift-off = 22 mm, sensitivity = 0.2509). Crack detection at the optimal lift-offs gives the highest detection sensitivity than other lift-offs for the fixed coil gap. Next sections explain principle of mutual inductance based Tx-Rx probe, the simulation and experimental studies carried out for the optimisation.

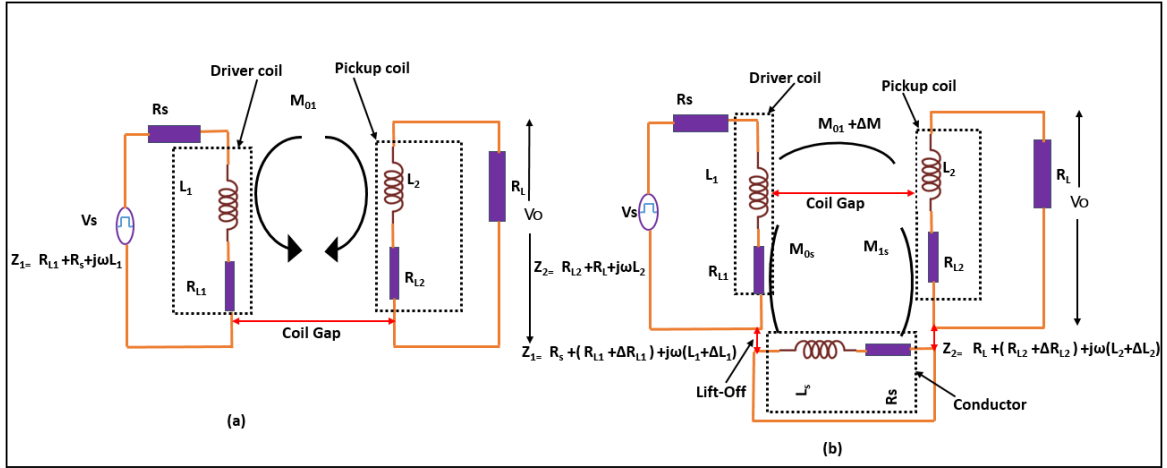
4.3 Mutual Inductance Based Tx-Rx probe Testing Method

A Tx-Rx type of PEC probe basically consists of a coplanar driver and pick-up coil pair (figure 4.2). The driver coil is excited with a time-changing current which develops a changing magnetic field. This field induces an eddy current in nearby electrical conductor. According to Faraday's law, an electromotive force (emf) is developed both in the drive and pick-up coils due to the changing magnetic flux emanating from the driver coil current [166]. The ratios of the induced emf to the rate of change of current producing it on the driver coil itself and on the pick-up coil are known as self-inductance and mutual inductance of the PEC probe, respectively. The coil geometries and their relative positions determine these self and mutual inductances. Also, the magnetic field developed by the probe induces eddy currents (EC) in the nearby conducting material. The ECs in the conductor develop an opposing magnetic field that generates an additional (EMF) in both coils according to Lenz's law. This opposing magnetic field changes the resultant mutual inductance of the probe as shown in figure 1b. Because EC develops magnetic flux that is not in phase with the exciting current, a lossy Self-inductance is generated by the coil coupling to the ECs it generates. Also, a lossy-mutual inductance is generated when a coil coupled to the ECs generated by a nearby coil. These lossy inductances are complex-valued and frequency-dependent [166] .To derive the relationship between mutual inductance among coils and test sample as a function of coil gap and lift-off, I start from the voltage developed in the pick-up coil in the absence of a test sample and then modify the parameters caused by eddy current flow in the conductor when the probe is above a conductor.



(a) Without sample and (b) with sample

Figure 4.2 Driver-Pickup PEC probes



(a) Without sample (b) With sample

Figure 4.3 Equivalent circuits of PEC probes

The output voltage of the pickup coil in the absence of a conductor, as illustrated in figure 4.3a, is derived in [167, 168] as

$$V_0 = \frac{-j\omega M_{01} V_s R_L}{Z_1 Z_2 + (\omega M_{01})^2} \quad 4.1$$

Where V_0 = pick-up Voltage, M_{01} = mutual inductance between driver and pick-up coil in absence of conductor, V_s = excitation voltage, R_L = load resistance, Z_1 = driver coil impedance, Z_2 = pick-up coil impedance, R_{L1} = resistance of driver coil, R_{L2} = resistance of pick-up coil, R_s = signal source resistance, L_1 = driver coil inductance, L_2 = pick-up coil inductance. When the probe is above a conductor, parameters are modified by the eddy current flow in the conductor as follows: $R_{L1} = R_{L1} + \Delta R_{L1}$, $L_1 = L_1 + \Delta L_1$, $R_{L2} = R_{L2} + \Delta R_{L2}$, $L_2 = L_2 + \Delta L_2$, $M_{01} = M_{01} + \Delta M$. where ΔR_{L1} , ΔR_{L2} , ΔL_1 , ΔL_2 , ΔM are variations of the parameters and other mutual inductances

M_{0s} = mutual inductance between driver coil and conductor, M_{1s} = mutual inductance between pick-up coil and conductor are introduced [169]. Pick-up voltage V_0 significantly depends on mutual inductance between driver and pick-up coil in absence of conductor as shown in (4.1). However, in presence of conductor (Fig 4.3 b) induced eddy current in the conductor disturbs the electromagnetic field, hence the pick-up voltage cannot be predicted based on mutual inductance of the driver and pick-up coils only. Therefore the modified relationship becomes

$$V_0 = \frac{-j\omega(M_{01}+\Delta M)V_s R_L}{(Z_1+\Delta Z_1)(Z_2+\Delta Z_2)+(\omega(M_{01}+\Delta M))^2} \quad 4.2$$

Change in mutual inductance ΔM as functions of Coil gap and lift-off has been reported in [75]. Also the transfer impedance from eddy current to driver coil $\Delta Z_1 = \Delta R_{L1} + j\omega \Delta L_1$ and to pick-up coil $\Delta Z_2 = \Delta R_{L2} + j\omega \Delta L_2$ defined as change in mutual impedance (transfer impedance) when the probe is above test sample and in the absence of the sample significantly depend on lift-off as shown in equation (3) [170].

$$\Delta Z(L) = r(L) \frac{\omega^2 M^2(L)}{r^2(L) + \omega^2 l^2(L)} - l(L) \frac{\omega^2 M^2(L)}{r^2(L) + \omega^2 l^2(L)} \quad 4.3$$

Where L = lift-off, r = resistance of eddy current circulation path, l = inductance of eddy current circulation path, M = mutual inductance between coil and eddy current circulation path. Putting equation (3) in (2) and M as M_{0s} , M_{1s} for driver and pickup coils.

$$V_0 = \frac{-j\omega(M_{01}+\Delta M)V_s R_L}{\left(Z_1 + r_1 \frac{\omega^2 M_{0s}^2}{r_1^2 + \omega^2 l_1^2} - j\omega l_1 \frac{\omega^2 M_{0s}^2}{r_1^2 + \omega^2 l_1^2}\right) \left(Z_2 + r_2 \frac{\omega^2 M_{1s}^2}{r_2^2 + \omega^2 l_2^2} - j\omega l_2 \frac{\omega^2 M_{1s}^2}{r_2^2 + \omega^2 l_2^2}\right) + \omega^2 (M_{01} + \Delta M)^2} \quad (4.4)$$

From (4.2) and (4.4), it can be seen that the pick-up voltage V_0 largely depends on mutual couplings among coils and test sample. Variations of mutual inductances as a result of the coil gap and lift-off invariably influences the value of pick-up voltage. Mutual inductance of the coils above a conductor is a superposition of one between coils in the air and that from the conductor given by $(M_{01} + \Delta M)$. It is the change in mutual inductance due to the conductor ΔM that bears the information signal about the conductor [75]. Therefore, the mutual inductance ΔM largely affects the sensitivity of the PEC probe which is defined as change in amplitude of the response signal due to presence of metal conductor. The analytical derivation of the mutual inductances among coils and sample as a function of coil gaps (d) and lift-off (L) is very complex and sometimes impossible depending on coil geometry, hence I choose numerical simulation approach. Numerical simulations [171, 172] are carried out as explained in the next section to understand the influence of lift-off and coil gap on the pick-up coil voltage.

4.4 Numerical Simulation Study

Figure 4.4 is the geometry and PEC probe configuration for the simulation study. To simulate the operation of the probe above a conductive sample, a 3D model was built in COMSOL Multiphysics software. The model is made up of rectangular block (400x300x50 mm) and two rectangular coils of 36 x25 mm each for both driver and pickup coil of the probe. The model is placed in a volume with electromagnetic properties of air to truncate the simulation volume. The material of the coil is setup as copper with electrical conductivity 5.998×10^7 S/m and relative permeability 1. The sample is setup as aluminium material with relative permeability 1 and electrical conductivity 3.5×10^7 S/m. A pulse signal at 1 kHz frequency is used for excitation of the driver coil. To reduce computation time and resources the model is simplified using 2D models [173] from the cross-sections of the 3D geometry. This simplifies the geometry without reducing the integrity of the model. The numerical model used is free tetrahedral finite element. Mesh convergence study is conducted using an iterative method to reduce the influence of meshing on the results. The number of mesh elements is increased by varying the size of the tetrahedral finite elements. The response parameter of interest which is the peak value of the pickup voltage is recorded with number of mesh elements and solve time in table 4. It can be seen from the table that as from 183000 mesh elements, the pickup voltage converges to 0.224 V and increasing the number of mesh element has no significant effect on the pickup voltage. Rather more time is required to solve the model. Hence, 183000 mesh elements is used in the simulation study. The simulation procedure is as follows: excitation was applied on driver coils and pick-up coil voltage is measured and recorded. Through changing of the lift-off ranging from 1 to 37 mm with a step of 4 mm and coil gaps (centre to centre) ranging from 25 mm to 70 mm with a step of 5 mm, their influence on the output voltage of the pick-up coil is analysed. The voltage V_0 is as a result of the equations (4.2), (4.3) and (4.4) which show that pick-up voltage V_0 depends on mutual inductance which invariably is a function of coil gap and lift-off. Hence variation of V_0 with coil gap and lift-off is obtained from the simulation. Reference-subtracted, of peak amplitudes of pick-up coil voltage, the reference being the probe in air, without the effect of the conductor [174] is used in the study and discussed in next sections.

Table 4.1 Mesh convergence study

Mesh elements	Pickup voltage (V)	Solve time (hh:mm:ss)
47481	0.066	00:00:05
61245	0.135	00:00:07
85253	0.224	00:00:10
113854	0.272	00:00:23
163899	0.273	00:01:32
183000	0.274	00:03:01
253946	0.274	00:22:47
512266	0.276	01:19:43
1661745	0.275	03:05:54

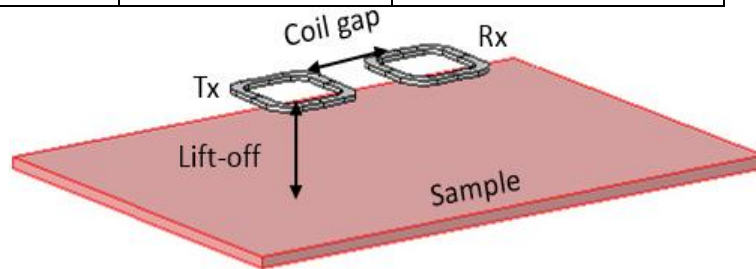


Figure 4.4 Simulation model showing driver, pick-up coils and test sample

4.4.1 Lift-off Influence

As mentioned in Section 4.3, the change in mutual inductance due to eddy current in the test sample carries the information about the condition of the sample. Hence the reference-subtracted signal used in this analysis is the voltage induced in the pick-up coil by eddy current in the sample which is obtained by subtracting pick-up coil voltage in presence and in absence of test sample. In order to analyse the influence of lift-off on the reference-subtracted signal, a plot of reference-subtracted voltage against lift-off is shown in figure 4.5.

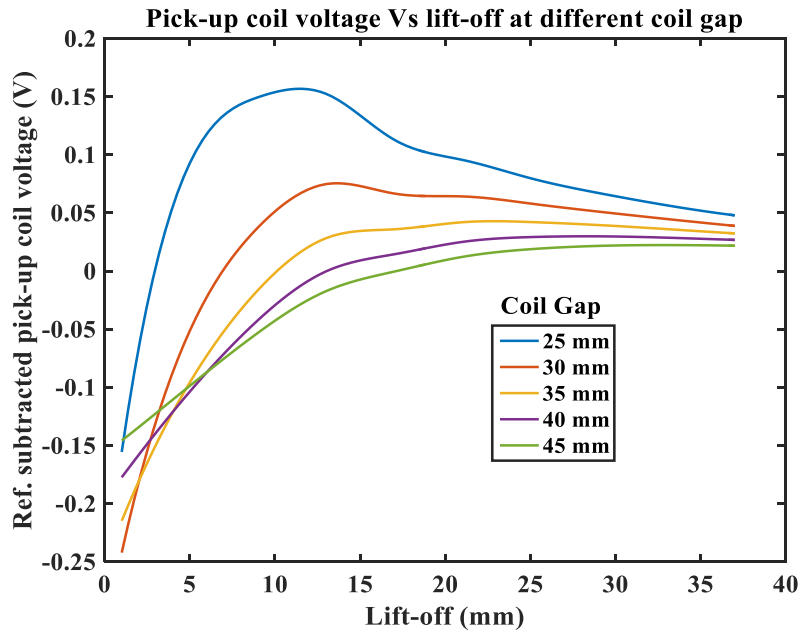


Figure 4.5 Lift-off influence on reference-subtracted signal from simulation

From figure 4.5, maximum values of reference-subtracted signal are located as indicated with arrows. The lift-off (L_o) and pick-up voltage (V_o) values are also indicated. Generally, sensitivity grows to a maximum value, then decays and tends to the voltage across the self-impedance of the pickup coil. The influence of coil gap and lift-off on the sensitivity of the probe is shown in table 4.2

Table 4.2 Influence of lift-off and coil gap on the sensitivity of driver pickup probe

Coil gap (mm)	Maximum lift-off (mm)	Sensitivity (V)
25	11	0.157
30	13	0.075
35	25	0.042
40	29	0.029
45	33	0.022

From table 4.1, the maximum point at coil gap of 25 mm occurred at $L_o = 11$ mm, $V_o = 0.157$ V. Also at coil gap 30 mm, maximum point occurred at the same $L_o = 13$ while with lower V_o (0.075 V). As the coil gap increased to 35 mm and above, maximum point occurred at higher L_o but with reduced V_o including coil gap 35 mm ($L_o = 25$ mm, $V_o = 0.042$ V), 40 mm ($L_o = 29$ mm, $V_o = 0.029$ V) and 45 mm ($L_o = 33$ mm, $V_o = 0.022$ V). This shows that although the sensitivity decreases with increase in coil gap, as coil gap increases beyond certain value, the probe sensitivity is maximum at a higher lift-off. The reason is that at maximum lift-off, the opposing eddy current signal equals the offset signal generated by the excitation field in the

pick-up coil. This almost eliminates the offset signal in the pick-up coil. At null offset, changes in eddy current caused by defect or any other factor in the test sample show a maximum percentage change of impedance of the pickup coil. This implies improved sensitivity at that coil gap/lift-off. In the experiment section, improved sensitivity is validated with surface crack detection of aluminium sample and compared sensitivity at various lift-off. And results show that highest sensitivity is achieved at the lift-off where reference-subtracted is maximum.

4.4.2 Coil Gap Influence

The relationship between the coil gap and reference-subtracted of pick-up coil voltage is obtained as shown in figure 4.6. There is similar behaviour of the signal as coil gap increases for every fixed lift-off. It can be observed that at lower lift-off, as coil gap increases the reference-subtracted signal first decreases before increasing. However, as lift-off increases eddy current influence is reduced and the signal only decays but with increase in signal amplitude. The reference-subtracted signal behaviour is hence a function of both coil gap and lift-off. Then sensitivity at high lift-off can be achieved by optimal combination of coil gap and lift-off especially where spatial constraints are required as in printed circuit board-based PEC probes.

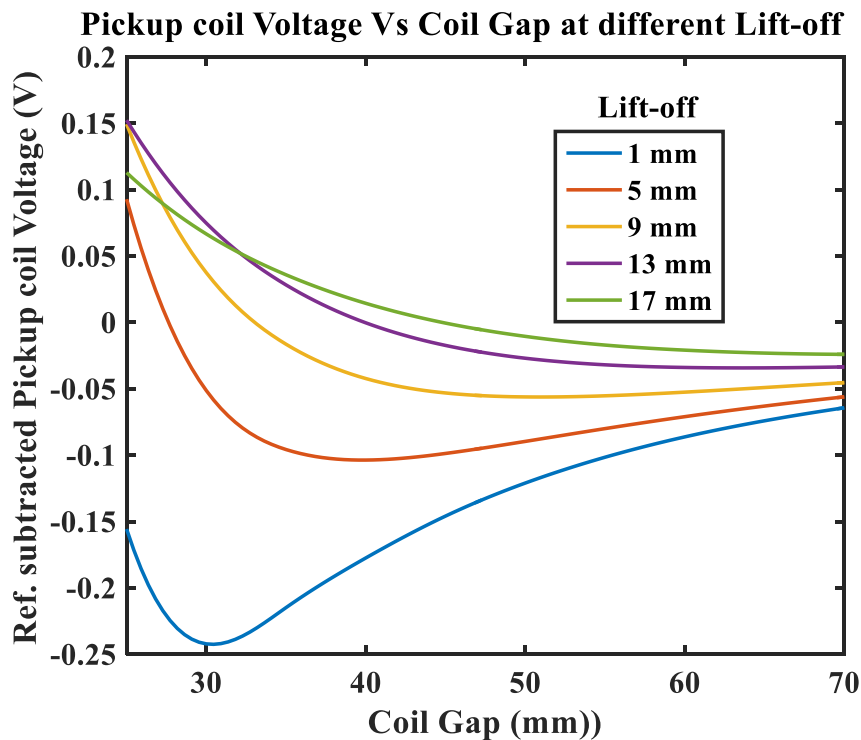
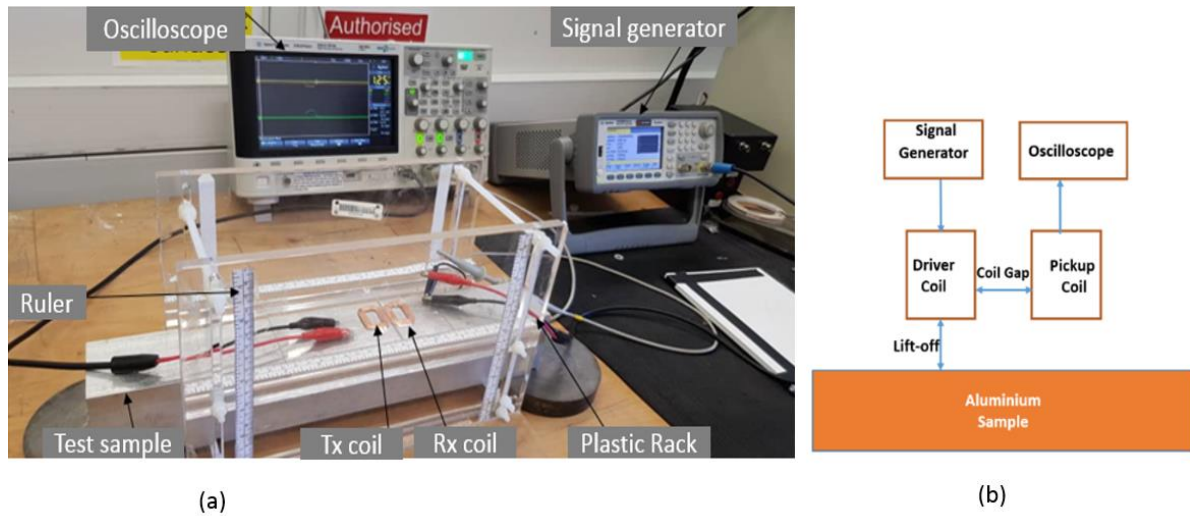


Figure 4.6 Coil gap influence on reference-subtracted signal from simulation

4.5 Experimental Study and Validation

Experimental validation of the numerical simulation is performed with two rectangular planar coils of equal size as driver and pick-up coils and dimensions as described in section 4.4.



(a) Instruments and sample setup (b) block diagram

Figure 4.7 Experimental setup for PEC probe

The Experimental setup and the block diagram of materials used in this work are shown in figure 4.7a and figure 4.7b respectively. The PEC probe as described in simulation including signal generator, oscilloscope, driver and pick-up coils are connected as shown in figure 4.7a above. Pulse signal of amplitude 5 V at frequency of 1 kHz was supplied to the driver coil and amplitude of output of the pick-up coil is read and recorded from the oscilloscope. For every measurement the voltage drop in the driver is kept constant at 460 mV by varying the amplitude of the pulse signal from the signal generator. Aluminium Sample measuring 400x65x50 mm is used. Lift-off is varied from 1 mm to 37 mm at a step of 4 mm. For every lift-off, coil gap is varied from 25 mm to 70 mm at a step of 5 mm and output voltage of the pick-up coil is read and recorded. Reference-subtracted signal is obtained by subtracting output voltage of pick-up coil in absence of sample and in presence of sample. The influence of lift-off and coil gap on the reference-subtracted signal is discussed below.

4.5.1 Lift-off Influence Analysis

The experimental results for lift-off influence on reference-subtracted of pick-up coil voltage are shown in figure 4. 8. The pick-up signal shows the same trend as in simulation result of figure 4.5. Again sensitivity grows and decays before and after maximum value respectively. Also as the coil gap increased to 35 mm and above, maximum point occurred at higher Lo but with reduced Vo. The difference in the simulation and experimental results is that the enhanced

sensitivity at higher lift-off seems to occur at the same value of lift-off for different coil gaps once the coil increases to 35 mm and above. This difference can be attributed to little variation in driver coil voltage as lift-off changes which is not kept constant in simulation study. This is as a result of the limitations of the simulation software.

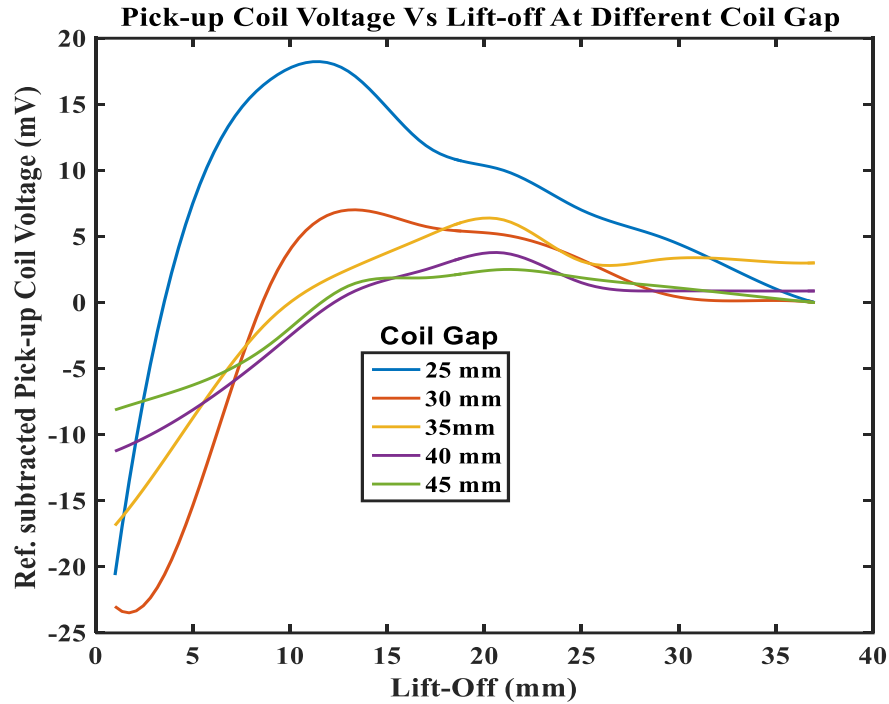


Figure 4.8 Reference-subtracted pick-up voltage vs lift-off at different coil gaps

4.5.2 Coil Gap Influence Analysis

The coil gap influence in figure 4.9 also agrees with the simulation results shown in figure 4.6. As coil gap increases, the signal amplitude decreases. It can be seen that at lower lift-off as the coil gap increases, reference-subtracted voltage decreases to a minimum value and then increases. Specifically the signal decreases to a minimum at 30 mm coil gap and then grows. However as lift-off increases the influence of test sample reduces and gradient of the signal decreases. So experiment validates that the pick-up voltage due to eddy current is influenced by coil gap and lift-off, and for every coil gap there is a lift-off where maximum sensitivity is achieved.

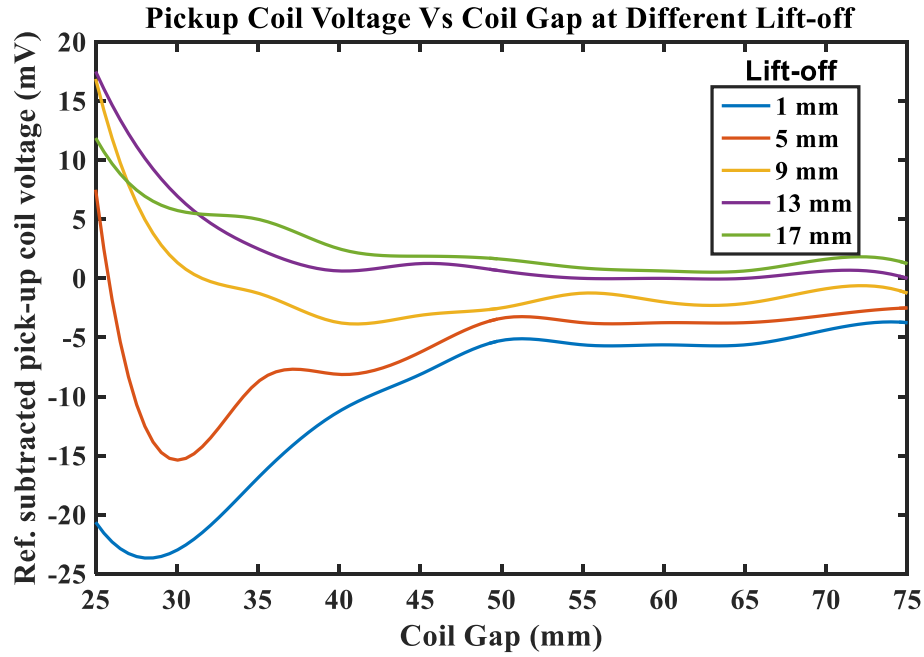


Figure 4.9 Reference-subtracted signal pick-up voltage vs coil gap at different lift-offs

The major source of noise apart from minor lift-off variations and hence signal-to-noise ratio (SNR) can be explained from the pick-up signal which consists of two parts: the offset signal generated by the excitation signal due to M_{01} and the signal induced by the eddy current in the sample due to ΔM . Hence, on the surface of a sample, the pick-up signal is the offset signal superimposed on the eddy current signal. Because analysis and quantification of defects mainly depend on eddy current signal, the offset signal is equivalent to noise. Hence signal-to-noise ratio (SNR) is defined as

$$SNR = \frac{\text{Max(PA)} + \text{Max(PE)}}{\text{Max(PA)}} \quad (4.5)$$

Where Max (PA) and Max (PE) are maximum of pick-up signal in air and eddy current signal respectively. Increase in lift-off reduces eddy current signal while the increase in coil gap reduces the offset signal. Therefore signal-to-noise ratio (SNR) decreases with increase in lift-off but increases with increase in coil gap. In addition, weak eddy current signal at high lift-off will be difficult to identify, hence the sensitivity of the probe to defects is significantly decreased. Increasing the coil gap will be helpful to reduce the offset signal but at the same time, the magnetic field strength in the sample will be reduced. However, there is coil gap/lift-off, the opposing eddy current signal cancels the offset signal generated by the excitation field in the pick-up coil. This almost eliminates the offset signal in the pick-up coil. At this null offset coil gap/lift-off, any change in eddy current caused by defect or any other factor in the test sample shows a maximum change of the response signal. Therefore, for every coil gap, there is a lift-off in which eddy current signal nulls the offset signal thereby improving SNR.

4.5.3 Comparison of Simulations and Experimental Results

To compare simulations and experimental results, SNR explained in Section 4.5.2 is used. The SNR shown in table 4.3 is used to compare the experimental and simulation results of the proposed approach. For a given coil gap, three lift-off values are selected: lift-off before the maximum SNR, at maximum SNR and after the maximum SNR. The maximum values of SNR are coloured blue and also underlined in the table. It can be seen that for every coil gap there is a lift-off where maximum SNR is achieved for both experimental and simulation results. For instance for coil gap 25 mm, three lift-off values of 9 mm, 13 mm and 17 mm are shown and

Table 4.3 Experimental and simulations results at selected lift-off and coil gaps

Experiment					Simulation				
Coil Gap (mm)	Lift-off (mm)	Max (PA) (mV)	Max (PE) (mV)	SNR	Coil Gap (mm)	Lift-off (mm)	Max (PA) (mV)	Max (PE) (mV)	SNR
25.00	9.00	93.13	17.50	1.18	25.00	9.00	92.06	14.94	1.16
	13.00	93.13	16.88	<u>1.20</u>		13.00	92.06	15.00	<u>1.19</u>
	17.00	93.13	11.88	1.13		17.00	92.06	11.29	1.12
30.00	9.00	41.75	7.00	1.03	30.00	9.00	45.50	3.74	1.10
	13.00	41.75	1.38	<u>1.17</u>		13.00	45.50	7.48	<u>1.16</u>
	17.00	41.75	5.75	1.14		17.00	45.50	6.66	1.15
35.00	17.00	26.25	6.25	1.19	35.00	17.00	30.90	3.58	1.12
	21.00	26.25	5.00	<u>1.24</u>		21.00	30.90	4.19	<u>1.14</u>
	25.00	26.25	3.13	1.12		25.00	30.90	4.21	1.13
40.00	17.00	18.75	3.75	1.13	40.00	17.00	22.70	1.44	1.06
	21.00	18.75	2.50	<u>1.20</u>		21.00	22.70	2.50	<u>1.13</u>
	25.00	18.75	1.88	1.10		25.00	22.70	2.90	1.13
45.00	17.00	13.75	2.50	1.14	45.00	17.00	17.44	1.13	1.06
	21.00	13.75	1.88	<u>1.18</u>		21.00	17.44	1.87	<u>1.10</u>
	25.00	13.75	1.88	1.14		25.00	17.44	1.78	1.10

the maximum SNR of 1.20 occurred at 13 mm lift-off while both lift-off values of 9 mm and 17 mm had lower values of 1.18 and 1.13 respectively for experimental result. Simulation results have the same trend of SNR but with different maximum values of 1.19 and lower values of 1.16 and 1.12. The same trend can be observed from other coil gap and lift-off values. The difference in values can be attributed to little variation in driver coil voltage as lift-off changes

which is kept constant only in the experiment but was varying in simulation study. This is as a result of the limitations of the simulation software. Hence there is a good agreement between simulation and experiment results that pick-up voltage due to eddy current is influenced by coil gap and lift-off and for every coil gap there, is a lift-off where maximum sensitivity (SNR) is achieved.

4.5.4 Performance Evaluation of the Proposed Technique for Crack Detection

To evaluate an improved sensitivity at optimal lift-off for a given coil gap, aluminium sample with artificial crack of width 1mm, depth 1mm and length 63mm shown in figure 4.10e is scanned at three selected lift-offs. First, at the optimal lift-off, second above optimal lift-off and third below the optimal lift-off respectively. Figure 4.10a shows variation of pick-up signal with lift-off without crack and it is observed that the optimal lift-off for coil gap 20 mm is established at 20 mm with a maximum pick-up signal amplitude of 0.0114 V. Two other lift-offs selected for scan are 4 mm with pick-up signal amplitude of 0.0069 V and 40 mm with signal amplitude of 0.0106 V. This is followed by scanning the aluminium sample with crack at lift-offs of 4 mm, 20 mm and 40 mm respectively so as to compare their amplitude change due to crack. As amplitude change feature is used for the crack detection, it is shown in figure 4.10b to figure 4.10c that lift-off 20 mm (optimal) scan has the highest amplitude change of 0.0117 V Figure 9c, while Lift-off 40 mm figure 9d and 4 mm figure 4,10b has 0.0109 V and 0.0062 V respectively. Therefore scanning at optimal lift-off of 20 mm has a stronger response than responses from other lift-offs with enhanced crack detection sensitivity. The experimental study has evaluated that optimal sensitivity can be achieved with optimized coils gap and lift-off. This is important in design and development of a new driver-pick-up pulse eddy current probe for a specific lift-off requirement.

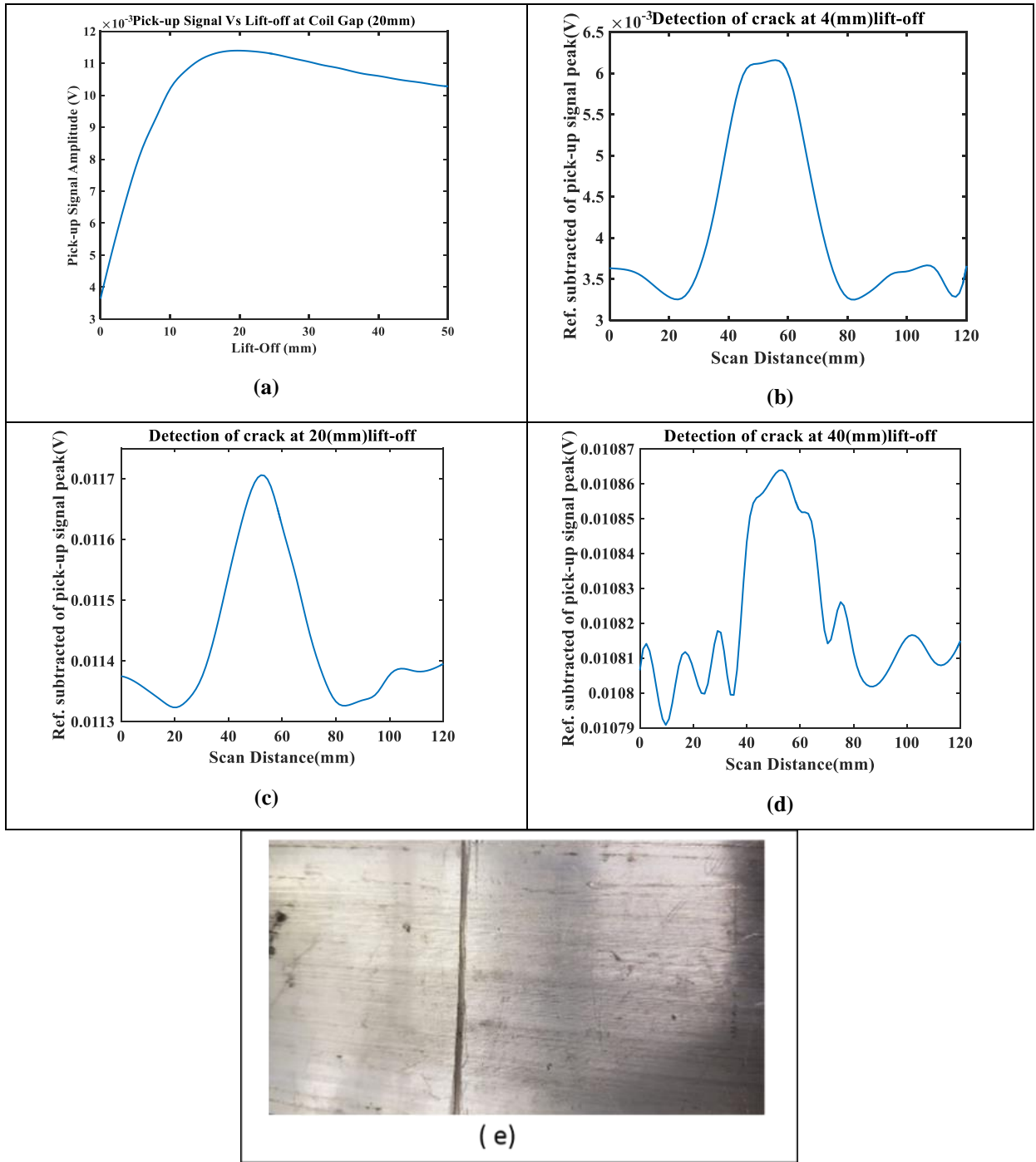


Figure 4.10 Comparison of crack detection at different lift-offs with fixed coil gap

4.4 Chapter summary

This chapter proposed a design optimization of mutual inductance based Tx-Rx PEC probe which gives high sensitivity to crack detection at high lift-off. The influence of coil gap and lift-off on detection sensitivity was used to optimize lift-off for every coil gap. Amplitude change was used as performance indicator to measure and evaluate the capability of the optimised probe through simulation and experimental studies. It was observed that, for every coil gap, there is an optimal lift-off at which highest detection sensitivity is achieved and increase in coil gap increases the optimal lift-off at the cost of reduced sensitivity. Experimental validation of the optimization approach was carried out by detecting a manmade crack on an aluminium sample. The results obtained show that the optimization approach gives a higher detection capability at the optimal lift-off than other lift-offs. This is a significant improvement can be used in inspection of buried and thick insulated structure, and weld areas where high lift-off is unavoidable requirement. Part of this chapter has been published in [175]. In next chapter, further improvement on defect detection at the optimal high lift-off is studied. This is because to improve detection sensitivity, SNR has to be improved and measurement errors have to be reduced.

Chapter 5. Investigation of signal conditioning of Tx-Rx probe for high lift-off inspection

In chapter 4, coil gap and lift-off parameters of Tx-Rx probe were optimized to improve sensitivity at high lift-off. It was observed that to obtain higher optimal lift-off, the coil gap has to be increased. To further improve defect detection at the optimal high lift-off, SNR has to be improved and measurement errors have to be reduced. Hence, in this chapter a modified AC bridge for high lift-off inspection is designed and investigated.

5.1 Introduction

It is highlighted in chapter 3 that the output of Rx circuit is dominated by the Rx coil self-impedance making the impedance change which bears the required information a small percentage of the output signal especially at high lift-off [79, 80]. Typically, the variation in coil impedance falls in the range of 5% to 10% of the self-impedance [81]. The inherent self-inductance of the Rx coil is also one of the sources of nonlinearity in the Rx output signal [82]. Due to the self-impedance of the Rx coil, in addition to multi-parameter influence, the required information is sometimes masked in noise. The dominance by the Rx self-impedance limits the subsequent amplification of the output signal, which is the key in applications with a low SNR [71]. Therefore, a circuit designed to remove the enormous self-impedance of Rx coil, thereby improving SNR and linearity range. Measurement errors due capacitive and electromagnetic interference are also reduced.

The impedance change of Tx-Rx due defect can be converted into electrical signals such as current, voltage, frequency, and phase using different circuits. Such circuits include an amplitude modulation circuit [83], a frequency modulation circuit, and bridge circuits [84, 85, 176]. Frequency output sensors can also be used as signal conditioning through oscillation for instance as in [82, 86, 87]. However, to balance the influence of coil self-impedance and improve sensitivity, bridge circuits are normally used as part of signal conditioning to convert the impedance change or magnetic field change into electrical signal [88]. Ac bridge circuit is operated in a balanced mode to null the offset due to self-impedance of Rx coil and to detect the impedance change as the balance is disturbed. Conventional ac bridges including Maxwell's bridge, Anderson bridge, Hay's bridge, etc. are used for this purpose [89]. However, a challenge of bridge circuits is limited linear range input-output characteristic [156, 177]. Another setback of conventional bridges is the measurement error due to stray capacitance between bridge nodal point and ground, and stray inductance of the inductive coils [157].

To address the problem of the ac bridge circuit, a modified Maxwell's bridge based on the operational amplifier is proposed. The proposed circuit removes the influence of self-impedance of the Rx coil, reduce measurement errors, and improve SNR and linear input-output characteristics. Such a measurement circuit suitable for capacitive sensors with large offset capacitance has been presented in [178, 179]. In the circuit of [178], a sensing capacitor in a T-network is connected in a negative feedback loop of an operation amplifier (opamp), while a reference capacitor in another T-network is connected in a positive feedback loop of the same opamp. The output of the two networks is then fed to an instrumentation amplifier which gives zero output voltage when the two capacitance values are equal and non-zero output voltage when there is a difference between the two capacitance values arising from the change in the measured parameter. By this technique the large offset capacitance of a capacitive human proximity sensor is removed and detection sensitivity improved.

The idea of the circuit of [178] is borrowed by using two Rx coils in the feedback networks of an opamp. The outputs of the two Rx coils are fed to the subtractor opamp. The subtractor gives zero output voltage when the two impedance values are equal and non-zero voltage when there is a difference in impedance values. Based on this idea, a simple circuit that removes the large self-impedance of Rx coil using opamp based bridge circuit is proposed. This circuit can be seen as a modified Maxwell's bridge considering the arrangement of the passive components of the circuit. The major aim is to remove the effect of self-impedance of the Rx coil from the mutual impedance of the PEC probe and the test sample. Part of the circuit of [180] which consists of two inverting opamps and a subtractor circuit to configure two Rx coils is used. Two Rx coils form the feedback loops of the two inverting opamps with both coils coupled to the Tx coil. Adopting the linear variable differential transformer approach [181], the two Rx coils are arranged into a push-pull configuration. That is the mutual inductance of Tx and one coil of Rx is made positive, while the mutual inductance of Tx and another coil of Rx is made negative through coil winding. Hence, the difference between the mutual inductances of the two Rx coils and Tx coil becomes twice that of one Rx coil.

To evaluate the performance of the proposed circuit, the modified Maxwell's bridge was compared with Maxwell's bridge in linearity range and in crack detection of aluminium sample. The results obtained show that the proposed circuit has an improved linearity range compared to conventional ac bridge. Also when compared in crack detection, the proposed circuit shows more sensitivity in crack detection. However, it is easier to map the crack geometry with Maxwell's bridge signal than the modified Maxwell's bridge signal. For instance, although there are equal extrema for both circuits, the symmetry with respect to the centre of the crack

for Maxwell's bridge response simplifies the mapping of the crack with the response signal than in the modified Maxwell's bridge.

To understand how self-impedance of Rx coil dominates the output signal of Tx-Rx PEC probe which leads to low SNR especially at high lift-off, I analyse the equivalent circuit of Tx-Rx PEC probe. Mutual inductance based PEC probe depends on the linking magnetic field of coils and sample. Time changing voltage or current in the Tx coil generates magnetic flux that couples both directly and indirectly through the sample with Rx coil. The equivalent circuit used to induce and extract the induced voltage from the Rx coil is in figure 5.1. I analyse the circuit without a sample and then introduce a sample and modify the circuit to include the influence of the sample. Without a sample as in figure 5.1a, the proximity of the Tx and Rx equivalent circuit results in mutual inductance of Tx and Rx ,where the mutually induced electromotive force (EMF) is given by the following equations.

$$\varepsilon_1 = -M_{12} \frac{di_2}{dt} \quad (5.1)$$

$$\varepsilon_2 = -M_{21} \frac{di_1}{dt} \quad (5.2)$$

$$L_1 \frac{di_1}{dt} + (r_1 + R_s) i_1 = M \frac{di_2}{dt} + V_s U(t) \quad (5.3)$$

$$L_2 \frac{di_2}{dt} + (r_2 + R_L) i_2 = M \frac{di_1}{dt} \quad (5.4)$$

M = Direct mutual inductance of Tx and Rx

\mathcal{M} = Mutual inductance of Tx and Rx through Sample

V_s = Excitation voltage

V_0 = Rx output Voltage

$U(t)$ = Unit step function

L_1, L_2 = Self-inductance of Tx and Rx

r_1, r_2 = Internal resistance of Tx and Rx coils

R_s = Source resistance

R_L = Load resistance

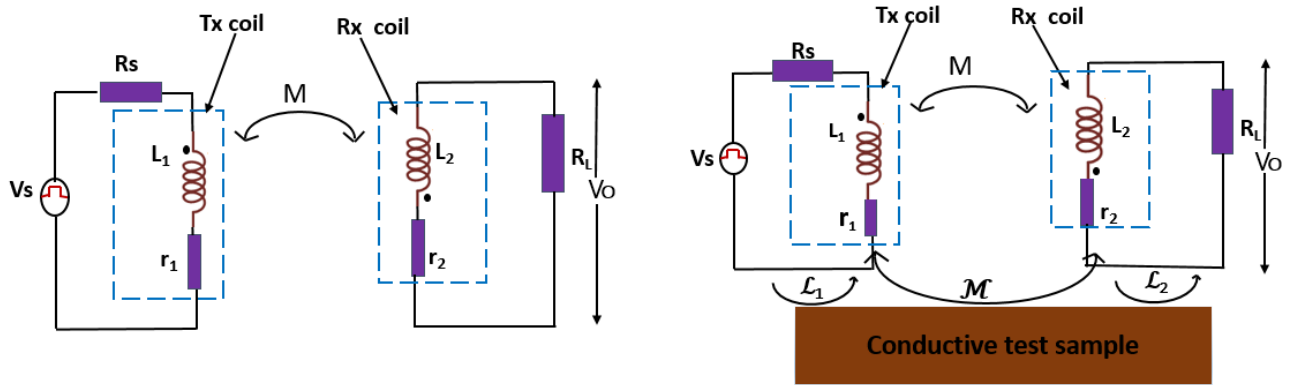
$\mathcal{L}_1, \mathcal{L}_2$ = self-couplings of Tx and Rx coils through the sample

i_1, i_2 = Tx and Rx current

$\mathcal{E}_1, \mathcal{E}_2$ = Mutually induced emf of Tx and Rx

M_{12}, M_{21} = ratio of \mathcal{E}_1 to current change in Rx and ratio of \mathcal{E}_2 to current change in Tx

$M_{12} = M_{21} = M$



(a) Without sample

(b) With sample

Figure 5.1 Tx-Rx equivalent circuit

In proximity to a sample figure 5.1b, the magnetic field developed by the probe induces eddy currents (EC) in a nearby conductive sample. The EC in the sample develop an opposing magnetic field that generates an additional EMF in both coils following Lenz's law [110]. While the Tx coil generates an electromagnetic field [182], the Rx coil measures the reflected field from the test sample as the voltage across the load resistance R_L [154]. It is from the induced voltage in the Rx coil that the status of the test sample is evaluated. However, the total field in the presence of a sample can be considered as a sum of the original field of the coil in the air plus a reflected field from the metal sample [69]. In presence of a sample, a Tx-Rx probe generates self-couplings of both Tx coil and Rx coil through the sample $\mathcal{L}_1, \mathcal{L}_2$ and a mutual coupling of Tx and Rx coils through the sample \mathcal{M} (remote coupling). Hence, the previous equations are modified to take an account of the self-couplings of Tx and Rx coils through the sample, and the mutual coupling of Tx and Rx through the sample [169]. Hence, total inductance of Rx, $L = L_2 + \mathcal{L}_2$, mutual inductance of Tx and Rx probe $M = M + \mathcal{M}$ and the internal resistance becomes of Rx $r = r_2 + \Delta r_2$. The Rx output voltage

$$V_o = (L_2 + \mathcal{M} + \mathcal{L}_2) \frac{di_2}{dt} + (r_2 + \Delta r_2) i_2 - M \frac{di_1}{dt} \quad (5.5)$$

Which is $V_o = R_L i_2$ becomes

From (5.5), the impedance change due to the mutual coupling of the sample and PEC probe (5.6), the direct mutual impedance of Tx and Rx coils (5.7) and self-impedance of the Rx coil (5.8) is extracted from output signal respectively as follows

$$\Delta Z = j\omega(\mathcal{M} + \mathcal{L}_2) + \Delta r_2 \quad (5.6)$$

$$Z_{TR} = j\omega M \quad (5.7)$$

$$Z = j\omega L_2 + r_2 \quad (5.8)$$

The impedance change due to the mutual coupling of the sample and probe ΔZ bears the information about the sample [75]. Whereas, Z_{TR} , the direct mutual impedance of Tx and Rx coils, in addition to Rx coil self-impedance Z form an offset that masks the required information signal [71]. Because of the large value of the offset, the impedance change, the required information signal is a very small percentage of the Rx output voltage yielding a very low SNR output. As can be seen in (5.6)-(5.8), only ΔZ is the required information signal, Z_{TR} is the offset due to direct coupling of Tx coil and Rx coil whereas Z is the offset due to self-impedance of Rx coil. Hence these two offsets are the main sources of noise that limit SNR of the response signal. In chapter 4, the problem of direct coupling Z_{TR} offset was mitigated. When a Tx-Rx PEC probe is in proximity of a conductive sample, the magnetic field of Tx coil couples directly with the Rx coil and forms an offset in Rx circuit. The Tx coil also couples indirectly through the sample with the Rx coil bearing the information about the test sample in the Rx circuit as in figure 5. 1b. Because the resultant value of these two couplings (M and \mathcal{M}) depend on coil gap and lift-off [75], coil gap and lift-off is optimized to minimize the offset (M) due to direct coupling of Tx and Rx coils . At the optimal lift-off, for every coil gap, the defect detection sensitivity was maximized.

Although the offset arising from the direct coupling of Tx and Rx is eliminated, the offset due to self-impedance of the Rx coil is another challenge which this work proposes to remove. As lift-off increases, the SNR decreases the more because the impedance change or the information signal generated by magnetic field of eddy current reaching the Rx coil diminishes whereas, the Rx coil self-impedance remains constant. Hence, at high lift-off, impedance change ΔZ becomes insignificant component of the output signal. Therefore, it is required to design a

measurement circuit that can remove the effect of self-impedance of the Rx coil to improve SNR of the output signal. The next section explains the design and the principle of the proposed signal conditioning to achieve this requirement.

5.3 Proposed Signal Conditioning Circuit

The major aim of the proposed signal conditioning circuit is to modify Maxwell's bridge using opamp circuit to remove the self-impedance of the Rx coil to improve SNR and linearity range at high lift-off. Hence, this section describes the modification and working of the proposed circuit. Maxwell's bridge of figure 5 2a is modified using three high impedance and low-noise opamps, and passive components as in figure 5 2b. Inductors (Coils) L2 and L3, and resistors R1 and R2 of Maxwell's bridge form the feedback loops of two (opamps) A1 and A2 respectively which are working in inverting modes. A pulse excitation V_e is applied to the Tx coil which is coupled to two Rx coils. The output of A₁ and A₂ are then fed into a subtractor opamp A₃ and output are measured as ΔV . The output voltages V_a and V_b of opamps A₁ and A₂ are given by

$$V_a = -V_s \frac{r_3 + j\omega L_3}{R_1} \quad (5.9)$$

$$V_b = -V_s \frac{r_2 + j\omega L_2}{R_2} \quad (5.10)$$

Where L_2 and L_3 , r_2 and r_3 are self-inductances and internal resistances of the feedback coils respectively. The voltage difference ΔV of the two outputs obtained at the output of op-amp A₃ is given by

$$\Delta V = \frac{V_s((r_3 + j\omega L_3))}{R_1} - \frac{(r_2 + j\omega L_2)}{R_2} \quad (5.11)$$

The complete Tx-Rx PEC probe circuit is configured as in figure 5.3a. Two coils L_2 and L_3 of the Rx circuit are coupled with the Tx coil above a test sample. The close proximity of Tx and Rx, in the presence of a sample, results in indirect coupling of Tx and Rx through the sample [169]. Hence, as explained in section 5.2, the total self-inductance of Rx coil₂ = $L_2 + \mathcal{L}_2$, and Rx coil₃ = $L_3 + \mathcal{L}_3$, internal resistance of Rx coil₂ = $r_2 + \Delta r_2$ and Rx coil₃ = $r_3 + \Delta r_3$. Applying the push-pull configuration of the two Rx coils, the mutual inductance of Tx and Rx coil₂ = $M + \mathcal{M}$, mutual inductance of Tx and Rx coil₃ = $-M - \mathcal{M}$. Also Self-inductance of Rx coil₂ = $L_2 + \mathcal{L}_2$ and Rx coil₃ = $L_3 - \mathcal{L}_3$. Substituting the changes in (5.11)

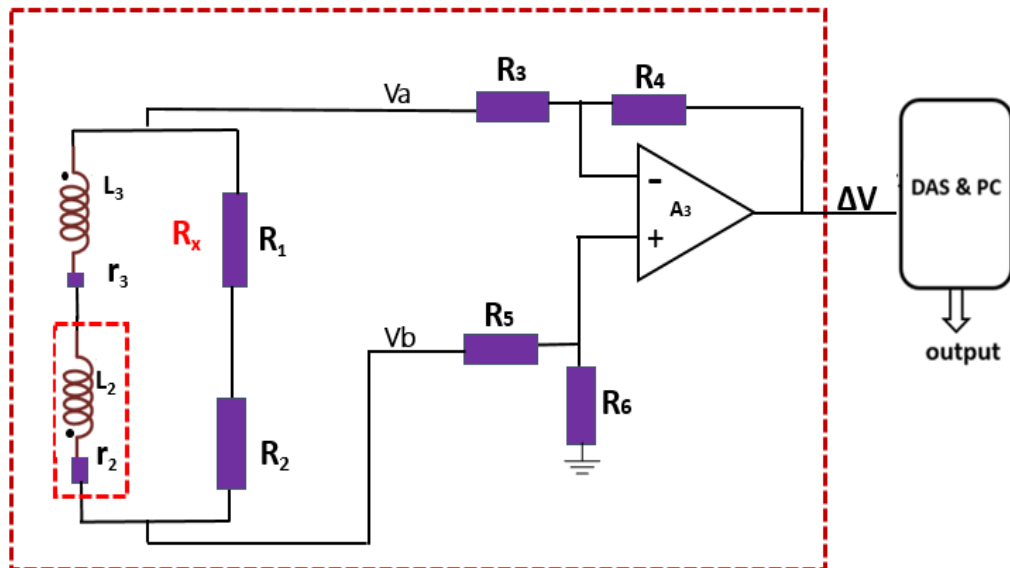
$$\Delta V = \frac{Vs(r_2 + \Delta r_2 + j\omega(L_2 + M + \mathcal{L}_2 + \mathcal{M}))}{R_2} \cdot \frac{R_1}{(r_3 + \Delta r_3 + j\omega(L_3 - M - \mathcal{L}_3 - \mathcal{M}))} \quad (5.12)$$

If I choose $\Delta r_2 = \Delta r_3$, $R_2 = R_1 = R$, $r_2 = r_3$, $L_3 = L_2$, $\mathcal{L}_2 = \mathcal{L}_3 = \mathcal{L}$ and substitute in (12), the Rx output voltage becomes

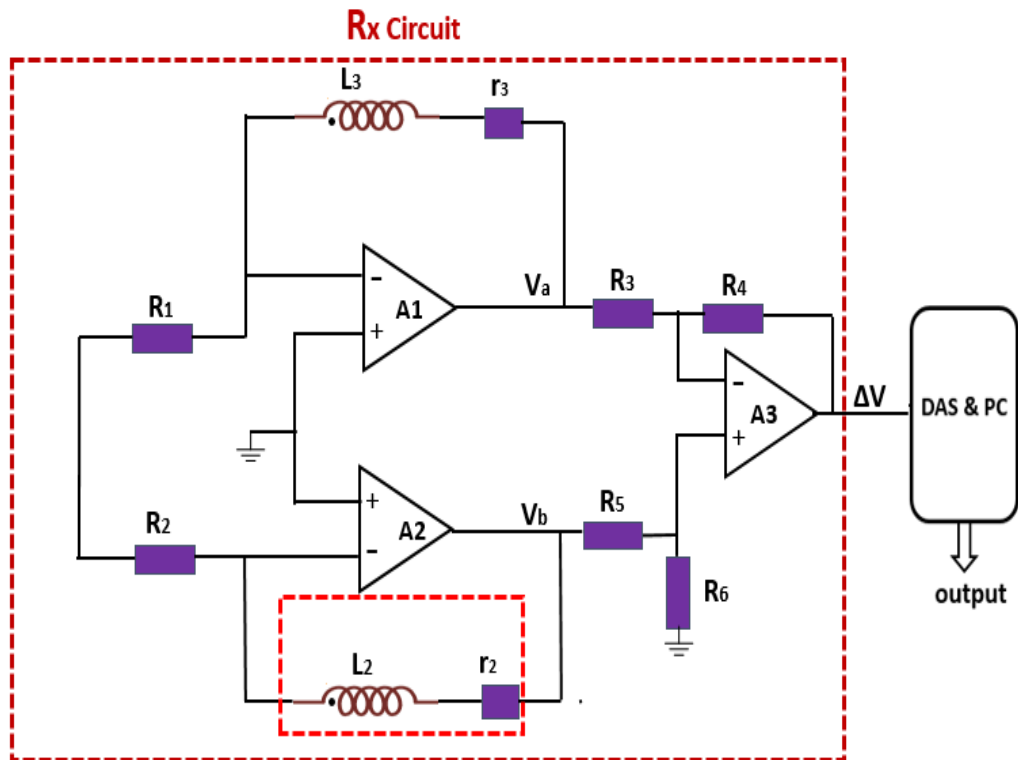
$$\Delta V = \frac{Vs(2j\omega(M + \mathcal{L} + \mathcal{M}))}{R} \quad (5.13)$$

From (5.13), it can be seen that self-impedance of the Rx coil is suppressed from the output voltage. The offset due to direct coupling of Tx and Rx coils (M) can be eliminated as explained in Section 5.2. Thereafter, the output signal ΔV becomes directly proportional to the impedance change of Rx coils ($\mathcal{L} + \mathcal{M}$). Hence, the output will be a minimum (ideally zero) without a sample. No offset output voltage will be present due to the self-impedance of the Rx coil or direct mutual impedance of Tx and Rx coils.

At high lift-off as highlighted in section 5.2, the change in impedance of Rx coil becomes insignificant compared to large Rx self-impedance. However, as the influence of Rx self-impedance has been removed by the conditioning circuit, the change in the impedance becomes a significant component of the output signal. Then, the output is fed to the computer (PC) via data acquisition system (DAS) for analog-to-digital conversion, digitization and low pass filtering which also reduces the effect of interference and noise on the output. Moreover, this configuration has a linear characteristic over a wide range of impedance change with improved sensitivity and stability.



(a) Maxwell's inductive bridge

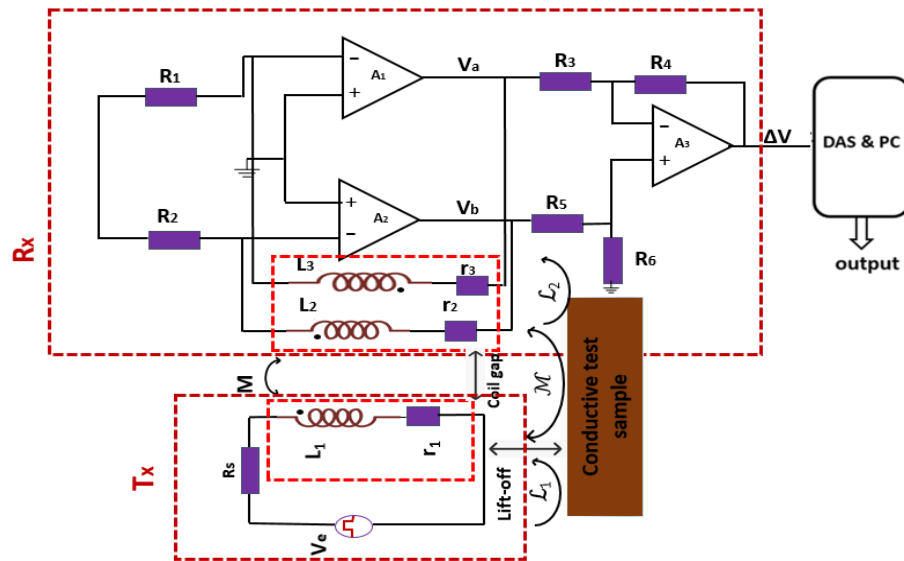


(b) Modified bridge circuit

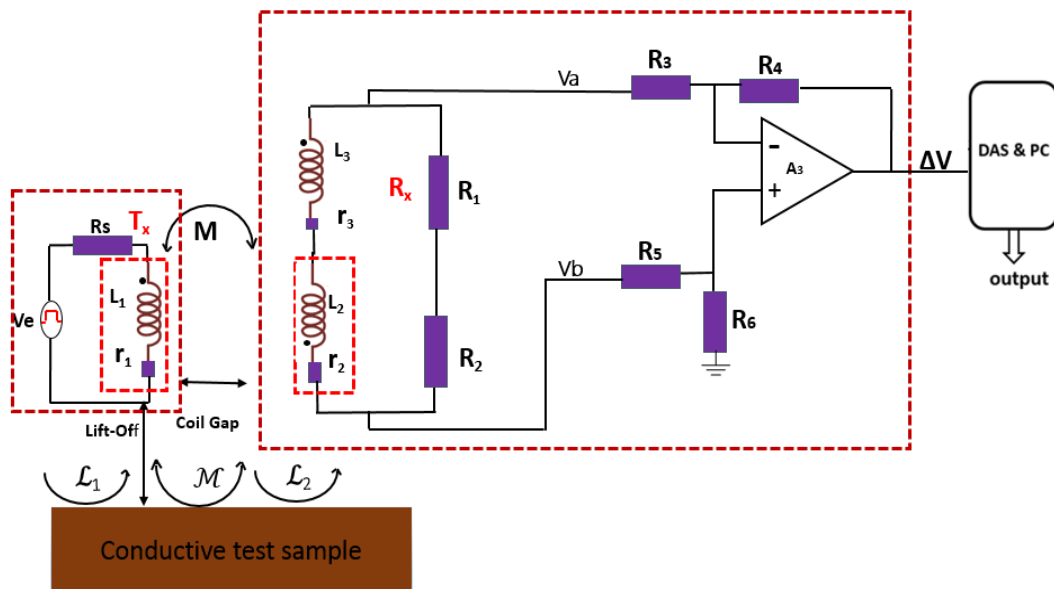
Figure 5.2 Different Signal Conditioning Circuit

The improved linearity range of the modified circuit may be explained, thus; for identical coils in the modified circuit, the edge effects are assumed to be identical. Additionally, in the push-pull inductance measurement circuit of figure 5.3a, these edge effects cancel each other. Also, the non-inverting terminals of opamp A1 and A2 are connected to a common ground. Therefore, the inverting terminals are at the virtual ground where one end of the Rx coils are connected and stray capacitance between the terminals of the coils is negligible. The same excitation signal is input to opamps A1 and A2 through input resistance R1 and R2. Hence, the other two terminals of the inductance coils are also at the same potential and the stray capacitance between these terminals is also negligible. The electromagnetic interference between the two Rx coils are similar and cancels each other when the differential voltages V1 and V2 are measured. Thus, the measurement error in the modified circuit is minimized. This is why the characteristic of the modified circuit is found to be quite linear even at high lift-off as reflected in the experimental results. However, the circuit may become unstable due to the derivative action and variations of the inductance in the feedback path. This instability can cause fluctuations in the output signal if the values of R1 and R2 are low. Increasing the resistances R1 and R2 reduces the quality factors of the feedback circuits and enhances stability [183] but reducing sensitivity as can be seen in (5.13). Hence, R1 and R2 should be carefully chosen. Through series of experiments with different values of R1 and R2, 20k was chosen for both R1 and R2

in this work, to achieve a stable output signal. As nodes V_a and V_b are connected to the differential amplifier's input gain-setting resistors, the input resistors are selected to reduce the loading effect or directing current away from the bridge, which can affect the bridge output.



(a) Modified bridge conditioning circuit



(b) Maxwell's bridge conditioning circuit

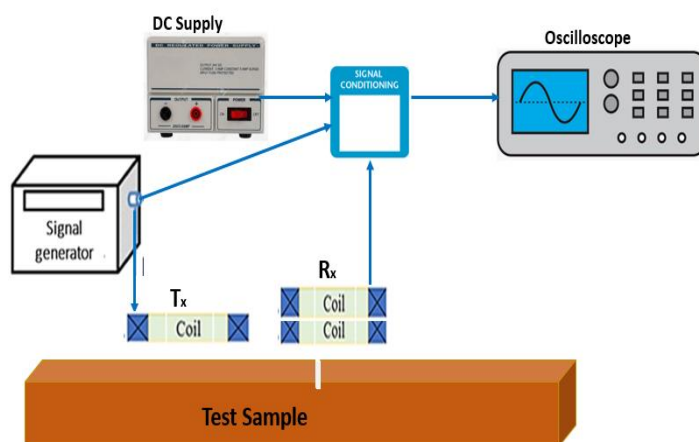
Figure 5.3 Tx-Rx probe above test sample with conditioning circuit

5.4 Experimental Setup

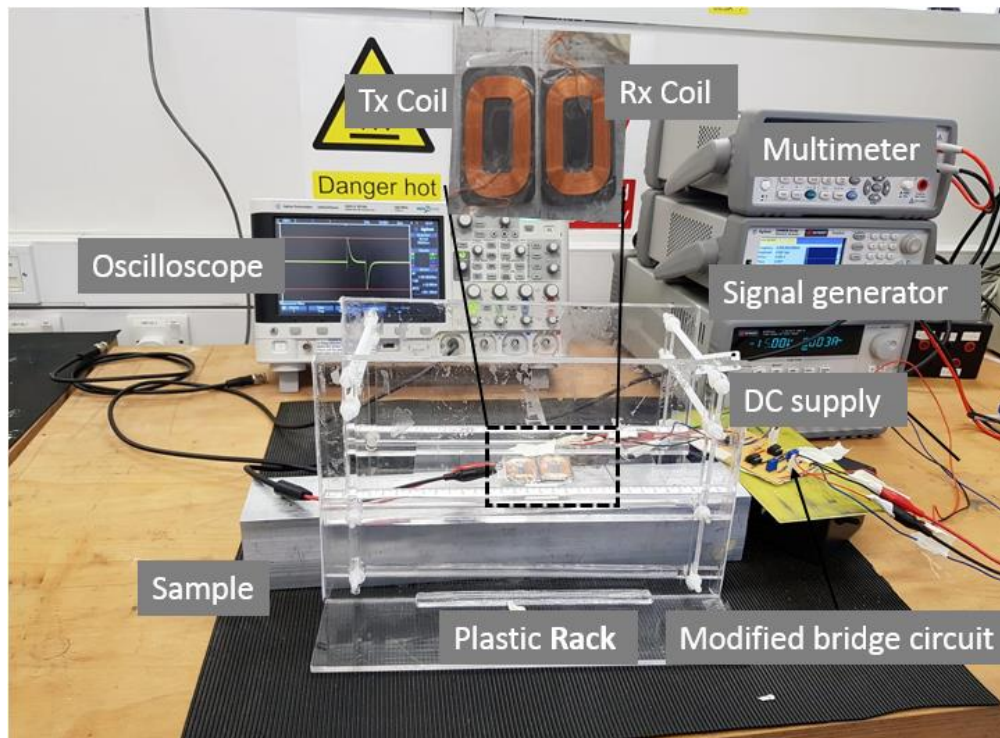
The experiment is carried out in three parts. In the first part, the influence of lift-off on R_x output voltage at a fixed coil gap with the Tx coil and Rx coil above the crack-free aluminium sample without the conditioning circuit is studied. The lift-off of Tx-Rx probe from the aluminium sample is increased from 0 mm to 55 mm at a step of 5 mm at fixed coil gaps of

1mm to 6mm at a step of 1mm and at each step the amplitude of the Rx output voltage is read and recorded with an oscilloscope. Although the expected lift-off is 30mm, the study is extended to 55mm so that whether the Rx output converges to its value when there is no sample can be observed. In the second part, lift-off variation is studied with Maxwell's bridge by varying the lift-off and coil gap as explained in the first part. Also the lift-off influence of the modified bridge is studied by repeating the same procedure as used in Maxwell's inductance bridge.

In the third part, the performance of the modified Maxwell's bridge and Maxwell's bridge with crack detection in the aluminium sample is studied. The probe is used to scan in the steps of 2 mm along with the aluminium sample with a crack. At each scan point, the value of Rx output voltage is read and recorded. The peak values of reference subtracted Rx output voltage is then plotted against the scan points. The values of circuit parameters used are $L_1 = L_2 = L_3 = 10.7\mu\text{H}$, $r_1 = r_2 = r_3 = 0.2\text{ohms}$, $R_1 = R_2 = 20\text{k}$, $R_3 = R_5 = 1\text{k}$, $R_4 = R_6 = 10\text{k}$, $A_1 = A_2 = A_3 = 741$ opamp. The Experimental setup and the block diagram of materials used is in figure 5.4. The PEC probe including signal generator, oscilloscope, one Tx coil and two Rx coils are connected as in figure 5.4a. Pulse signal of amplitude 4 V, pulse width 20us, frequency 4 kHz was supplied to the Tx circuit and amplitude of the output of the Rx coil is read and recorded. Aluminium Sample measuring 400 mm x 50 mm x 50 mm is used for both lift-off influence study and for crack detection. Rx coil is identical to Tx coil, a rectangular coil with an inner diameter 12 mm, outer diameter 25 mm, length 36 mm and 15 turns.



(a) Block diagram



(b) Instruments and sample Setup

Figure 5.4 Experimental setup

5.5 Experimental Results and Discussions

Based on the experimental setups and procedures described in the previous section, measurement data is collected from each experiment. In this section, the results of the experiments are discussed under lift-off influence and linearity, sensitivity to crack detection and SNR, and comparison of the conditioning circuits.

5.5.1 Lift-off Influence and linearity range

In this section, I explain how lift-off variation affects the linearity of the input-output characteristic of the Tx-Rx PEC probe without conditioning circuits, with the modified circuit and with Maxwell's inductance bridge circuit. The response of the Rx circuit with pulse signal is in Figure 5.5. The amplitude of the response signal for every lift-off variation is extracted. The static characteristic curve of the Tx-Rx coils without conditioning circuit in figure 5.6a reveals a good linearity response. It can be observed that there is relative linearity from 1mm to 55 mm lift-off. Hence, PEC testing in the lift-off range will not be affected by non-linearity. However, the large value of the self-impedance (offset) of Rx coil made amplitude of the output signal very high compared to those with conditioning circuit. The static characteristic curve for the modified circuit in figure 5.6b depicts almost the same linearity as that of figure 5.6a. The static characteristic curve of Maxwell's bridge circuit in figure 5.6c depicts good linearity at a low lift-off but as the lift-off increases to about 15.00 mm, non-linearity sets in, as reflected in

the zigzag nature of the graph. The nonlinearity exists at higher lift-off due to the limited linearity range of Maxwell's bridge circuit. Hence, PEC testing can only be taken without measurement errors at lift-off lower than 15 mm with Maxwell's bridge conditioning circuit. Whereas that of the modified circuit is extended to about 50.00 mm.

The percentage deviations from the linearity of Maxwell's inductance bridge and the modified circuit for different coil gaps are in figure 5. 7. The deviation of the modified circuit figure 5.7b is found to be smaller than that of Maxwell's bridge figure 5. 7a for coil gaps 1mm to 6mm as shown in the boxes on the graphs. From this, it can be concluded that the modified Maxwell's bridge has a better linearity range and characteristics than convectional Maxwell's bridge. Figure 5. 8a and figure 5.8b show curves and error bars of the measured data of eight repeated experiments with both Maxwell's bridge and the modified Maxwell's bridge.

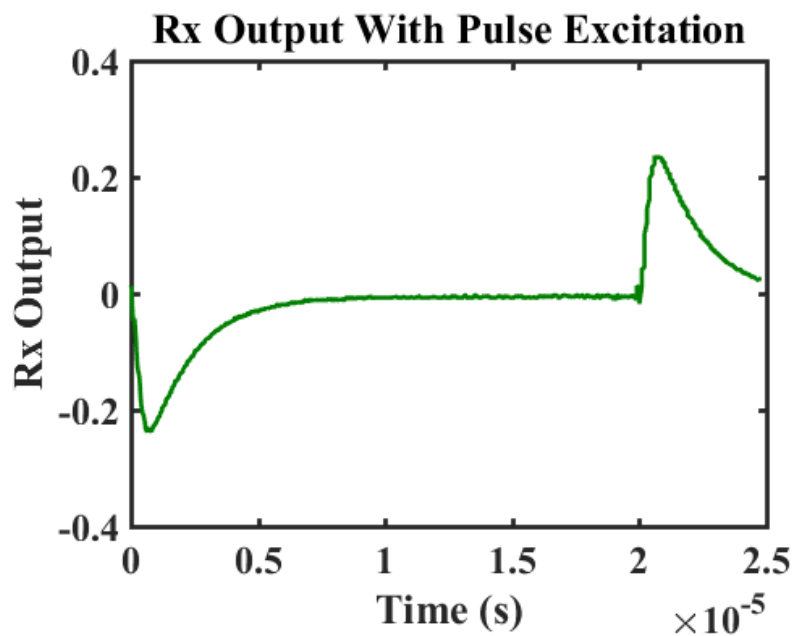
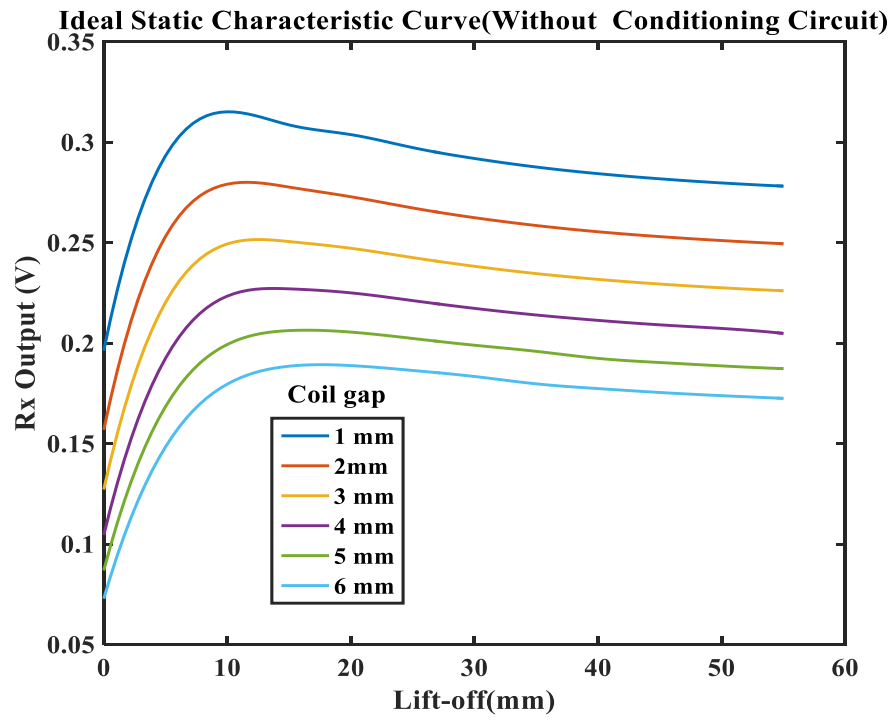
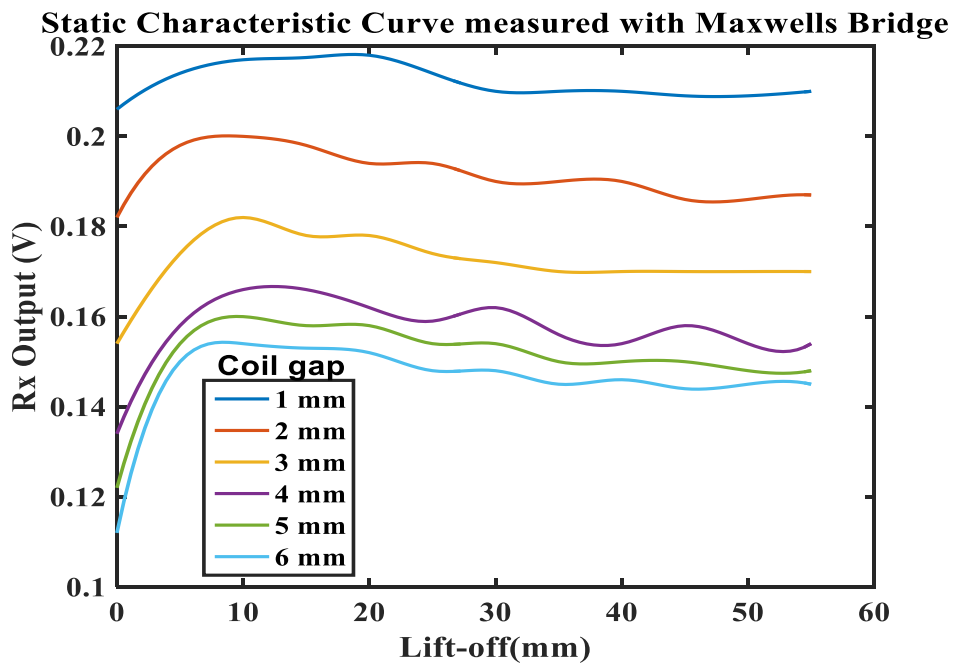


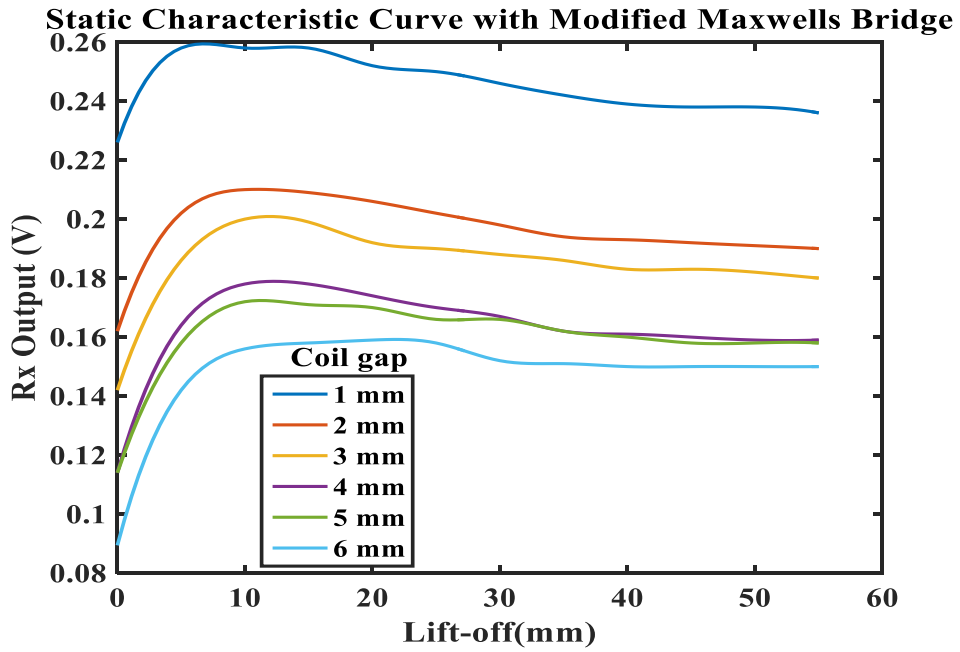
Figure 5.5 Response signal of Rx with repeated pulse excitation of Tx coil



(a) Ideal curve

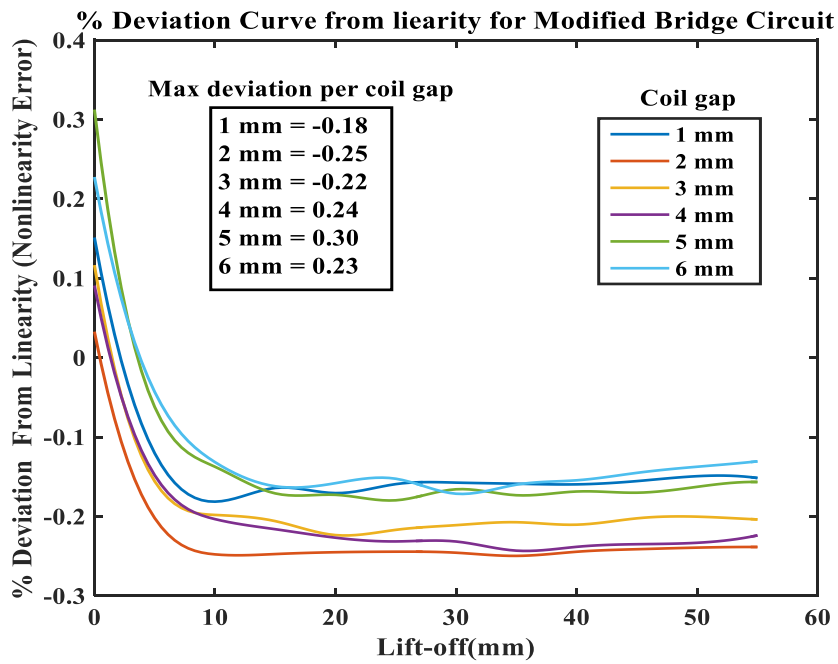


(b) Maxwell's bridge

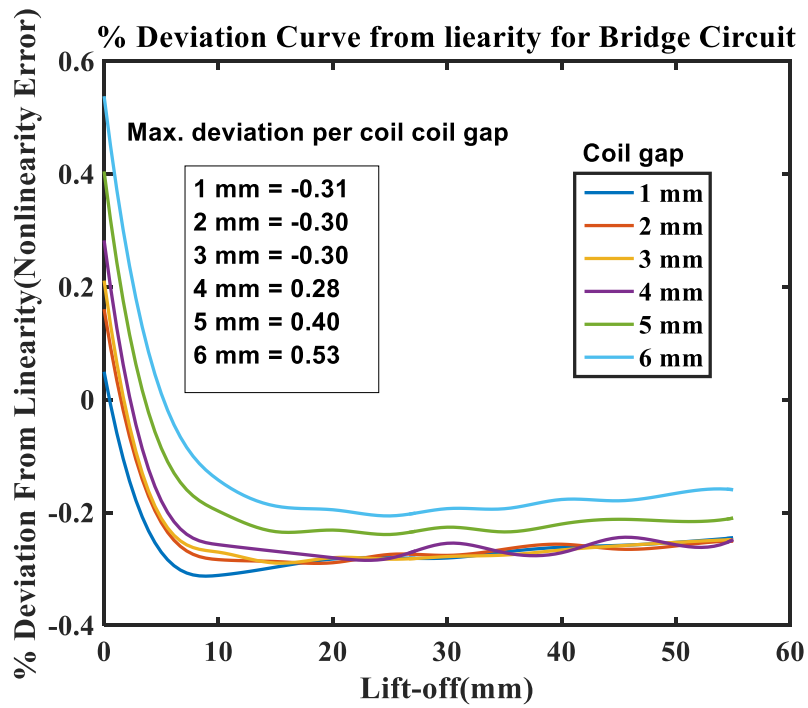


(c) Modified Maxwell's bridge

Figure 5.6 Static characteristic curve of Tx-Rx probe

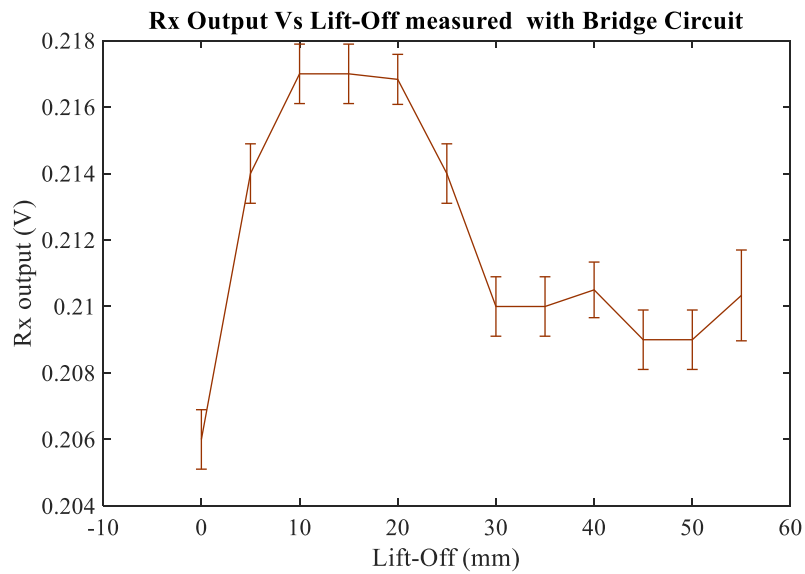


(a) Maxwell's bridge

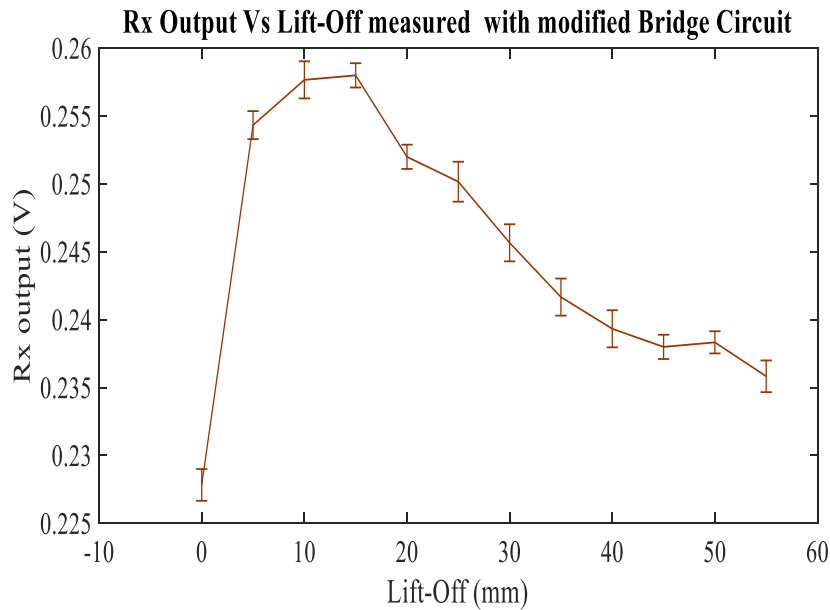


(b) Modified Maxwell's bridge

Figure 5.7 Percentage deviation from the ideal linearity



(a) Maxwell's inductance bridge



(b) Modified circuit

Figure 5.8 Measurement errors of the Circuits

5.5.2 Sensitivity to Crack Detection and SNR

In this subsection, an application of the proposed circuit in surface crack detection of an aluminium (Al) sample is discussed and its performance compared with conventional Maxwell's bridge in sensitivity and SNR. The modified Maxwell's bridge and Maxwell's bridge are used for artificial crack detection in the aluminium sample. At a fixed coil gap of (4.00 mm) and lift-off (30.00 mm), the aluminium sample is scanned with a Tx-Rx probe and the Rx output voltage is read and recorded as described in section 5.4. The peak values of reference subtracted output voltage of the Rx coil connected to the modified Maxwell's bridge and Maxwell's bridge one after the other are plotted in figure 5.9. With reference to the centre of the crack which is at 30mm from the start point of the scan distance, it can be observed that the two circuits show different response shapes due to the crack influence. The response of Maxwell's bridge is symmetrical with respect to the centre of the crack, with minima when the centre of Tx-Rx coils is at the edges of the crack and a maximum when the centre of Tx-Rx coils is at the centre of the crack. The response of the modified Maxwell's bridge is not symmetrical with respect to the centre of the crack with maxima when the centre of Tx-Rx coils

is at the edges of the crack and a minimum when the centre of Tx-Rx coils is at the centre of the crack. However, considering sensitivity as amplitude change, the amplitude of the response signal changes from 12.50 mV to 0.00 mV due to the first edge of the crack, from 0.00mV to 19.80mV at the centre of the crack and from 19.80mv to 6.30mV due to the last edge of the crack for Maxwell's bridge. Whereas that of modified Maxwell's bridge changes from 0.00 mV to 27.00 mV due to the first edge of the crack, from 27.00mV to 0.00mV at the centre of the crack and from 0.00mV to 29.50 mV due to the last edge of the crack. Hence, the change in amplitude for the modified Maxwell's bridge is far greater than that of Maxwell's bridge. Therefore, it is concluded that the modified Maxwell's bridge has better sensitivity to crack than Maxwell's bridge. However, it is easier to build a relationship between the extracted amplitude feature, and the detected crack with Maxwell's bridge than the modified Maxwell's bridge based on crack response shape. For instance, although there are equal extrema for both circuits, the symmetry with respect to the centre of the crack for Maxwell's bridge response simplifies the mapping of the crack with the response signal than in the modified bridge. Hence, it is easier to characterize crack with Maxwell's bridge than the modified Maxwell's bridge.

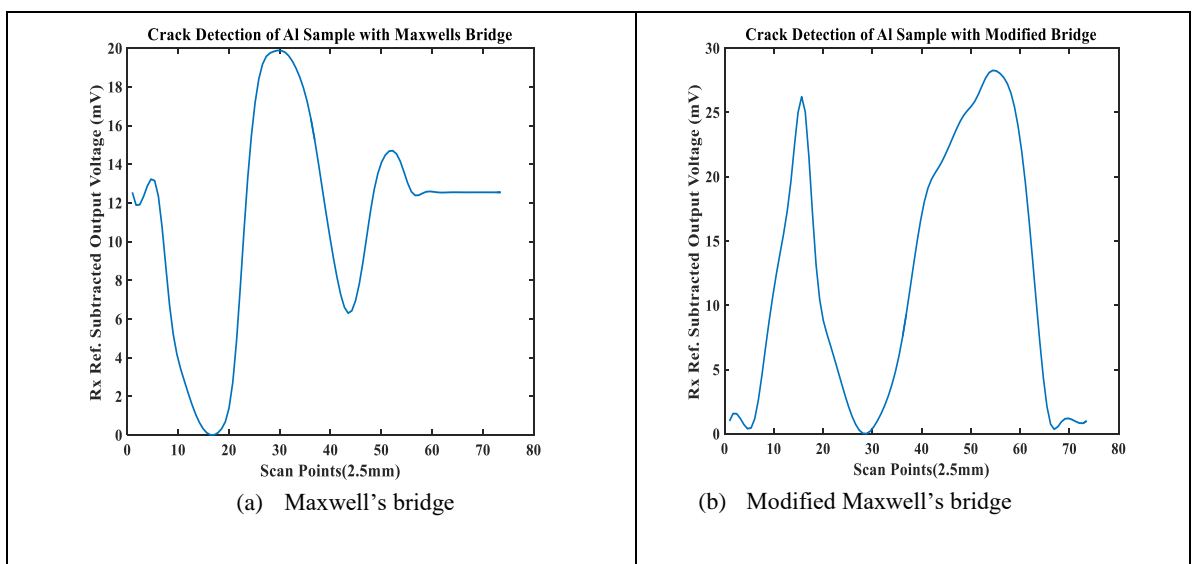


Figure 5.9 Crack detection of the aluminium sample

To explain how the circuits perform in SNR, SNR is defined as a ratio of the impedance change due to the presence of a crack to the output signal. Lift-off noise, self-impedance, the direct

mutual impedance of Tx and Rx coils (offset), and impedance change due to crack on the sample are the components of the output signal. Hence, on the surface of a sample, the output signal is the offset superimposed on the impedance change [184]. Because analysis and quantification of defects mainly depend on the impedance change, the offset signal is equivalent to noise. Hence, signal-to-noise ratio (SNR) is defined as

$$SNR = \frac{Max(Vc)}{Max(Vnc)} \quad (5.14)$$

Where Max (Vc) and Max (Vnc) are the maximum values of the output signal of the sample with and without crack. The experimental SNR and the peak induced signal voltages by Maxwell's bridge and modified Maxwell's bridge signifies higher sensitivity to crack than the conventional Maxwell's bridge.

Table 5.1 SNR and peaks of Maxwell's bridge and modified Maxwell's bridge

	Maxwell Bridge (mV)	Modified Maxwell's bridge (mV)
No Crack	318.50	207.75
Crack	511.50	572.25
SNR	1.61	2.75

5.5 Performance Comparison

The modified circuit has higher SNR and sensitivity to crack detection, especially at high lift-off compared to conventional Maxwell's bridge. However, it is easier to build a link between amplitude features of the output signal crack geometries with Maxwell's bridge than the modified circuit. The modified Maxwell's bridge in comparison to related works also shows improved linearity performance. For instance in the multiplier type bridge interface of [185, 186], the maximum nonlinearity error is 2% of the full scale. A direct microcontroller interface to resistive sensors in bridge form is presented in [187]. The nonlinearity error is 0.3%, but the use of a microcontroller interface is an added cost. A scheme for non-symmetric impedance bridge is presented in [188]. The nonlinearity is 0.4% and also requires special attention on circuit stability. The circuit of [89] is simple and low cost, because only two opamps with passive components are required. However, the maximum linearity deviation (1%) is far more than that of the proposed circuit. The relative error as reported in [189] is about 0.2% but the major limitation is the complexity of the condition circuit. Compared to the mentioned papers, the proposed circuit with maximum linearity deviations between 0.18% and 0.30% has shown improved performance. The simplicity and low cost of the components of the modified Maxwell's bridge is also another advantage.

5.6 Chapter summary

A modified Maxwell's bridge based on the opamp circuit of Tx-Rx PEC probe is proposed and investigated for high lift-off PEC testing. The analysis of three performance metrics of SNR, linearity range and sensitivity at high lift-off for the new signal conditioning circuit has been carried out. It is shown that the modified Maxwell's bridge has a higher SNR of 2.75 against 1.61 for Maxwell's bridge for coil gap 4.00 mm and lift-off 20.00 mm. The lift-off linearity range for the modified Maxwell's bridge is 0.00 mm to 55.00 mm whereas the bridge has 0.00 mm to 15.00 mm. The crack detection by Tx coil based on amplitude change is found to be 27.00 mV for modified Maxwell's bridge against 12.50 mV for Maxwell's bridge while that of Rx coil detection is 23.50 mV for the modified Maxwell's bridge against 9.00 mV Maxwell's bridge. However, it is easier to build a relationship between crack geometry and bridge response based on crack influence shapes than the modified Maxwell's bridge. Also as a result of the modifications, a large impedance change can be measured and amplified by the signal conditioning circuit as self-impedance of Rx coil has been removed. Small linearity range of conventional Maxwell's bridge is extended with improved sensitivity. The modified Maxwell's bridge hence has good measurement accuracy. Finally, the circuit becomes much simpler and cost-effective and no bridge balancing is needed. In the next chapter different excitation signals are studied and compared based on the modified Maxwell's bridge for crack quantitative non-destructive evaluation (QNDE) at high lift-off.

Chapter 6. Selection of Excitation Mode for High Lift-off Inspection

In chapter 5, a signal conditioning approach has been used to improve SNR at high lift-off by removing the offset caused by self-impedance of the Rx coil through a modified Maxwell's bridge. Because high lift-off inspection is prone to noise, high SNR excitation mode is also required for such application. However, each type of excitation modes presents merits and demerits that prevent the selection of an absolute best excitation mode. In this chapter, different excitation modes including single frequency, multi-frequency, sweep-frequency and pulse excitations are reviewed. From the review, PEC and SFEC were comparatively studied to ascertain their performances for defect quantification at high lift-off. Experiments were used for this study in crack detection and quantitative non-destructive evaluation QNDE of aluminium sample. Pulse features show more linear relationship with depth cracks whereas SFEC is better for crack detection at high lift-off.

6.1 Introduction

Excitation modes used to interrogate test samples are essential part of EC testing system. The SNR of the system depends much on the type of excitation mode used in specific applications such as high lift-off inspection. Commonly used EC excitation modes for NDT&E are single frequency, multi-frequency, sweep-frequency and pulse [12]. Many researchers are engaging in the development of EC excitation modes capable of providing as much information as possible about the presence, the location, and the geometry of defects. Signals characterized by a wide spectral content capable of penetrating different layers of material under test are gradually replacing the classical sinusoidal excitation approach, using either single frequency at different times or multiple frequencies at a time [13, 120, 190, 191]. The detection and quantification of defects like crack depth at high lift-off is one of the major challenges of EC testing. This is because the combined effects of high lift-off and crack depth makes the interpretation of the response signal difficult. Furthermore, at high lift-off, the impedance change of transmitter- receiver (Tx-Rx) probe as may be caused by cracks becomes minimal, making crack depth measurement a challenge. Hence excitation mode that possess high SNR, and signal strength are required for high lift-off defect detection and QNDE. However, each type of excitation mode presents merits and demerits that prevent the choice of an absolute best excitation mode. Performance of excitation modes in EC testing also depends significantly on frequency components of the excitation mode and lift-off [90]. For instance Single frequency EC sinusoidal excitations for a single-coil probe lose sensitivity beyond 5mm lift-off [109]. The aim of selecting appropriate excitation mode is for the EC system to provide as much

information as possible about the presence and geometry of defects for a specific application. In the case of lift-off dependent inspection like thick insulated structures or weld areas, signals with wide spectral content are required for different lift-off inspection. This is because different optimal frequency excitations are needed to detect quantification at different lift-off values [192]. Hence EC signals are analysed in the frequency domain to enhance defect characterization by providing an additional dimension of information to traditional phasor measurements at a single excitation frequency. The Sweep Frequency Eddy Current (SFEC) excitation mode offers high precision and broad bandwidth. However, for higher spectral resolution and accuracy requirements, the sweep duration is longer, leading to lengthy inspection times [100]. A solution to this problem might be multi-frequency (MUF) EC when the excitation signal contains several frequency components. Implementation of such an excitation becomes increasingly sophisticated with a growing number of desired frequencies [193]. Pulse Eddy Current (PEC) technique, where the Tx-Rx probe is excited with a pulse, mitigates the broad-band excitation challenge. The PEC technique which is mainly a time-domain method uses different time-domain features for defect detection and quantification. Such features include peak amplitude, the time to peak, the peak height, rising point and zero crossings. Advanced signal analysis techniques are needed in order to extract test case related features from a time-domain PEC signal, for example principal component analysis PCA for PEC [107, 132, 194-197]. Hence, there have been efforts to facilitate PEC response interpretation by frequency domain analysis. Different defect types or sizes will require that different amounts of the total field have to be affected in order to be able to detect the defects. For instance in Tx-Rx probe, the mutual inductance of Tx coil, Rx coil, and test sample at a given lift-off and coil gap depends on excitation mode and frequency. And certain amount of mutual inductance has to be attained before defects can be detected [69]. Also the prospect of defect quantification through a simple procedural change without need for complex signal processing is a valuable complementary technique for any ECT method. Based on these requirements, pulse and sweep-frequency excitation modes for quantification of crack at high lift-off is experimentally studied and compared. The factors analysed and compared are crack detection at high lift-off, SNR and QNDE capability.

6.2 Experimental Studies

The experimental study is based on the system diagram of figure 6. 1. It is divided into two categories namely, the data acquisition section and the data processing section. The data acquisition section comprises the control unit (PC) used to generate the excitation signal, the probe, x-y scanner, test sample and the signal conditioning circuit. The PC is connected to a

movable platform called the x-y scanner through the controller of the scanner. The Tx-Rx probe is also attached to the x-y scanner. The scanning is line scan and once the probe position is determined, the PC then sends a trigger signal to the x-y scanner controller and an excitation signal is sent to the sample under test (SUT) via the Tx-Rx probe. The x-y scanner then scans the sample while data is captured through the signal conditioning circuit by the PC. The captured raw data is then sent to the data processing unit which is made up of data acquisition system and Matlab software in the PC. Once the data acquisition and storage are completed, the data processing unit processes the data and the features are extracted through quantitative and qualitative analysis. QNDE methods are then used for defect evaluation and characterization. This process is carried out using the pulse and sweep-frequency excitation modes one after the other and their performances are compared based on SNR, QNDE and crack depth detection at different lift-offs for different crack depths.

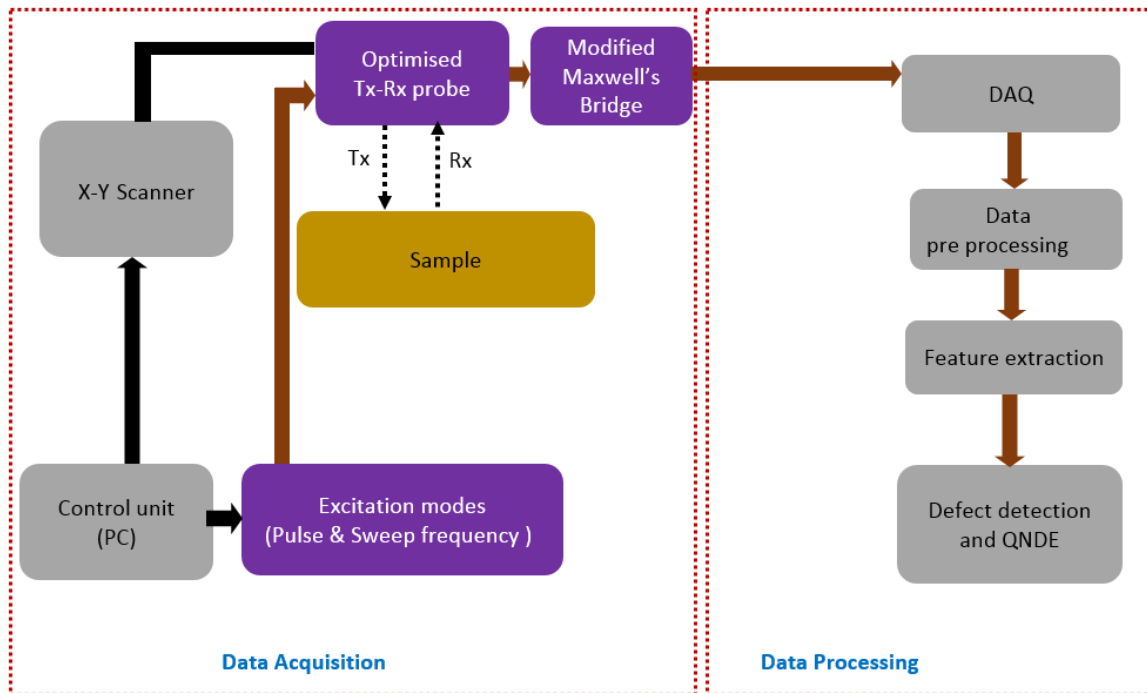


Figure 6.1 System block diagram for the study

6.3 Experimental Setup and Samples

Two identical, rectangular coils were used as Tx-Rx coils as the EC probe for scanning the sample under test. The two coils were configured and connected to the measurement circuit via the signal conditioning box to the PC as shown in Figure 6.2. A coil gap of 2mm between Tx-Rx was used and the probe was placed at lift-off of 5mm and increased to 15mm at a step of 5mm above the sample without crack to generate reference signal and then with sample bearing

artificial cracks. At each lift-off, the sample is scanned at a scan step of 2.5 mm interval for 99 scan points covering a distance of 245 mm of the sample length. For each scan point of the sample along the scan-axis, Rx output was captured and recorded by the PC using Matlab software. The pulse excitation signal is set at 4V Peak to Peak, 1 kHz frequency, 20 μ s bandwidth, and 8.4ns rise and fall time. Matlab software was used for data processing and feature extraction. Reference subtracted amplitude features were extracted from the Rx output, mapped and compared with dedicated crack parameters. Reference subtracted signal is the difference between the amplitude of sample with crack and sample without crack. After testing the sample with pulse excitation, sweep-frequency excitation was also used to repeat the same process as pulse signal. Sweep-frequency signal was set at 4Vpeak to peak with start frequency of 1 kHz to match with the fundamental frequency of the pulse signal. The frequency was increased to 200 kHz at a step of 5 kHz for every scan point and the acquired data were processed exactly as in pulse excitation using same Matlab software.

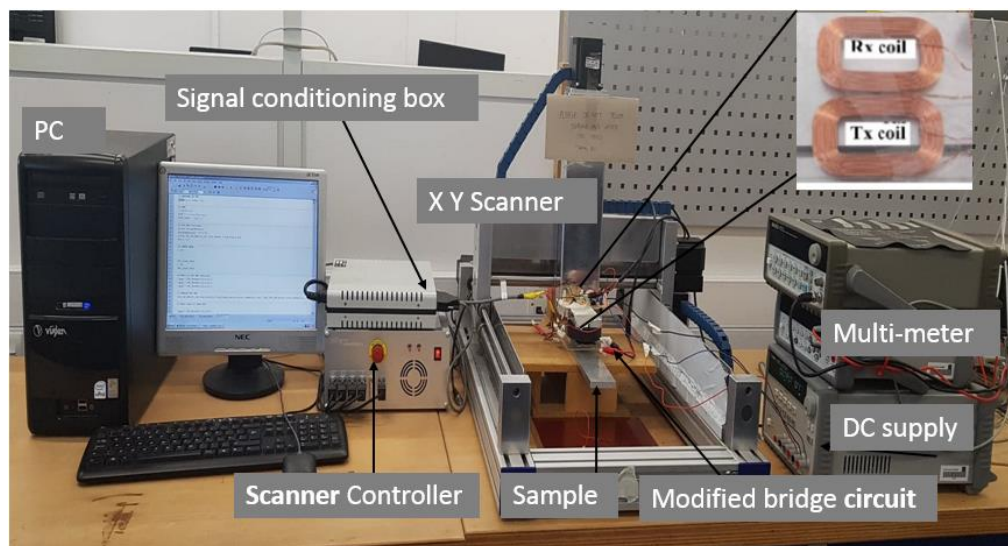


Figure 6.2 Experimental setup

Figure 6.3 shows the Aluminium (Al) sample used for the testing. The Al sample has a 50mm width by 300mm length by 10mm height with four different artificial surface cracks. The cracks are 2 mm, 4mm, 6mm, and 8mm deep and each having 3.3 mm width along the scan side. The probe was made up of two identical wire-wound rectangular spiral coils, one for Tx coil and the other for Rx coil. Each coil was made up of 15 turns of 26 AWG Cu-wire with 36mm length by 25mm width. The scan dimensions and directions including distance between cracks are shown in figure 6.4. The cracks on the sample are scanned as surface crack. That is the openings of the cracks are facing the probe so as to study the combined influence of lift-off and crack depth on the response signal. This makes the study simple as the lift-off influence and crack depth with less influence of the sample thickness are investigated.



Figure 6.3 Aluminium test sample with artificial cracks

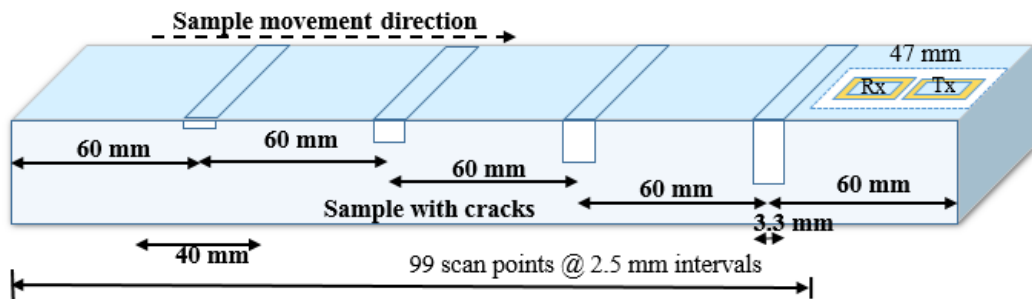


Figure 6.4 Sample and scan dimensions

6.4 Results and Discussion

The experimental results are presented and discussed under lift-off influence on response signals of the excitation modes. After which the time-domain performance of PEC is presented and explained along with the SFEC in crack depth detection and quantification. This is followed by the frequency domain performance of PEC also along with SFEC. Then the SNR for both excitation modes are discussed

6.4.1 Influence of lift-off on Rx time domain response of PEC and SFEC

The influence of lift-off on Rx time-domain response for PEC and SFEC without defect is shown in figure 6.5. The optimal lift-off for the chosen coil gap of 2mm for both PEC and SFEC is at 15mm. However, at all the lift-off values the amplitude of SFEC is greater than that of the PEC in time domain. This can be explained as, due to the SFEC signal contains sinusoidal tones with equal amplitude distribution [102]. Whereas in PEC, amplitudes of frequency components decrease with increasing frequency.

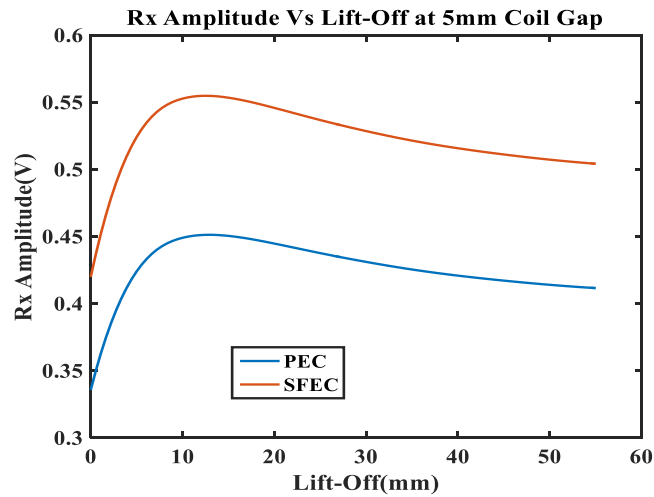


Figure 6.5 Lift-off influence of PEC and SFEC at fixed Coil gap

6.4.2 PEC time domain and SFEC crack detection at different Lift-offs

The time domain amplitude of PEC and SFEC amplitude as performance indicator calculated by subtracting the reference signal from the output signal is to detect the crack position as indicated with red circles of figure 6.6. From figure 6.6, it can be seen that the output of both excitation modes detects the crack with decreasing amplitude as lift-off increases. However, output of SFEC is higher in amplitude for each of the cracks as shown in table 6.1.

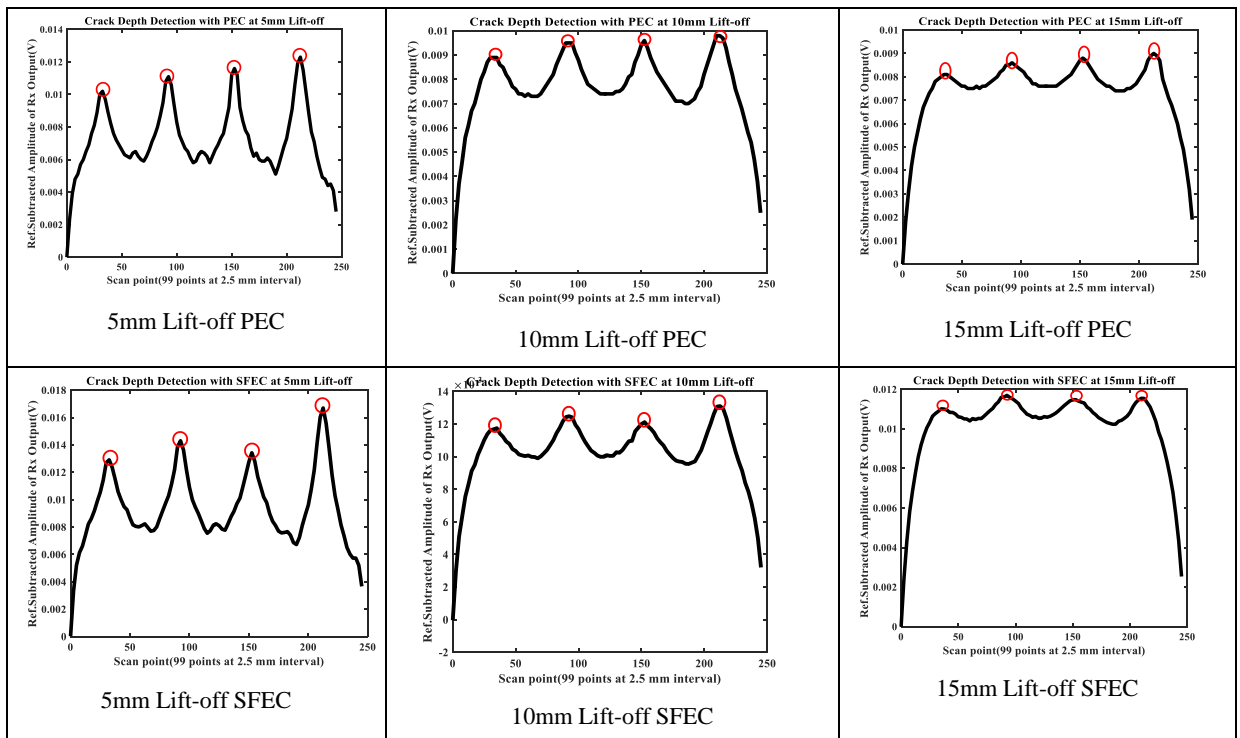


Figure 6.6 Crack detection of PEC and SFEC at different Lift-offs

Table 6.1 Performance of PEC and SFEC in crack depth detection

Crack depth (mm)	Excitation mode & Signal Amplitude (V)	
	PEC	SFEC
2	0.0102	0.0129
4	0.0111	0.0143
6	0.0116	0.0134
8	0.0112	0.0167

For table 6.1, at 5mm lift-off scan, PEC and SFEC give the following outputs for the crack depths (2mm crack depth, PEC = 0.0102V, SFEC=0.0129V), (4mm crack depth, PEC= 0.0111V, SFEC= 0.0143V), (6mm crack depth, PEC= 0.0116V, SFEC= 0.0134V), (8 mm crack depth, PEC= 0.0112V, SFEC= 0.0167V). However, in mapping of the crack depth to the response signal, the PEC performs better as explained in next section.

6.4.3 QNDE of crack depths with PEC and SFEC at different lift-offs

The relationship between the response signal of PEC and SFEC, and crack depth is shown in Figure 6.7. Although the amplitude change of SFEC is higher at every scan lift-off, PEC response is more linearly mapped to crack depth at lower lift-offs. However, as the lift-off increases, the response signals for both excitation modes show almost the same deviation from linearity with crack depth variation as can be seen in figure 6.7. This is due to the degrading SNR as lift-off increases which distorts the response signal.

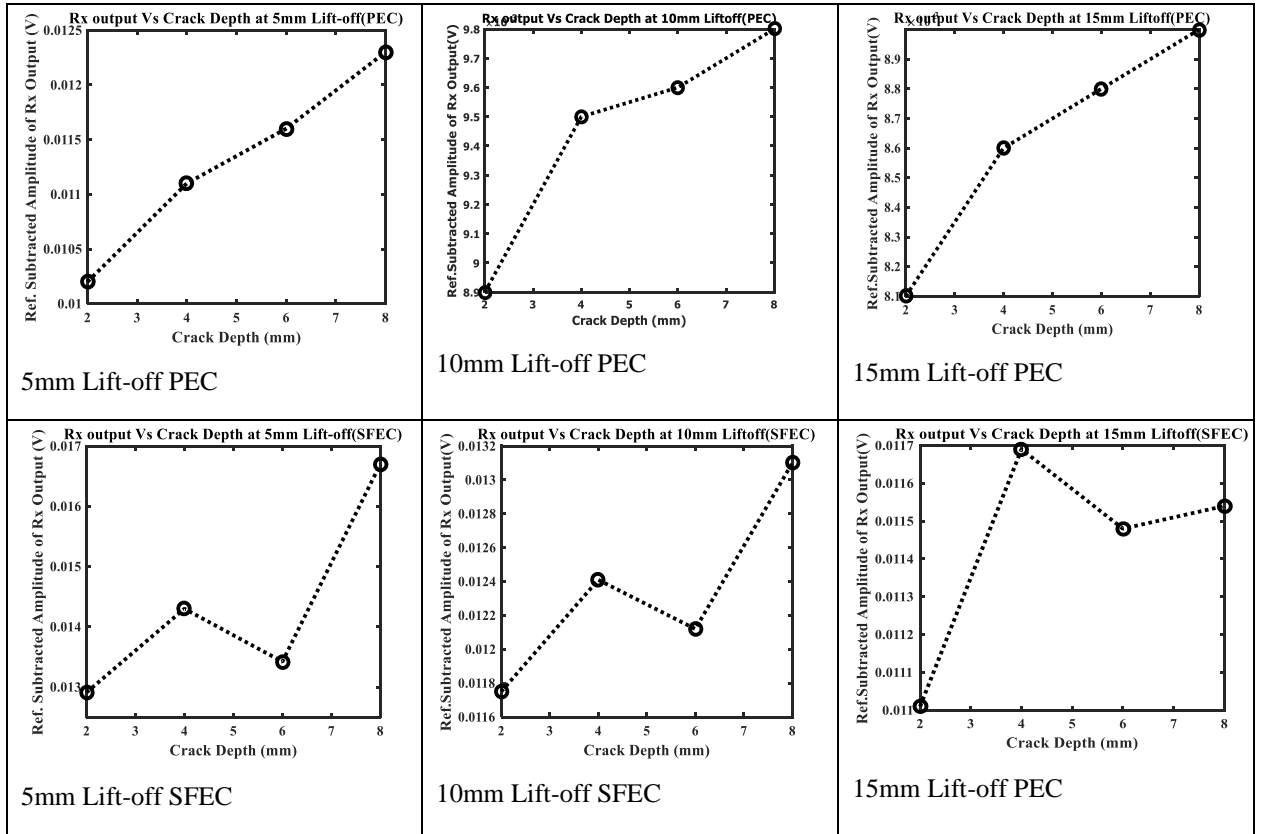


Figure 6.7 Crack depth mapping of PEC and SFEC responses at different Lift-offs

During the experiments the repeatability of the measurements was verified. Six repeated measurements of the crack depth for the four cracks are taken for both PEC and SFEC as shown in tables 6.2 and 6.3 respectively. Repeatability error (r) is then calculated by the formula $r = 2(2)^{1/2}\sigma$ where σ is the standard deviation [198]. It can be observed from table 6.2 that the percentage errors of measurements for both PEC and SFEC do not exceed 1%. Such repeatability is very important from the point of view of accuracy of the results. However, it is indicated that the crack depth measurement results of the PEC method have a better repeatability than the SFEC. The vibration effect of the scanning system and measurement errors due to the weak coupling of Tx and Rx coils could have led to the poor repeatability of the SFEC.

Table 6.2 Repeatability of PEC measurements

Crack depth (mm)	1st	2nd	3rd	4th	5th	6th	Repeatability Error (%)
2	0.0102	0.0130	0.0102	0.0092	0.0104	0.0105	0.36
4	0.0111	0.0121	0.0109	0.0138	0.0091	0.0110	0.44
6	0.0116	0.0109	0.0091	0.0104	0.0131	0.0128	0.43
8	0.0123	0.0115	0.0144	0.0104	0.0135	0.0130	0.41

Table 6.3 Repeatability of SFEC measurements

Crack depth (mm)	1st	2nd	3rd	4th	5th	6th	Repeatability Error (%)
2	0.0139	0.0137	0.0141	0.0098	0.0120	0.0124	0.46
4	0.0133	0.0129	0.0149	0.0126	0.0091	0.0145	0.58
6	0.0138	0.0141	0.0093	0.0132	0.0121	0.0120	0.50
8	0.0167	0.0176	0.0161	0.0151	0.0144	0.0149	0.34

6.4.4 PEC Frequency Domain Vs SFEC Crack Detection

The frequency-domain responses of PEC and SFEC are shown in figure 6.8. The one sided fast Fourier transformed PEC indicated that only the low-frequency components are of significant amplitude while the high-frequency components decays to almost zero as in figure 6.8a. On the other hand the SFEC possess an optimal frequency after which the amplitude decays as in figure 6.8b. The influence of lift-off on one-sided Fourier transform PEC signal shown in figure 6.8c. The optimal frequency of SFEC slightly depends on lift-off because the mutual inductance of Tx-Rx probe varies with lift-off and also coil gap. Hence for every lift-off there is an optimal frequency as shown in figure 6.8d.

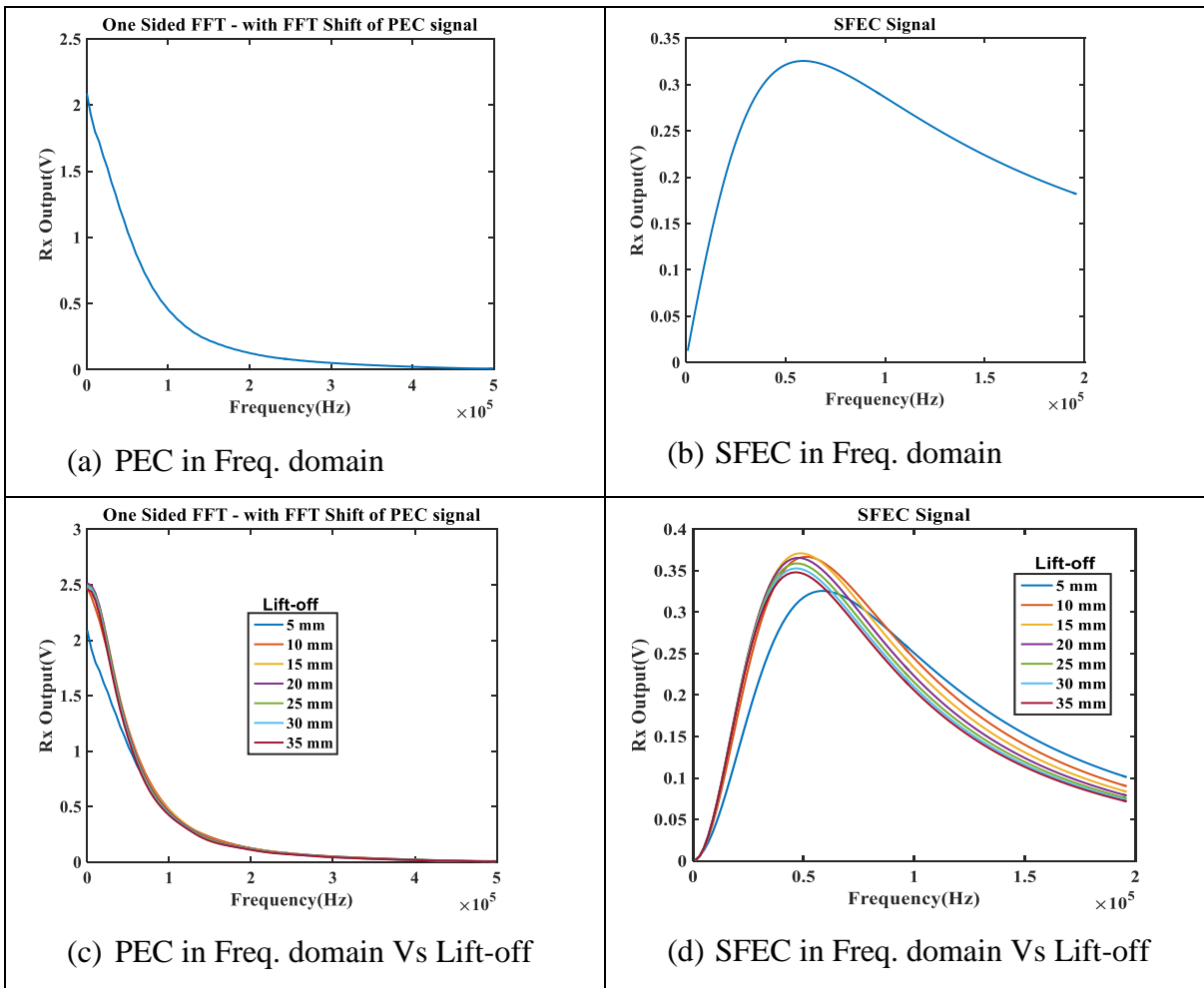


Figure 6.8 Frequency domain response of PEC and SFEC

Figure 6.9 shows the result of crack depth detection of PEC in the frequency domain. There are peaks at crack positions and a trough at the centre position of the sample which coincide so closely with the variation of lift-off. The peak amplitude of the PEC signal changes with the variation of the defect depth. As the lift-off increases the trough becomes higher while the amplitude change due to crack depth becomes smaller. The explanation is that the PEC peak amplitude is influenced differently by both crack depth and lift-off. However, the peak amplitude of the PEC signal is not linearly mapped to crack depth variation as depicted by SFEC. This may be due to combined effect of lift-off and crack depth. Hence it is possible to separate the influence of lift-off on PEC response in frequency domain than in time domain.

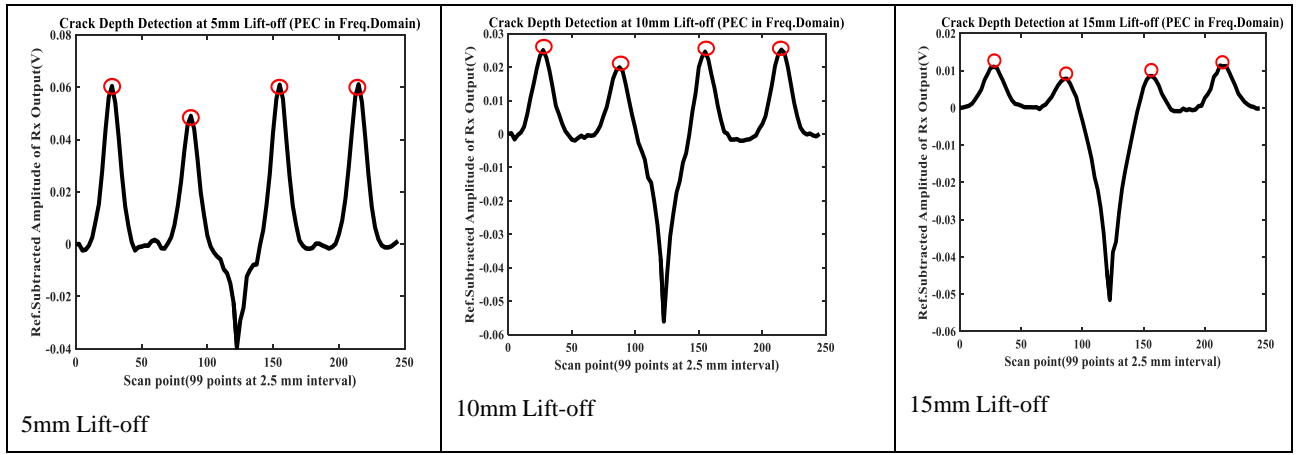


Figure 6.9 Crack depth detection of PEC based on frequency domain.

6.5 Performance evaluation and Comparison

Generally, the frequency domain signals show higher SNR compared to time domain signal of PEC. The SNR also decreases with increase in lift-off for all the excitation modes. In time domain, the PEC excitation mode has higher SNR to crack detection at low lift-off than at high lift-off. In frequency domain, PEC shows more SNR than in time domain. However, SFEC and frequency domain PEC show better detection capability of crack both at low and high lift-offs but lacks linearity mapping of response to crack depth variation. To build a link between amplitude features of the output signal to crack depth, the PEC mode in time domain is therefore preferable to SFEC. But for crack detection especially at high lift-off, frequency domain signals performed better than time domain signal of PEC.

To explain how the excitation modes perform in SNR, SNR is defined as a ratio of the Voltage amplitude change due to the presence of a crack to the output signal. Lift-off noise and impedance change due to crack on the sample are the components of the output signal. Hence, on the surface of a sample, the output signal is the lift-off noise superimposed on the impedance (or voltage) change. Because analysis and quantification of defects mainly depend on the impedance change, the (SNR) is defined as

$$SNR = \frac{Max(Vc)}{Max(Vnc)} \quad (6.1)$$

Where Max (Vc) and Max (Vnc) are the amplitudes of the response signal of the sample with and without crack respectively. The experimental SNR the peak induced signal voltages by PEC and SFEC is hence calculated and shown in the table 6.4 below in addition to crack detection and QNDE performances of the modes.

Table 6.4 Comparison of PEC and SFEC performances for high lift-off (Lo) testing

Lo (mm)	SNR			Crack depth detection limit (mm)			QNDE		
	PEC		SFEC	PEC		SFEC	PEC		SFEC
	Time domain	Freq. domain	Freq. domain	Time domain	Freq. domain	Freq. domain	Time domain	Freq. domain	Freq. domain
5	1.05	1.95	1.88	2	2	2	high	low	low
10	1.04	1.86	1.85	2	2	2	high	low	low
15	1.03	1.83	1.84	4	2	2	high	very low	low

6.6 Chapter Summary

This chapter presents a comparative review of different EC excitation modes and studied the performances of two of the excitation modes including PEC and SFEC in high lift-off crack depth detection and quantification. Specifically, a discussion on the merits and demerits of different excitation modes and their various applications were reviewed. Details of the experimental set up and material samples with defects were presented for the comparative study. The major comparison factors are SNR, crack depth detection limit and QNDE performance of the two modes at different lift-offs. PEC response were analysed in both time domain and frequency domain and compared with SFEC; reason being that for the mutual inductance based Tx-Rx probe, defect detection and quantification capability at a given lift-off depends on frequency components of the excitation mode. From the experimental results, PEC in time domain performed better for crack depth quantification at low lift-off. Whereas, PEC in frequency domain performed better than SFEC in crack detection at high lift-off. One can therefore conclude that combined features of PEC response in time domain and frequency domain can used in crack depth detection and quantification at lift-off high lift-off. Whereas the SFEC can be used in crack depth detection at high lift-off. Among other things the study brought to light the better SNR of PEC in time domain compared to SFEC at tested lift-offs. However, the above conclusions are based on the particular experimental setup used in this study. The spatial resolution of the scanning system and the samples available for this particular study are the limitations of this setup, otherwise, it would have been possible to estimate the crack depths with the PEC even at a higher lift-off. Therefore defect quantification at high lift-off is an area of the proposed research that needs more investigation.

Chapter 7. Conclusion and Further Work

In this chapter, the research is summarised based on the simulations and the experimental studies. Conclusions are drawn from the potentials of the mutual inductance based Tx-Rx EC probe for high lift-off inspection. The chapter then concludes by presenting the future work in terms of improving the system QNDE capability and extension of inspection lift-off as required by harsh environment like high temperature.

7.1 Research Conclusions

A review of electromagnetic NDE techniques for defect detection and characterization has been conducted. Major benefits and limitations of these techniques and the potential for high lift-off inspections have been assessed. High lift-off inspection arising from thick insulated or buried structure and weld areas using mutual inductance based Tx-Rx EC probe has been investigated. The investigation reveals that both coil gap and lift-off have significant effects on the resultant mutual inductance, hence the sensitivity of Tx-Rx EC probe above a metallic conductor. In effect, the optimisation of these two parameters (coil gap and lift-off) provides a technique that can be used to fix a Tx-Rx coil gap for a given lift-off requirement.

- The finding becomes valuable in the inspection of buried or thick insulated structures and weld zones where high lift-off is a major requirement. Also for a varied lift-off inspection, the coil gap can be controlled to achieve the optimal lift-off as the inspection lift-off varies like in structures with varied insulation thickness.
- This technique can be used in the design and development of a printed circuit Tx-Rx EC probe for a specific lift-off application by fixing the coil gap on the printed circuit board that is optimal for the required lift-off.
- This approach can be put into practical use in internal pipeline inspection where weld joints determine the inspection lift-off. In such a case, the coil gap is fixed based on the lift-off resulting from the thickness of the weld. The Tx and Rx coils are also made small so that the curvature of the pipe surface will not have significant effect on the response signal.

The influence of self-impedance of the Rx coil on SNR was investigated. A modified Maxwell's bridge to eliminate the influence of Rx self-impedance has been designed and investigated for high lift-off inspection. The circuit improved SNR by at least 1.14 compare to conventional AC bridge circuit as shown in table 5.1. The modified circuit was evaluated by crack detection of aluminium sample at a lift-off 30mm and compared with the conventional Maxwell's inductance bridge in terms of SNR and linearity range. The approach provides a means of

improving linearity range and reduction of measurement errors associated with the conventional AC bridges. Also, the need for balancing AC bridges is eliminated.

- The method is useful for signal conditioning of sensing system that is prone to low SNR. The dominating offsets in the response signal can be removed with such circuit thereby making the output signal proportional to the measured parameter change only.

Performance of different EC excitation modes was studied for high lift-off inspection. The study demonstrated that each type of excitation modes presents merits and demerits that prevent the choice of an absolute best excitation mode. Hence, selection of best excitation mode depends on specific applications. After review of excitation modes, PEC and SFEC were selected and comparatively study for crack depth detection and quantification at high lift-off. Experiments for estimation of crack depth at high lift-off are carried out for both excitation modes. Pulse features show more linear relationship with depth cracks. Whereas, SFEC is better for cracks detection at high lift-off.

- The comparative study of the excitation modes reveals the different performances of PEC in time and frequency domains for high lift-off testing in terms of crack depth detection and quantification. Selection of time or frequency domain analysis of PEC based on the priority of defect detection or QNDE
- Also, the study demonstrated more enhancements in high lift-off inspection with Tx-Rx excitation mode selection in comparison to single-frequency mode with limited lift-off of 5mm (a big challenge in EC testing system)

However, the conclusions drawn from this study are based on the simulation and experimental setups used in the investigations. These includes optimisation of the Tx-Rx probe through numerical simulation with Comsol Multiphysics software and the simple experimental setup as explained in chapter 4. Also the investigation of a modified Maxwell's bridge in chapter 5 is based on a simple opamp front-end signal conditioning. Lastly in chapter 6, the optimised probe and the modified Maxwell's bridge are integrated and used for pulse and sweep frequency excitations comparison and QNDE of crack depths.

7.2 Future work Suggestions

The proposed work has shown promising results in defect detection and characterization at high lift-off resulting from thick insulated structures, buried structures or weld zones. Even with the improved results of this approach, there are many other ways to improve system performance.

Feature extraction and defect quantification though not addressed in this work are worth considering and exploring with Tx-Rx probe measurements. In order that the improved SNR at high lift-off achieved in this research work can be extended to defect quantification. Future work in this area based on the Tx-Rx probe system will be geared towards the improvement of the system to have an integrated NDT&E approach that can be used for varied lift-off or for ultra-high lift-off inspections as required in harsh environment like high temperature. Such application can be found in nuclear station where hot storage tanks are to be inspected at lift-off of more than 80cm. Complex geometries such as changing pipe diameters due to multi-diameter pipeline structure are also unavoidable in practice. And these geometries are characterized with some weld joints, amongst others. The limited lift-off of the current EC system is a serious concern as high lift-off requirements limits the EC applications

In terms of probe enhancement for improvement of lift-off sensitivity, there are several parameters of Tx-Rx probe that could be enhanced and optimised. The Tx-Rx probe approach allows greater flexibility in design. This is because with Tx-Rx probes containing separate excitation and receive coils, Tx and Rx parts of the EC system including Tx and Rx coils can be separately designed and optimised for specific applications. Also coil size, shape, orientation, lift-off and separation of Tx-Rx coils (coil gap) are all parameters that could be optimized. The mitigation of direct mutual coupling interference between Tx and Rx coils can be extended to flexible EC sensor array for complex geometry inspection. With flexible EC sensor array selected excitation frequency mode can be applied to enhance crack detection especially in areas where surface scanning is difficult and the probe is required to be in a fixed position.

Signal conditioning and excitation modes optimisation is another area that can be explored. For signal conditioning wireless power approaches are currently being used to improve coupling by increasing current at resonance. The technique could be used to improve signal strength at high lift-off. Nonlinear- parity-time-symmetric circuitry could be explored to improve signal strength at high lift-off. This is because in our study of coil gap and lift-off optimisation, the optimal lift-off could be increased by increasing the coil gap but sensitivity reduces. With the Nonlinear parity-time-symmetric technique, as the coil gap increases the Rx received voltage decreases but the circuit keeps compensating for the decrease in the received voltage. Compressed pulse excitation and code modulated excitation modes are currently being explored for different applications. The interference between the Tx and Rx coils is a challenge that could be tackled with excitation modes modifications. The prospect of detection and characterisation

of defect via a simple procedural parameter change, without the need for complex data processing is a valuable complementary technique to any EC system.

References

- [1] D. E. Bray, and R. K. Stanley, *Nondestructive evaluation: a tool in design, manufacturing and service*: CRC press, 2014.
- [2] M. Fallahpour, J. T. Case, M. T. Ghasr, and R. Zoughi, "Piecewise and Wiener Filter-Based SAR Techniques for Monostatic Microwave Imaging of Layered Structures," *IEEE Transactions on Antennas and Propagation*, vol. 62, no. 1, pp. 282-294, 2014.
- [3] Z. Liu, and Y. Kleiner, "State of the art review of inspection technologies for condition assessment of water pipes," *Measurement*, vol. 46, no. 1, pp. 1-15, 2013.
- [4] E. H. A. Duisterwinkel, E. Talmishnikh, D. Krijnders, and H. J. Wörtche, "Sensor Motes for the Exploration and Monitoring of Operational Pipelines," *IEEE Transactions on Instrumentation and Measurement*, vol. 67, no. 3, pp. 655-666, 2018.
- [5] R. E. Malkin, A. C. Franklin, R. L. T. Bevan, H. Kikura, and B. W. Drinkwater, "Surface reconstruction accuracy using ultrasonic arrays: Application to non-destructive testing," *NDT & E International*, vol. 96, pp. 26-34, 2018/06/01/, 2018.
- [6] H. Q. Pham, B. V. Tran, D. T. Doan, V. S. Le, Q. N. Pham, K. Kim, C. Kim, F. Terki, and Q. H. Tran, "Highly Sensitive Planar Hall Magnetoresistive Sensor for Magnetic Flux Leakage Pipeline Inspection," *IEEE Transactions on Magnetics*, pp. 1-5, 2018.
- [7] J. Feng, F. Li, S. Lu, J. Liu, and D. Ma, "Injurious or Noninjurious Defect Identification From MFL Images in Pipeline Inspection Using Convolutional Neural Network," *IEEE Transactions on Instrumentation and Measurement*, vol. 66, no. 7, pp. 1883-1892, 2017.
- [8] Nurmalia, N. Nakamura, H. Ogi, and M. Hirao, "EMAT pipe inspection technique using higher mode torsional guided wave T(0,2)," *NDT & E International*, vol. 87, pp. 78-84, 2017/04/01/, 2017.
- [9] M. P. Papaelias, M. C. Lugg, C. Roberts, and C. L. Davis, "High-speed inspection of rails using ACFM techniques," *NDT & E International*, vol. 42, no. 4, pp. 328-335, 2009.
- [10] J. R. Bowler, and N. Bowler, "Theory of four-point alternating current potential drop measurements on conductive plates," *Proceedings of the Royal Society of London A: Mathematical, Physical and Engineering Sciences*, vol. 463, no. 2079, pp. 817-836, 2007-03-08 00:00:00, 2007.
- [11] J. García-Martín, J. Gómez-Gil, and E. Vázquez-Sánchez, "Non-destructive techniques based on eddy current testing," *Sensors*, vol. 11, no. 3, pp. 2525-2565, 2011.
- [12] D.-G. Park, C. S. Angani, B. P. C. Rao, G. Vértesy, D.-H. Lee, and K.-H. Kim, "Detection of the subsurface cracks in a stainless steel plate using pulsed eddy current," *Journal of Nondestructive Evaluation*, vol. 32, no. 4, pp. 350-353, 2013.
- [13] G. Yang, A. Tamburrino, L. Udpa, S. S. Udpa, Z. Zeng, Y. Deng, and P. Que, "Pulsed eddy-current based giant magnetoresistive system for the inspection of aircraft structures," *IEEE transactions on magnetics*, vol. 46, no. 3, pp. 910-917, 2009.
- [14] A. Yin, B. Gao, G. Yun Tian, W. L. Woo, and K. Li, "Physical interpretation and separation of eddy current pulsed thermography," *Journal of Applied Physics*, vol. 113, no. 6, pp. 064101, 2013.
- [15] G. Tian, Y. Gao, K. Li, Y. Wang, B. Gao, and Y. He, "Eddy current pulsed thermography with different excitation configurations for metallic material and defect characterization," *Sensors*, vol. 16, no. 6, pp. 843, 2016.
- [16] Y.-K. Zhu, G.-Y. Tian, R.-S. Lu, and H. Zhang, "A review of optical NDT technologies," *Sensors*, vol. 11, no. 8, pp. 7773-7798, 2011.
- [17] Y. He, G. Y. Tian, M. Pan, D. Chen, and H. Zhang, "An investigation into eddy current pulsed thermography for detection of corrosion blister," *Corrosion Science*, vol. 78, pp. 1-6, 2014.
- [18] C. Xu, X. Gong, W. Zhang, and G. Chen, "An investigation on eddy current pulsed thermography to detect surface cracks on the tungsten carbide matrix of polycrystalline diamond compact bit," *Applied Sciences*, vol. 7, no. 4, pp. 429, 2017.
- [19] D. Huang, K. Li, G. Y. Tian, A. I. Sunny, X. Chen, C. Tang, J. Wu, H. Zhang, and A. Zhao, "Thermal pattern reconstruction of surface condition on freeform-surface using eddy current pulsed thermography," *Sensors and Actuators A: Physical*, vol. 251, pp. 248-257, 2016.
- [20] P. Jianping, Z. Kang, Y. Kai, H. Zhu, Z. Yu, P. Chaoyong, and G. Xiaorong, "The early stage wheel fatigue crack detection using eddy current pulsed thermography," *AIP Conference Proceedings*, vol. 1806, no. 1, pp. 100010, 2017.

- [21] D. Ayala–Cabrera, M. Herrera, J. Izquierdo, S. J. Ocana–Levario, and R. Pérez–García, “GPR-based water leak models in water distribution systems,” *Sensors*, vol. 13, no. 12, pp. 15912-15936, 2013.
- [22] P. G. G. Slaats, G. A. M. Mesman, L. P. M. Rosenthal, and H. Brink, “Tools to monitor corrosion of cement-containing water mains,” *Water science and technology*, vol. 49, no. 2, pp. 33-39, 2004.
- [23] Z.-y. Han, Y. Han, and W.-m. Zheng, “The Design of a High Speed Real-time and Fixed-point FFT Processor [J],” *Journal of Circuits and Systems*, vol. 1, pp. 004, 2002.
- [24] L. Li, A. E.-C. Tan, K. Jhamb, and K. Rambabu, “Buried object characterization using ultra-wideband ground penetrating radar,” *Microwave Theory and Techniques, IEEE Transactions on*, vol. 60, no. 8, pp. 2654-2664, 2012.
- [25] F. Parrini, M. Fratini, M. Pieraccini, C. Atzeni, G. De Pasquale, P. Ruggiero, F. Soldovieri, and A. Brancaccio, "ULTRA: Wideband ground penetrating radar 2006 European Radar Conference." pp. 182-185.
- [26] S. Nounouh, K. Haddadi, and T. Lasri, “Cancellation technique for CW ground penetrating radar applications,” *IEEE Microwave and Wireless Components Letters*, vol. 25, no. 5, pp. 343-345, 2015.
- [27] M. Li, R. Birken, N. X. Sun, and M. L. Wang, “Compact slot antenna with low dispersion for ground penetrating radar application,” *IEEE Antennas and Wireless Propagation Letters*, vol. 15, pp. 638-641, 2015.
- [28] A. De Coster, and S. Lambot, “Full-Wave Removal of Internal Antenna Effects and Antenna–Medium Interactions for Improved Ground-Penetrating Radar Imaging,” *IEEE Transactions on Geoscience and Remote Sensing*, vol. 57, no. 1, pp. 93-103, 2018.
- [29] H. G. Ramos, and A. L. Ribeiro, “Present and future impact of magnetic sensors in NDE,” *Procedia Engineering*, vol. 86, pp. 406-419, 2014.
- [30] Y. Sun, S. Liu, R. Li, Z. Ye, Y. Kang, and S. Chen, “A new magnetic flux leakage sensor based on open magnetizing method and its on-line automated structural health monitoring methodology,” *Structural Health Monitoring*, vol. 14, no. 6, pp. 583-603, 2015.
- [31] G. Kopp, and H. Willems, “Sizing limits of metal loss anomalies using tri-axial MFL measurements: A model study,” *NDT & E International*, vol. 55, pp. 75-81, 4//, 2013.
- [32] W. Han, J. Xu, P. Wang, and G. Tian, “Defect Profile Estimation from Magnetic Flux Leakage Signal via Efficient Managing Particle Swarm Optimization,” *Sensors*, vol. 14, no. 6, pp. 10361, 2014.
- [33] M. R. Kandroodi, B. N. Araabi, M. M. Bassiri, and M. N. Ahmadabadi, “Estimation of depth and length of defects from magnetic flux leakage measurements: verification with simulations, experiments, and pigging data,” *IEEE Transactions on Magnetics*, vol. 53, no. 3, pp. 1-10, 2016.
- [34] D. L. Atherton, “Magnetic inspection is key to ensuring safe pipelines,” *NDT and E International*, vol. 1, no. 30, pp. 40, 1997.
- [35] T. Azizzadeh, and M. S. Safizadeh, “Three-Dimensional Finite Element and Experimental Simulation of magnetic flux leakage-type NDT for Detection of Pitting Corrosions,” *URL: <http://www.NDT.net/article/IranNDT2017/papers/520.pdf>*, 2017.
- [36] H. Zhang, L. Liao, R. Zhao, J. Zhou, M. Yang, and R. Xia, “The non-destructive test of steel corrosion in reinforced concrete bridges using a micro-magnetic sensor,” *Sensors*, vol. 16, no. 9, pp. 1439, 2016.
- [37] Y. Lijian, L. Gang, Z. Guoguang, and G. Songwei, "Sensor development and application on the oil-gas pipeline magnetic flux leakage detection," 2009 International Conference on Electronic Measurement & Instruments. pp. 2-876-2-878.
- [38] R. LeTessier, R. W. Coade, and B. Geneve, “Sizing of cracks using the alternating current field measurement technique,” *International Journal of Pressure Vessels and Piping*, vol. 79, no. 8-10, pp. 549-554, 2002.
- [39] H. Rowshandel, G. L. Nicholson, C. L. Davis, and C. Roberts, “A combined threshold and signature match method for the automatic detection of rail RCF cracks using an ACFM sensor” 6th IET Conference on Railway Condition Monitoring, 2014.
- [40] M. J. Knight, F. P. Brennan, and W. D. Dover, “Effect of residual stress on ACFM crack measurements in drill collar threaded connections,” *Ndt & E International*, vol. 37, no. 5, pp. 337-343, 2004.

- [41] W. Li, X. a. Yuan, G. Chen, X. Yin, and J. Ge, "A feed-through ACFM probe with sensor array for pipe string cracks inspection," *NDT & E International*, vol. 67, pp. 17-23, 2014.
- [42] J. Ge, W. Li, G. Chen, X. Yin, Y. Wu, X. Yuan, and M. Zhao, "New parameters for the ACFM inspection of different materials," *Insight-Non-Destructive Testing and Condition Monitoring*, vol. 58, no. 6, pp. 313-317, 2016.
- [43] L. Wei, C. Guoming, Y. Xiaokang, Z. Chuanrong, and L. Tao, "Analysis of the lift-off effect of a U-shaped ACFM system," *NDT & E International*, vol. 53, pp. 31-35, 2013.
- [44] F. Noorian, and A. Sadr, "Computation of transient Eddy currents in EMATs using discrete Picard Method" 2010 18th Iranian Conference on Electrical Engineering, pp. 727-731.
- [45] Q. Feng, R. Li, B. Nie, S. Liu, L. Zhao, and H. Zhang, "Literature review: Theory and application of in-line inspection technologies for oil and gas pipeline girth weld deflection," *Sensors*, vol. 17, no. 1, pp. 50, 2017.
- [46] H. Selim, M. Delgado Prieto, J. Trull, L. Romeral, and C. Cojocar, "Laser Ultrasound Inspection Based on Wavelet Transform and Data Clustering for Defect Estimation in Metallic Samples," *Sensors (Basel, Switzerland)*, vol. 19, no. 3, pp. 573, 2019.
- [47] T. E. G. Álvarez-Arenas, J. Camacho, and C. Fritsch, "Passive focusing techniques for piezoelectric air-coupled ultrasonic transducers," *Ultrasonics*, vol. 67, pp. 85-93, 2016.
- [48] S. Dequan, G. Guili, X. Peng, and G. Zhiwei, "Defects Detection System for Steel Tubes Based on Electromagnetic Acoustic Technology," *Procedia Engineering*, vol. 29, pp. 252-256, //, 2012.
- [49] W.-B. Na, and T. Kundu, "A combination of PZT and EMAT transducers for interface inspection," *The Journal of the Acoustical Society of America*, vol. 111, no. 5, pp. 2128-2139, 2002.
- [50] Y. Gao, G. Y. Tian, P. Wang, H. Wang, B. Gao, W. L. Woo, and K. Li, "Electromagnetic pulsed thermography for natural cracks inspection," *Scientific reports*, vol. 7, pp. 42073, 2017.
- [51] X. Gao, F. Podd, W. Van Verre, D. Daniels, and A. Peyton, "Investigating the Performance of Bi-Static GPR Antennas for Near-Surface Object Detection," *Sensors*, vol. 19, no. 1, pp. 170, 2019.
- [52] E. C. Ashigwuike, O. J. Ushie, R. Mackay, and W. Balachandran, "A study of the transduction mechanisms of electromagnetic acoustic transducers (EMATs) on pipe steel materials," *Sensors and Actuators A: Physical*, vol. 229, pp. 154-165, 2015.
- [53] Y. Shi, C. Zhang, R. Li, M. Cai, and G. Jia, "Theory and application of magnetic flux leakage pipeline detection," *Sensors*, vol. 15, no. 12, pp. 31036-31055, 2015.
- [54] J. Zhang, M. Yuan, S.-J. Song, and H.-J. Kim, "Precision measurement of coating thickness on ferromagnetic tube using pulsed eddy current technique," *International Journal of Precision Engineering and Manufacturing*, vol. 16, no. 8, pp. 1723-1728, 2015.
- [55] Y. He, F. Luo, M. Pan, X. Hu, J. Gao, and B. Liu, "Defect classification based on rectangular pulsed eddy current sensor in different directions," *Sensors and Actuators A: Physical*, vol. 157, no. 1, pp. 26-31, 2010.
- [56] D. Roy, R. Chakraborty, and B. K. Kaushik, "Comparative study of E-shaped coil and evolution of new methodology for crack detection using eddy current testing," *Insight-Non-Destructive Testing and Condition Monitoring*, vol. 55, no. 10, pp. 553-557, 2013.
- [57] Y. Li, B. Yan, D. Li, Y. Li, and D. Zhou, "Gradient-field pulsed eddy current probes for imaging of hidden corrosion in conductive structures," *Sensors and Actuators A: Physical*, vol. 238, pp. 251-265, 2016/02/01/, 2016.
- [58] N. Ulapane, A. Alempijevic, J. Valls Miro, and T. Vidal-Calleja, "Non-destructive evaluation of ferromagnetic material thickness using Pulsed Eddy Current sensor detector coil voltage decay rate," *NDT & E International*, vol. 100, pp. 108-114, 2018/12/01/, 2018.
- [59] X. Chen, and Y. Lei, "Electrical conductivity measurement of ferromagnetic metallic materials using pulsed eddy current method," *NDT & E International*, vol. 75, pp. 33-38, 2015/10/01/, 2015.
- [60] Y. R. Smith, J. R. Nagel, and R. K. Rajamani, "Eddy current separation for recovery of non-ferrous metallic particles: A comprehensive review," *Minerals Engineering*, vol. 133, pp. 149-159, 2019/03/15/, 2019.

- [61] Q. Cao, D. Liu, Y. He, J. Zhou, and J. Codrington, "Nondestructive and quantitative evaluation of wire rope based on radial basis function neural network using eddy current inspection," *NDT & E International*, vol. 46, pp. 7-13, 2012/03/01/, 2012.
- [62] R. Yang, Y. He, and H. Zhang, "Progress and trends in nondestructive testing and evaluation for wind turbine composite blade," *Renewable and Sustainable Energy Reviews*, vol. 60, pp. 1225-1250, 2016/07/01/, 2016.
- [63] C. De Michelis, C. Rinaldi, C. Sampietri, and R. Vario, "2 - Condition monitoring and assessment of power plant components," *Power Plant Life Management and Performance Improvement*, J. E. Oakey, ed., pp. 38-109: Woodhead Publishing, 2011.
- [64] C. S. Angani, D. G. Park, C. G. Kim, P. Leela, P. Kollu, and Y. M. Cheong, "The pulsed eddy current differential probe to detect a thickness variation in an insulated stainless steel," *Journal of Nondestructive Evaluation*, vol. 29, no. 4, pp. 248-252, 2010.
- [65] M. Fan, B. Cao, A. I. Sunny, W. Li, G. Tian, and B. Ye, "Pulsed eddy current thickness measurement using phase features immune to liftoff effect," *NDT & E International*, vol. 86, pp. 123-131, 2017/03/01/, 2017.
- [66] M. Fan, B. Cao, G. Tian, B. Ye, and W. Li, "Thickness measurement using liftoff point of intersection in pulsed eddy current responses for elimination of liftoff effect," *Sensors and Actuators A: Physical*, vol. 251, pp. 66-74, 2016/11/01/, 2016.
- [67] D. Zhou, M. Pan, Y. He, and B. Du, "Stress detection and measurement in ferromagnetic metals using pulse electromagnetic method with U-shaped sensor," *Measurement*, vol. 105, pp. 136-145, 2017/07/01/, 2017.
- [68] G. Mroz, W. Reimche, W. Frackowiak, O. Bruchwald, and H. J. Maier, "Setting Discrete Yield-stress Sensors for Recording Early Component Loading Using Eddy-current Array Technology and Induction Thermography," *Procedia Technology*, vol. 15, pp. 484-493, 2014/01/01/, 2014.
- [69] L. Xie, B. Gao, G. Y. Tian, J. Tan, B. Feng, and Y. Yin, "Coupling pulse eddy current sensor for deeper defects NDT," *Sensors and Actuators A: Physical*, vol. 293, pp. 189-199, 2019.
- [70] K. Zhang, Y. He, and Z. Dong, "Pulsed eddy current nondestructive testing for defect evaluation and imaging of automotive lightweight alloy materials," *Journal of Sensors*, vol. 2018, 2018.
- [71] R. R. Robaina, H. T. Alvarado, and J. A. Plaza, "Planar coil-based differential electromagnetic sensor with null-offset," *Sensors and Actuators A: Physical*, vol. 164, no. 1-2, pp. 15-21, 2010.
- [72] A. K. Soni, B. Sasi, S. Thirunavukkarasu, and B. P. C. Rao, "Development of eddy current probe for detection of deep sub-surface defects," *IETE Technical Review*, vol. 33, no. 4, pp. 386-395, 2016.
- [73] Z. Liu, J. Yao, C. He, Z. Li, X. Liu, and B. Wu, "Development of a bidirectional-excitation eddy-current sensor with magnetic shielding: Detection of subsurface defects in stainless steel," *IEEE Sensors Journal*, vol. 18, no. 15, pp. 6203-6216, 2018.
- [74] Y. He, F. Luo, M. Pan, X. Hu, B. Liu, and J. Gao, "Defect edge identification with rectangular pulsed eddy current sensor based on transient response signals," *NDT & e International*, vol. 43, no. 5, pp. 409-415, 2010.
- [75] W. Dehui, H. Tianfu, W. Xiaohong, and S. Lingxin, "Analytical model for mutual inductance between two rectangular coils in driver pickup mode for eddy current testing," *Nondestructive Testing and Evaluation*, vol. 33, no. 1, pp. 20-34, 2018.
- [76] G. Klein, J. Morelli, and T. W. Krause, "Model based optimization of driver-pickup separation for eddy current measurement of gap," *AIP Conference Proceedings*, vol. 1949, no. 1, pp. 110006, 2018.
- [77] S. K. Burke, G. R. Hugo, and D. J. Harrison, "Transient eddy-current NDE for hidden corrosion in multilayer structures," *Review of Progress in Quantitative nondestructive evaluation*, pp. 307-314: Springer, 1998.
- [78] N. Ulapane, L. Nguyen, J. V. Miro, A. Alempijevic, and G. Dissanayake, "Designing a pulsed eddy current sensing set-up for cast iron thickness assessment" 2017 12th IEEE Conference on Industrial Electronics and Applications (ICIEA), pp. 901-906.
- [79] W. Li, Y. Ye, K. Zhang, and Z. Feng, "A thickness measurement system for metal films based on eddy-current method with phase detection," *IEEE Transactions on Industrial Electronics*, vol. 64, no. 5, pp. 3940-3949, 2017.
- [80] Z. Qu, Q. Zhao, and Y. Meng, "Improvement of sensitivity of eddy current sensors for nano-scale thickness measurement of Cu films," *NDT & E International*, vol. 61, pp. 53-57, 2014.

- [81] M. Jagiella, S. Fericean, and A. Dorneich, "Progress and recent realizations of miniaturized inductive proximity sensors for automation," *IEEE sensors journal*, vol. 6, no. 6, pp. 1734-1741, 2006.
- [82] V. Gunasekaran, B. George, S. Aniruddhan, D. D. Janardhanan, and R. V. Palur, "Performance Analysis of Oscillator-Based Read-Out Circuit for LVDT," *IEEE Transactions on Instrumentation and Measurement*, no. 99, pp. 1-9, 2018.
- [83] M. R. Nabavi, and S. Nihtianov, "Eddy-current sensor interface for advanced industrial applications," *IEEE Transactions on Industrial Electronics*, vol. 58, no. 9, pp. 4414-4423, 2010.
- [84] H. Wang, Y. Liu, W. Li, and Z. Feng, "Design of ultrastable and high resolution eddy-current displacement sensor system. IECON 2014 - 40th Annual Conference of the IEEE Industrial Electronics Society" pp. 2333-2339.
- [85] H. Wang, and Z. Feng, "Ultrastable and highly sensitive eddy current displacement sensor using self-temperature compensation," *Sensors and Actuators A: Physical*, vol. 203, pp. 362-368, 2013.
- [86] G. Y. Tian, Z. X. Zhao, R. W. Baines, and P. Corcoran, "Blind sensing [eddy current sensor]," *Manufacturing Engineer*, vol. 76, no. 4, pp. 179-182, 1997.
- [87] G. Y. Tian, *Eddy current frequency output sensors for precision engineering*, 2001.
- [88] Z. Liu, A. D. Koffman, B. C. Waltrip, and Y. Wang, "Eddy current rail inspection using AC bridge techniques," *Journal of research of the National Institute of Standards and Technology*, vol. 118, pp. 140, 2013.
- [89] S. Chattopadhyay, and S. C. Bera, "Modification of the Maxwell–Wien bridge for accurate measurement of a process variable by an inductive transducer," *IEEE Transactions on Instrumentation and Measurement*, vol. 59, no. 9, pp. 2445-2449, 2010.
- [90] S. Bajracharya, E. Sasaki, and H. Tamura, "Numerical study on corrosion profile estimation of a corroded steel plate using eddy current," *Structure and Infrastructure Engineering*, pp. 1-14, 2019.
- [91] A. K. Soni, and B. P. Rao, "Lock-in Amplifier Based Eddy Current Instrument for Detection of Sub-surface Defect in Stainless Steel Plates," *Sensing and Imaging*, vol. 19, no. 1, pp. 32, 2018.
- [92] R. J. Ditchburn, S. K. Burke, and M. Posada, "Eddy-Current Nondestructive Inspection with Thin Spiral Coils: Long Cracks in Steel," *Journal of Nondestructive Evaluation*, vol. 22, no. 2, pp. 63-77, 2003/06/01, 2003.
- [93] F. Thollon, B. Lebrun, N. Burais, and Y. Jayet, "Numerical and experimental study of eddy current probes in NDT of structures with deep flaws," *NDT & E International*, vol. 28, no. 2, pp. 97-102, 1995.
- [94] C. N. Owston, "Eddy-current testing at microwave frequencies," *Non-Destructive Testing*, vol. 2, no. 3, pp. 193-196, 1969.
- [95] W. Yin, J. Tang, M. Lu, H. Xu, R. Huang, Q. Zhao, Z. Zhang, and A. Peyton, "An Equivalent-Effect Phenomenon in Eddy Current Non-Destructive Testing of Thin Structures," *IEEE Access*, vol. 7, pp. 70296-70307, 2019.
- [96] K. A. Bartels, and J. L. Fisher, "Multifrequency eddy current image processing techniques for nondestructive evaluation," *Proceedings, International Conference on Image Processing 1995* pp. 486-489 vol.1.
- [97] Z. Liu, K. Tsukada, K. Hanasaki, and M. Kurisu, "Two-dimensional eddy current signal enhancement via multifrequency data fusion," *Journal of Research in Nondestructive Evaluation*, vol. 11, no. 3, pp. 165-177, 1999.
- [98] A. Bernieri, G. Betta, L. Ferrigno, and M. Laracca, "Crack depth estimation by using a multi-frequency ECT method," *IEEE Transactions on Instrumentation and Measurement*, vol. 62, no. 3, pp. 544-552, 2013.
- [99] D. J. Pasadas, A. L. Ribeiro, H. G. Ramos, B. Feng, and P. Baskaran, "Eddy current testing of cracks using multi-frequency and noise excitation," 2018 IEEE International Instrumentation and Measurement Technology Conference (I2MTC) , pp. 1-6.
- [100] Y. Shen, C. Lee, C. C. H. Lo, N. Nakagawa, and A. M. Frishman, "Conductivity profile determination by eddy current for shot-peened superalloy surfaces toward residual stress assessment," *Journal of Applied Physics*, vol. 101, no. 1, pp. 014907, 2007.

- [101] W. Cheng, and H. Hashizume, "Characterization of multilayered structures by swept-frequency eddy current testing," *AIP Advances*, vol. 9, no. 3, pp. 035009, 2019.
- [102] C. Huang, X. Wu, Z. Xu, and Y. Kang, "Ferromagnetic material pulsed eddy current testing signal modeling by equivalent multiple-coil-coupling approach," *NDT & E International*, vol. 44, no. 2, pp. 163-168, 2011.
- [103] D. J. Harrison, "Eddy-current inspection using Hall sensors and transient excitation," *Defence Research Agency Technical Report DRA/SMC/TR941008, DRA Farnborough, UK*, 1994.
- [104] J. S. R. Giguère, B. A. Lepine, and J. M. S. Dubois, "Detection of cracks beneath rivet heads via pulsed eddy current technique," *AIP Conference Proceedings*, vol. 615, no. 1, pp. 1968-1975, 2002.
- [105] I. Zainal Abidin, C. Mandache, G. Y. Tian, and M. Morozov, "Pulsed eddy current testing with variable duty cycle on rivet joints," *NDT & E international*, vol. 42, no. 7, pp. 599-605, 2009.
- [106] V. K. Babbar, P. R. Underhill, C. Stott, and T. W. Krause, "Finite element modeling of second layer crack detection in aircraft bolt holes with ferrous fasteners present," *NDT & E International*, vol. 65, pp. 64-71, 2014.
- [107] X. Qiu, P. Zhang, J. Wei, X. Cui, C. Wei, and L. Liu, "Defect classification by pulsed eddy current technique in con-casting slabs based on spectrum analysis and wavelet decomposition," *Sensors and Actuators A: Physical*, vol. 203, pp. 272-281, 2013/12/01/, 2013.
- [108] Y. He, F. Luo, M. Pan, F. Weng, X. Hu, J. Gao, and B. Liu, "Pulsed eddy current technique for defect detection in aircraft riveted structures," *NDT & e International*, vol. 43, no. 2, pp. 176-181, 2010.
- [109] A. N. AbdAlla, M. A. Faraj, F. Samsuri, D. Rifai, K. Ali, and Y. Al-Douri, "Challenges in improving the performance of eddy current testing," *Measurement and Control*, vol. 52, no. 1-2, pp. 46-64, 2019.
- [110] M. E. Ibrahim, and S. K. Burke, "Mutual Impedance of Eddy-Current Coils Above a Second-Layer Crack of Finite Length," *Journal of Nondestructive Evaluation*, vol. 38, no. 2, pp. 50, 2019.
- [111] R. Ghoni, M. Dollah, A. Sulaiman, and F. M. Ibrahim, "Defect characterization based on eddy current technique: Technical review," *Advances in Mechanical Engineering*, vol. 6, pp. 182496, 2014.
- [112] A. S. Repelianto, and N. Kasai, "The Improvement of Flaw Detection by the Configuration of Uniform Eddy Current Probes," *Sensors*, vol. 19, no. 2, pp. 397, 2019.
- [113] B.-H. Bae, J.-M. Choi, and S.-Y. Kim, "Eddy current testing probe with dual half-cylindrical coils," *Review of Scientific Instruments*, vol. 71, no. 2, pp. 567-570, 2000.
- [114] S. P. Sullivan, S. P. Smith, and F. L. Sharp, "Simultaneous absolute and differential operation of eddy current bobbin probes for heat exchanger tube inspection," *Materials evaluation*, vol. 58, no. 5, 2000.
- [115] N. M. Rodrigues, L. S. Rosado, and P. M. Ramos, "A portable embedded contactless system for the measurement of metallic material conductivity and lift-off," *Measurement*, vol. 111, pp. 441-450, 2017/12/01/, 2017.
- [116] A. L. Ribeiro, F. Alegria, O. Postolache, and H. M. G. Ramos, "Eddy current inspection of a duralumin plate" 2009 IEEE Instrumentation and Measurement Technology Conference, pp. 1367-1371.
- [117] J. Fang, and T. Wen, "A wide linear range eddy current displacement sensor equipped with dual-coil probe applied in the magnetic suspension flywheel," *Sensors*, vol. 12, no. 8, pp. 10693-10706, 2012.
- [118] A. Sophian, G. Tian, and M. Fan, "Pulsed Eddy Current Non-destructive Testing and Evaluation: A Review," *Chinese Journal of Mechanical Engineering*, vol. 30, no. 3, pp. 500-514, 2017/05/01, 2017.
- [119] L. M. Vallese, "Diffusion of pulsed currents in conductors," *Journal of Applied Physics*, vol. 25, no. 2, pp. 225-228, 1954.
- [120] A. Sophian, G. Y. Tian, D. Taylor, and J. Rudlin, "Design of a pulsed eddy current sensor for detection of defects in aircraft lap-joints," *Sensors and Actuators A: Physical*, vol. 101, no. 1-2, pp. 92-98, 2002.
- [121] H. L. Libby, *Introduction to electromagnetic nondestructive test methods*: Krieger, 1971.

- [122] Y. He, B. Gao, A. Sophian, and R. Yang, *Transient electromagnetic-thermal nondestructive testing: pulsed eddy current and transient eddy current thermography*: Butterworth-Heinemann, 2017.
- [123] M. Lu, L. Yin, A. J. Peyton, and W. Yin, "A novel compensation algorithm for thickness measurement immune to lift-off variations using eddy current method," *IEEE Transactions on Instrumentation and Measurement*, vol. 65, no. 12, pp. 2773-2779, 2016.
- [124] M. B. Kishore, D. G. Park, J. R. Jeong, J. Y. Kim, L. J. Jacobs, and D. H. Lee, "Detection of Deep Subsurface Cracks in Thick Stainless Steel Plate," *Journal of Magnetism*, vol. 20, no. 3, pp. 312-316, 2015.
- [125] A. Sophian, G. Tian, and M. Fan, "Pulsed eddy current non-destructive testing and evaluation: A review," *Chinese Journal of Mechanical Engineering*, vol. 30, no. 3, pp. 500, 2017.
- [126] C. S. Angani, H. G. Ramos, A. L. Ribeiro, and T. J. Rocha, "Evaluation of transient eddy current oscillations response for thickness measurement of stainless steel plate," *Measurement*, vol. 90, pp. 59-63, 2016.
- [127] M. Smetana, T. Strapacova, and L. Janousek, "Pulsed excitation in eddy current non-destructive testing of conductive materials," *Advances in electrical and electronic engineering*, vol. 7, no. 1-2, pp. 326-329, 2011.
- [128] L. Obrutsky, B. Lepine, J. Lu, R. Cassidy, and J. Carter, "Eddy current technology for heat exchanger and steam generator tube inspection," *Proc. 16th WCNDT, Montreal (Canada)*, vol. 30, 2004.
- [129] Y. Yating, and G. Jia, "Investigation of signal features of pulsed eddy current testing technique by experiments," *Insight-Non-Destructive Testing and Condition Monitoring*, vol. 55, no. 9, pp. 487-491, 2013.
- [130] K. Zhang, Z. Dong, Z. Yu, and Y. He, "Shape Mapping Detection of Electric Vehicle Alloy Defects Based on Pulsed Eddy Current Rectangular Sensors," *Applied Sciences*, vol. 8, no. 11, pp. 2066, 2018.
- [131] M. Morozov, G. Y. Tian, and P. J. Withers, "The pulsed eddy current response to applied loading of various aluminium alloys," *NDT & E International*, vol. 43, no. 6, pp. 493-500, 2010.
- [132] A. Sophian, G. Y. Tian, D. Taylor, and J. Rudlin, "A feature extraction technique based on principal component analysis for pulsed eddy current NDT," *NDT & e International*, vol. 36, no. 1, pp. 37-41, 2003.
- [133] B. Lebrun, Y. Jayet, and J.-C. Baboux, "Pulsed eddy current signal analysis: application to the experimental detection and characterization of deep flaws in highly conductive materials," *NDT & e international*, vol. 30, no. 3, pp. 163-170, 1997.
- [134] J. C. Moulder, and J. A. Bieber, "Pulsed eddy-current measurements of corrosion and cracking in aging aircraft," *MRS Online Proceedings Library Archive*, vol. 503, 1997.
- [135] T. Clauzon, F. Thollon, and A. Nicolas, "Flaws characterization with pulsed eddy currents NDT," *IEEE transactions on Magnetism*, vol. 35, no. 3, pp. 1873-1876, 1999.
- [136] D. Zhou, Y. Li, X. Yan, L. You, Q. Zhang, X. Liu, and Y. Qi, "The investigation on the optimal design of rectangular PECT probes for evaluation of defects in conductive structures," *International Journal of Applied Electromagnetics and Mechanics*, vol. 42, no. 2, pp. 319-326, 2013.
- [137] Z. Xu, X. Wu, J. Li, and Y. Kang, "Assessment of wall thinning in insulated ferromagnetic pipes using the time-to-peak of differential pulsed eddy-current testing signals," *NDT & E International*, vol. 51, pp. 24-29, 2012.
- [138] Y. Li, H. Jing, I. Zainal Abidin, and B. Yan, "A gradient-field pulsed eddy current probe for evaluation of hidden material degradation in conductive structures based on lift-off invariance," *Sensors*, vol. 17, no. 5, pp. 943, 2017.
- [139] Y. Li, S. Ren, B. Yan, I. Zainal Abidin, and Y. Wang, "Imaging of subsurface corrosion using gradient-field pulsed eddy current probes with uniform field excitation," *Sensors*, vol. 17, no. 8, pp. 1747, 2017.
- [140] D. Rifai, A. Abdalla, R. Razali, K. Ali, and M. Faraj, "An eddy current testing platform system for pipe defect inspection based on an optimized eddy current technique probe design," *Sensors*, vol. 17, no. 3, pp. 579, 2017.
- [141] Z. Wang, and Y. Yu, "Traditional Eddy Current–Pulsed Eddy Current Fusion Diagnostic Technique for Multiple Micro-Cracks in Metals," *Sensors*, vol. 18, no. 9, pp. 2909, 2018.

- [142] M. Alamin, G. Y. Tian, A. Andrews, and P. Jackson, "Principal component analysis of pulsed eddy current response from corrosion in mild steel," *IEEE Sensors Journal*, vol. 12, no. 8, pp. 2548-2553, 2012.
- [143] H. Tian, S. Yamada, M. Iwahara, H. Watanabe, and H. Tooyama, "Eddy-current scratch inspection with high probe lift-off," 2005 IEEE International Magnetics Conference (INTERMAG), pp. 425-426.
- [144] H. E. Martz, C. M. Logan, D. J. Schneberk, and P. J. Shull, *X-ray Imaging: fundamentals, industrial techniques and applications*: CRC Press, 2016.
- [145] G. Mook, O. Hesse, and V. Uchanin, "Deep penetrating eddy currents and probes," *Materials Testing*, vol. 49, no. 5, pp. 258-264, 2007.
- [146] W. Yin, R. Binns, S. J. Dickinson, C. Davis, and A. J. Peyton, "Analysis of the liftoff effect of phase spectra for eddy current sensors," *IEEE Transactions on Instrumentation and Measurement*, vol. 56, no. 6, pp. 2775-2781, 2007.
- [147] L. A. N. M. Lopez, D. K. S. Ting, and B. R. Upadhyaya, "Removing Eddy-Current probe wobble noise from steam generator tubes testing using Wavelet Transform," *Progress in Nuclear Energy*, vol. 50, no. 7, pp. 828-835, 2008.
- [148] L. Shu, H. Songling, Z. Wei, and Y. Peng, "Improved immunity to lift-off effect in pulsed eddy current testing with two-stage differential probes," *Russian journal of nondestructive testing*, vol. 44, no. 2, pp. 138-144, 2008.
- [149] G. Y. Tian, Y. Li, and C. Mandache, "Study of lift-off invariance for pulsed eddy-current signals," *IEEE transactions on magnetics*, vol. 45, no. 1, pp. 184-191, 2009.
- [150] A. Mohan, and S. Poobal, "Crack detection using image processing: A critical review and analysis," *Alexandria Engineering Journal*, 2017/02/15/, 2017.
- [151] D. Dhital, and J. R. Lee, "A Fully Non-Contact Ultrasonic Propagation Imaging System for Closed Surface Crack Evaluation," *Experimental Mechanics*, vol. 52, no. 8, pp. 1111-1122, 2012.
- [152] B. Shan, S. Zheng, and J. Ou, "A stereovision-based crack width detection approach for concrete surface assessment," *KSCE Journal of Civil Engineering*, vol. 20, no. 2, pp. 803-812, 2016.
- [153] S. K. Burke, and R. J. Ditchburn, "Mutual impedance of planar eddy-current driver-pickup spiral coils," *Research in Nondestructive Evaluation*, vol. 19, no. 1, pp. 1-19, 2008.
- [154] X. Sheng, Y. Li, M. Lian, C. Xu, and Y. Wang, "Influence of Coupling Interference on Arrayed Eddy Current Displacement Measurement," *Materials Evaluation*, vol. 74, no. 12, pp. 1675-1683, 2016.
- [155] A. De Marcellis, C. Reig, and M.-D. Cubells-Beltrán, "Current-based measurement technique for high sensitivity detection of resistive bridges with external balancing through control voltages," *IEEE Sensors Journal*, vol. 17, no. 2, pp. 404-411, 2017.
- [156] P. R. Nagarajan, B. George, and V. J. Kumar, "A Linearizing Digitizer for Wheatstone Bridge Based Signal Conditioning of Resistive Sensors," *IEEE Sensors Journal*, vol. 17, no. 6, pp. 1696-1705, 2017.
- [157] S. Chattopadhyay, B. R. Maity, and S. Pal, "Accurate measurement of Q'factor of an inductive coil using a modified maxwell wein bridge network," *Sensors & Transducers*, vol. 105, no. 6, pp. 10, 2009.
- [158] G. Betta, P. Burrascano, L. Ferrigno, M. Laracca, M. Ricci, and G. Silipigni, "An experimental comparison of complex excitation sequences for eddy current testing," *ACTA IMEKO*, vol. 4, no. 1, pp. 128-134, 2015.
- [159] J. Kral, R. Smid, H. M. G. Ramos, and A. L. Ribeiro, "The lift-off effect in eddy currents on thickness modeling and measurement," *IEEE Transactions on Instrumentation and Measurement*, vol. 62, no. 7, pp. 2043-2049, 2013.
- [160] G. Y. Tian, Y. He, I. Adewale, and A. Simm, "Research on spectral response of pulsed eddy current and NDE applications," *Sensors and Actuators A: Physical*, vol. 189, pp. 313-320, 2013.
- [161] Y. Yu, Y. Yan, F. Wang, G. Tian, and D. Zhang, "An approach to reduce lift-off noise in pulsed eddy current nondestructive technology," *NDT & E International*, vol. 63, pp. 1-6, 2014.
- [162] V. Arjun, B. Sasi, B. P. C. Rao, C. K. Mukhopadhyay, and T. Jayakumar, "Optimisation of pulsed eddy current probe for detection of sub-surface defects in stainless steel plates," *Sensors and Actuators A: Physical*, vol. 226, pp. 69-75, 2015/05/01/, 2015.

- [163] D. Zhou, J. Wang, Y. He, D. Chen, and K. Li, "Influence of metallic shields on pulsed eddy current sensor for ferromagnetic materials defect detection," *Sensors and Actuators A: Physical*, vol. 248, pp. 162-172, 2016.
- [164] G. Klein, J. Morelli, and T. W. Krause, "Model based optimization of driver-pickup separation for eddy current measurement of gap." p. 110006.
- [165] T. P. Theodoulidis, and E. E. Kriezis, "Impedance evaluation of rectangular coils for eddy current testing of planar media," *NDT & E International*, vol. 35, no. 6, pp. 407-414, 2002/09/01/, 2002.
- [166] D. R. Desjardins, T. W. Krause, A. Tetervak, and L. Clapham, "Concerning the derivation of exact solutions to inductive circuit problems for eddy current testing," *NDT & E International*, vol. 68, pp. 128-135, 2014.
- [167] H. Zhou, B. Zhu, W. Hu, Z. Liu, and X. Gao, "Modelling and practical implementation of 2-coil wireless power transfer systems," *Journal of Electrical and Computer Engineering*, vol. 2014, pp. 27, 2014.
- [168] C. Liu, and Y. Dong, "Resonant enhancement of a passive coil-capacitance loop in eddy current sensing path," *Measurement*, vol. 45, no. 3, pp. 622-626, 2012.
- [169] D. Desjardins, T. W. Krause, and L. Clapham, "Transient response of a driver-pickup coil probe in transient eddy current testing," *NDT & E International*, vol. 75, pp. 8-14, 2015.
- [170] D. Vyroubal, and D. Zele, "Experimental optimization of the probe for eddy-current displacement transducer," *IEEE transactions on instrumentation and measurement*, vol. 42, no. 6, pp. 995-1000, 1993.
- [171] Z. Chen, N. Yusa, and K. Miya, "Some advances in numerical analysis techniques for quantitative electromagnetic nondestructive evaluation," *Nondestructive testing and evaluation*, vol. 24, no. 1-2, pp. 69-102, 2009.
- [172] S. Xie, Z. Chen, T. Takagi, and T. Uchimoto, "Quantitative non-destructive evaluation of wall thinning defect in double-layer pipe of nuclear power plants using pulsed ECT method," *NDT & E International*, vol. 75, pp. 87-95, 2015.
- [173] S. Xie, Z. Chen, T. Takagi, and T. Uchimoto, "Development of a very fast simulator for pulsed eddy current testing signals of local wall thinning," *NDT & E International*, vol. 51, pp. 45-50, 2012.
- [174] Y. He, G. Tian, H. Zhang, M. Alamin, A. Simm, and P. Jackson, "Steel corrosion characterization using pulsed eddy current systems," *IEEE Sensors Journal*, vol. 12, no. 6, pp. 2113-2120, 2012.
- [175] D. I. Ona, G. Y. Tian, R. Sutthaweeikul, and S. M. Naqvi, "Design and optimisation of mutual inductance based pulsed eddy current probe," *Measurement*, vol. 144, pp. 402-409, 2019/10/01/, 2019.
- [176] H. Zhang, M. Zhong, F. Xie, and M. Cao, "Application of a Saddle-Type Eddy Current Sensor in Steel Ball Surface-Defect Inspection," *Sensors*, vol. 17, no. 12, pp. 2814, 2017.
- [177] A. D. Marcellis, C. Reig, and M. Cubells-Beltrán, "Current-Based Measurement Technique for High Sensitivity Detection of Resistive Bridges With External Balancing Through Control Voltages," *IEEE Sensors Journal*, vol. 17, no. 2, pp. 404-411, 2017.
- [178] C. Baby, and B. George, "A simple analog front-end circuit for grounded capacitive sensors with offset capacitance," 2013 IEEE International Instrumentation and Measurement Technology Conference (I2MTC), pp. 1372-1375.
- [179] S. Malik, T. Islam, K. Kishore, K. Kumar, S. A. Akbar, and B. A. Botre, "A simple analog interface for capacitive sensor with offset and parasitic capacitance," 2015 Annual IEEE India Conference (INDICON), pp. 1-4.
- [180] N. Mandal, and G. Rajita, "An accurate technique of measurement of flow rate using rotameter as a primary sensor and an improved op-amp based network," *Flow Measurement and Instrumentation*, vol. 58, pp. 38-45, 2017.
- [181] G. Spiezia, R. Losito, M. Martino, A. Masi, and A. Pierno, "Automatic test bench for measurement of magnetic interference on LVDTs," *IEEE Transactions on Instrumentation and Measurement*, vol. 60, no. 5, pp. 1802-1810, 2011.
- [182] F. Mocholí Belenguer, A. Mocholí Salcedo, V. Milián Sánchez, and J. H. Arroyo Núñez, "Double Magnetic Loop and Methods for Calculating Its Inductance," *Journal of Advanced Transportation*, vol. 2018, 2018.

- [183] G. R. Guerreiro, and J. Navarro, "Design for stability of active inductor with feedback resistance," 2014 27th Symposium on Integrated Circuits and Systems Design (SBCCI), pp. 1-6.
- [184] S. K. Burke, and M. E. Ibrahim, "Mutual impedance of air-cored coils above a conducting plate," *Journal of Physics D: Applied Physics*, vol. 37, no. 13, pp. 1857, 2004.
- [185] A. De Marcellis, G. Ferri, and P. Mantenuto, "Analog Wheatstone bridge-based automatic interface for grounded and floating wide-range resistive sensors," *Sensors and Actuators B: Chemical*, vol. 187, pp. 371-378, 2013.
- [186] P. Mantenuto, A. De Marcellis, and G. Ferri, "Uncalibrated analog bridge-based interface for wide-range resistive sensor estimation," *IEEE Sensors Journal*, vol. 12, no. 5, pp. 1413-1414, 2011.
- [187] E. Sifuentes, O. Casas, F. Reverter, and R. Pallas-Areny, "Direct interface circuit to linearise resistive sensor bridges," *Sensors and Actuators A: physical*, vol. 147, no. 1, pp. 210-215, 2008.
- [188] G. De Graaf, and R. F. Wolffenbuttel, "Systematic approach for the linearization and readout of nonsymmetric impedance bridges," *IEEE transactions on instrumentation and measurement*, vol. 55, no. 5, pp. 1566-1572, 2006.
- [189] V. Stornelli, G. Ferri, A. Leoni, and L. Pantoli, "The assessment of wind conditions by means of hot wire sensors and a modified Wheatstone bridge architecture," *Sensors and Actuators A: Physical*, vol. 262, pp. 130-139, 2017/08/01/, 2017.
- [190] N. Ulapane, and L. Nguyen, "Review of Pulsed-Eddy-Current Signal Feature-Extraction Methods for Conductive Ferromagnetic Material-Thickness Quantification," *Electronics*, vol. 8, no. 5, pp. 470, 2019.
- [191] G. Y. Tian, and A. Sophian, "Defect classification using a new feature for pulsed eddy current sensors," *Ndt & E International*, vol. 38, no. 1, pp. 77-82, 2005.
- [192] M. Fan, Q. Wang, B. Cao, B. Ye, A. Sunny, and G. Tian, "Frequency optimization for enhancement of surface defect classification using the eddy current technique," *Sensors*, vol. 16, no. 5, pp. 649, 2016.
- [193] Y. Li, B. Yan, D. Li, H. Jing, Y. Li, and Z. Chen, "Pulse-modulation eddy current inspection of subsurface corrosion in conductive structures," *NDT & E International*, vol. 79, pp. 142-149, 2016.
- [194] P. F. Horan, P. R. Underhill, and T. W. Krause, "Real time pulsed eddy current detection of cracks in F/A-18 inner wing spar using discriminant separation of modified principal components analysis scores," *IEEE Sensors Journal*, vol. 14, no. 1, pp. 171-177, 2014.
- [195] M. Pan, Y. He, G. Tian, D. Chen, and F. Luo, "Defect characterisation using pulsed eddy current thermography under transmission mode and NDT applications," *NDT & E International*, vol. 52, pp. 28-36, 2012.
- [196] C. A. Stott, P. R. Underhill, V. K. Babbar, and T. W. Krause, "Pulsed eddy current detection of cracks in multilayer aluminum lap joints," *IEEE Sensors Journal*, vol. 15, no. 2, pp. 956-962, 2015.
- [197] J. A. Buck, P. R. Underhill, S. G. Mokros, J. E. Morelli, V. K. Babbar, B. Lepine, J. Renaud, and T. W. Krause, "Pulsed eddy current inspection of support structures in steam generators," *IEEE Sensors Journal*, vol. 15, no. 8, pp. 4305-4312, 2015.
- [198] H. Mandal, S. K. Bera, S. Saha, P. K. Sadhu, and S. C. Bera, "Study of a modified LVDT type displacement transducer with unlimited range," *IEEE Sensors Journal*, vol. 18, no. 23, pp. 9501-9514, 2018.

